Characterization of a Mouse Model of Soft Tissue Sarcoma: Intraoperative Molecular Imaging and miRNA Regulation of Metastasis

by

Jeffrey Mito

Department of Pharmacology and Cancer Biology
Duke University

Date:_______________________
Approved:

____
David Kirsch, Supervisor

____
Xiao-Fan Wang

____
Christopher Counter

____
Corinne Linardic

____
Gerard Blobe

Dissertation submitted in partial fulfillment of
the requirements for the degree of Doctor of Philosophy in the Department of
Pharmacology and Cancer Biology in the Graduate School
of Duke University

2012

ABSTRACT

Characterization of a Mouse Model of Soft Tissue Sarcoma: Intraoperative Molecular Imaging and miRNA Regulation of Metastasis

by

Jeffrey Mito

Department of Pharmacology and Cancer Biology
Duke University

Date:_______________________
Approved:

____
David Kirsch, Supervisor

____
Xiao-Fan Wang

____
Christopher Counter

____
Corinne Linardic

____
Gerard Blobe

An abstract of a dissertation submitted in partial
fulfillment of the requirements for the degree
of Doctor of Philosophy in the Department of
Pharmacology and Cancer Biology in the Graduate School
of Duke University

2012

Abstract

Soft Tissue Sarcomas are a rare group of mesenchymal tumors with over 50 recognized subtypes. These tumors are a diverse group of malignancies that primarily arise from the connective tissue, fat and muscle. In the United States, there are estimated to be approximately 11,000 new diagnoses a year with an annual mortality rate approaching 40%. Unfortunately, with such a diversity of subtypes of soft tissue sarcoma, and the relative scarcity of patient samples, there is a need for animal models that faithfully recapitulate the biology of these tumors. Such animal models would be useful for dissecting the underlying biology of soft tissue sarcomas and to evaluate novel therapies. One such model is the *LSL-Kras*^{G12D}*; p53*$^{Flox/Flox}$(referred to here as *KP* mice) mouse model of soft tissue sarcoma. These tumors are generated in a spatial and temporally restricted fashion and closely mimic the natural history of human soft tissue sarcomas, including a predilection to develop lung metastases. Here I will characterize this model of soft tissue sarcoma by: 1) performing cross species genomic comparisons to show that the sarcomas arising in *KP* mice most closely resembles Undifferentiated Pleomorphic Sarcoma , 2) utilizing this mouse model to identify cathepsin proteases as molecular markers of soft tissue sarcoma. I will then use cathepsin activated imaging probes for intraoperative molecular imaging to identify microscopic residual cancer in real time. Finally, 3) I identify a novel mechanism through which MAPK signaling regulates miRNA biogenesis

and the development of distant metastases in the *KP* mouse model of soft tissue sarcoma.

Contents

List of Tables

List of Figures

1. Introduction

1.1 Overview of Soft Tissue Sarcomas

Soft tissue sarcomas are a rare group of mesenchymal tumors that can arise at any site within the body. Soft tissue sarcomas arise from muscle, fat, connective tissue, and the peripheral nervous system. Every year, there are approximately 11,000 newly diagnosed cases of soft tissue sarcoma in the United States, which represents less than 1% of all new cancer diagnoses [1]. As with most types of cancer, incidence increases with age for most soft tissue sarcomas, with a peak incidence around age 65 [2]. However, several types of soft tissue sarcoma, including alveolar and embryonal rhabdomyosarcoma, are more common in childhood [2].

Anatomically, the majority of soft tissue sarcomas occur in the extremities, but other frequent locations include the torso, retroperitoneum, and the head and neck [3]. As the primary tumor grows, it will displace normal tissue around it, leading to compression of normal structures around the tumor, forming a pseudocapsule. The presence of this pseudocapsule can lead to poorly defined tumor margins that can provide challenges for complete surgical resection. Moreover, as soft tissue sarcomas grow in size, patients are at increased risk for metastatic spread of the primary tumor [4]. Thus, early intervention is important for patient outcomes. For soft tissue sarcomas, hematogenous dissemination to the lungs is the most common site of distant metastasis. As a result approximately 30% of soft tissue sarcoma patients will go onto develop fatal lung metastases [5].

1.2 Classification and Etiology of Soft Tissue Sarcomas

There are over 50 recognized subtypes of soft tissue sarcomas that are thought to originate from a broad spectrum of tissues including muscle, fat and the peripheral nervous system, among others [6]. Many soft tissue sarcomas are typically classified based on their presumed tissue of origin, such as liposarcoma, synovial sarcoma, and rhabdomyosarcoma. Conversely, less well defined tumors, such as undifferentiated pleomorphic sarcoma (UPS), are classified based on their histologic appearance.

Furthermore, when histologic appearance alone is not adequate to arrive at a diagnosis, immunohistochemistry is often used to aid in the identification of soft tissue sarcomas. Stains commonly used to identify tumors of myogenic origin include desmin, an intermediate filament protein [7], and myogenin [8]. For tumors of neurectoderm origin, such as malignant peripheral nerve sheath tumors (MPNST), staining for S100 can aid in the diagnosis of less differentiated variants [9]. Additionally, staining for cytokeratin can rule out tumors of epithelial origin or aid in the diagnosis of synovial sarcoma [10].

Besides the histologic subtype, one of the most important prognostic indicators of soft tissue sarcoma is tumor grade. Generally, a pathologist will consider tumor differentiation, mitotic activity and the presence of necrosis when assigning a grade to a tumor [11]. For patients with large high grade tumors, five-year metastasis rates will approach 50% [12]. Thus, identifying these patients early for aggressive therapy, including systemic chemotherapy, may improve their outcomes [13]. However, additional studies are needed to clarify the role of chemotherapy in therapy for soft tissue sarcomas as other studies have failed to show significant benefits in survival [14].

Others have speculated that understanding the etiology of soft tissue sarcomas may lead to better therapies by risk stratifying patients for cytotoxic therapy or targeted therapies that inhibit the pathways driving tumor development and progression [15]. Unlike many carcinomas, there are no defined precursor lesions or well established risk factors. In some cases, the development of soft tissue sarcoma has been linked to prior treatment with chemo- or radio-therapy [16, 17], or certain genetic abnormalities such as Li-Fraumeni syndrome, characterized by somatic mutation in p53 [18], and neurofibromatosis [19]. However, for most patients, there are no well defined risk factors and sarcomas arises de novo.

1.3 Translocation Associated Soft Tissue Sarcomas

Soft tissue sarcomas can generally be put into one of two large groups, those with well defined pathognomonic translocations and those without. Sarcomas with well defined translocations include: Ewing’s sarcoma, alveolar rhabdomyosarcoma (aRMS), and synovial sarcoma, among others.

Ewing’s sarcoma is a small round cell tumor typically found within the bone or soft tissue. These tumors tend to peak in incidence in childhood and are defined by a translocation between EWS and a member of the ETS transcription factor family, most commonly FLI1 [20]. This translocation results in the EWS domain providing a strong transcriptional activator fused with the FLI1 DNA-binding domain. A number of studies have identified several downstream targets that maybe involved in transformation including upregulation of Id2 [21] and hTERT [22], and downregulation of p21 [23] among other targets.

aRMS is a tumor predominantly of childhood and is defined by the presence of round or oval shaped cells with areas of central clearing that are thought to be due to poor cellular organization [24]. Although predominantly a diagnosis based on histologic appearance, the majority of aRMS have translocations between either the *PAX3* or *PAX7* gene and *FOXO1 [25, 26]*. *PAX3* and *PAX7* are myogenic transcription factors involved in muscle development [27]. For the majority of translocations in aRMS, the DNA binding domain of *PAX3* or *PAX7* is fused to the transactivating domain of *FOXO1* leading to aberrant transcriptional activity of *PAX3/7* target genes [27].

Synovial sarcoma is named for its resemblance to synovial cells. There are two histologic subtypes: mono- and bi-phasic. These tumors tend to occur in young adults in the extremities. Synovial sarcomas are often associated with joint capsules and tendons. The translocation most associated with synovial sarcoma involves fusion of the SYT gene on chromosome 18 with one of three homologous SSX genes on the X chromosome [28, 29].

1.4 Soft Tissue Sarcomas with Complex Karyotypes

In contrast to tumors defined by specific translocations, the majority of soft tissue sarcomas have no well defined translocations and tend to have complex karyotypes. Examples of sarcomas with complex karyotypes include UPS, leiomyosarcomas, fibrosarcoma, embryonal rhabdomyosarcoma, and MPNSTs among others. Despite this diversity, some have hypothesized that inactivation of the p53 pathway maybe a common feature that links this heterogeneous group of tumors [30].

UPS, formally known as malignant fibrous histiocytoma, is one of the most common soft tissue sarcoma of adulthood [31]. These tumors typically are high grade pleomorphic sarcomas, often with no clear line of differentiation based on histology or immunohistochemical staining [32, 33]. Thus, in recent years, UPS has become a diagnosis of exclusion.

Leiomyosarcomas are thought to arise from smooth muscle and display differentiation characteristics associated with smooth muscle. As such, they can occur at any site within the body that contains blood vessels. One better characterized site for the formation of leiomyosarcoma is within the uterine wall, although data has suggested that uterine leiomyosarcoma maybe distinct from leiomyosarcomas at other sites [34]. Recent work dissecting the molecular pathways responsible for leiomyosarcomas often have implicated the loss of the tumor suppressor *PTEN* [35], which results in activation of the PI3K pathway in leiomyosarcomas development [36].

Embryonal Rhabdomyosarcoma (eRMS) typically develops in young children and is the most common pediatric soft tissue tumor. In total, eRMS represents up to 50% of all rhabdomyosarcoma [37]. eRMS is histologically composed of rhabdomyoblasts that tend to be arranged in sheets or nests of rhabdomyoblast and lack an alveolar pattern that defines aMRS [37]. Indeed, recent work has suggested that eRMS may overlap with translocation negative aRMS and that these two groups of tumors (eRMS and translocation negative aRMS) may represent a single disease [38]. Mutations in a number of signaling pathways have been observed including those involved in growth factor and Ras signaling [39].

MPNSTs are soft tissue sarcomas derived from cells of neuroectodermal origin. MPNSTs tend to be highly cellular with many spindle cells and high mitotic rates [40]. They typically arise from peripheral nerves and occur in up to 13 percent of patients with type I neurofibromatosis [41]. These patients have germline mutations in the tumor suppressor *NF1* and develop often disfiguring neurofibromas that can progress to MPNSTs [42].

1.5 Therapy and Outcomes

Over the past several decades, therapy for soft tissue sarcomas has greatly improved. Thanks to improved surgical techniques and the addition of radiation therapy, for patients with extremity tumors, the amputation rate has dropped from 50% to less than 10% [43]. Conventional therapy for soft tissue sarcoma patients is surgical resection of the primary tumor. The goal of the surgery is to completely remove the primary tumor with wide surgical margins while preserving as many critical structures, such as nerves, as possible. Surgeons strive to perform the resection without cutting into the tumor or the pseudocapsule around it. Furthermore, violation of the tumor during oncologic resection has been linked to higher rates of local failure in soft tissue sarcoma patients [44].

As soft tissue sarcomas tend to be highly locally invasive, the addition of radiation therapy either before or after surgery has been shown to improve local control rates in sarcoma patients [45, 46]. With combined radiation therapy and surgery, local control rates approach 90% [45]. However, there are many risk factors that will increase the patient's risk for local recurrence and worse outcome. Three of the most important prognostic factors associated with patient outcome include margin status, tumor size and histologic grade [47]. These same risk factors are not only important for local control of the primary tumor, but also are risk factors for the development of metastatic disease.

For most soft tissue sarcomas, the most common site of metastatic disease is to the lungs [48]. Similarly, with few exceptions, soft tissue sarcomas rarely metastasize to lymph nodes. The development of distant metastases to the lung is the highest cause of mortality for sarcoma patients. When patients develop lung metastases, the median survival is 11-15 months [48, 49]. For patients with unresectable metastatic disease, systemic chemotherapy is the best option available to many sarcoma patients. With current chemotherapeutic regiments, response rates can range from 16-40% of patients. However, complete responses are rare and there are questionable benefits on overall survival [50-52]. Thus understanding of the molecular mechanisms underlying sarcoma biogenesis and tumor progression may lead to new therapies for sarcoma patients. However, there are relatively few patient samples and cell lines available to study. Therefore, the use of animal models of soft tissue sarcomas will likely accelerate the development of future therapies [53].

1.6 Mouse Models of Soft Tissue Sarcoma

Xenograft Models and Knockout Mice

Many of the earliest animal models of soft tissue sarcoma utilized transplanted human cell lines into immunocompromised mice. Cell lines from several subtypes of sarcomas with simple or complex karyotypes are available including: synovial sarcoma (SW982), rhabdomyosarcoma (RD and RH4), Ewing's sarcoma (RD-ES), fibrosarcoma (HT1080), Liposarcoma (SW872), and leiomyosarcoma (HTB88). These cell line models have been the primary research tool for soft tissue sarcomas for decades and have led to insights into sarcoma biology including tumor progression and metastasis [54, 55]. Moreover, they are model systems for testing new therapies that target the molecular pathways underlying tumor development and maintenance [56]. These xenograft systems also have several advantages: being able to rapidly screen compounds for efficacy, manipulate the cell lines *in vitro* such as adding or knockdown genes of interest, and the ability to generate a large number of synchronized tumors for studies.

However, despite these many advantages, there are some inherent disadvantages to these systems. The most pronounced weakness of these systems lies in appropriately modeling the tumor-stromal cell interactions between human tumor cells and the mouse stroma. This is further complicated by the need to use immunocompromised animals, which greatly hinders important tumor-immune system interactions that can impact tumor growth [57], metastasis [58], or response to therapy [59]. Thus, autochthonous mouse models of soft tissue sarcoma may provide better tumor-stromal cell interactions that more faithfully reflect the sarcoma biology of humans.

Some of the earliest knockout mice developed to study cancer were generated by targeted deletion of *p53* [60]. Similar to human patients with Li-Fraumeni syndrome, mice with homozygous loss of *p53* were tumor prone and developed a wide spectrum of tumors including lymphomas, osteosarcomas, and soft tissue sarcomas.

Another hereditary cancer predisposition syndrome that leads to the development of soft tissue sarcomas is neurofibromatosis. These patients typically have inactivation of the Ras-GTPase activating protein *NF1* [61]. This leads to reduced GTP hydrolysis of GTP-bound Ras, reducing negative feedback on Ras: increasing Ras pathway activity. The consequences of this are the development of neurofibromas in the peripheral nerves of patients. In time, these neurofibromas can go on to develop into MPNSTs. However, unlike humans, heterzygous *Nf1* knockout mice fail to develop neurofibromas [62]. However, chimeric mice with a mix of *NF1* null and *NF1* wild type mice, or mice carrying a *NF1* mutation in cis- with heterozygous loss of *p53*, mice develop MPNSTs [63].

Genetically Engineered Mouse Models of Soft Tissue Sarcoma

Over the past several decades, our ability to manipulate the mouse genome has increased significantly. From the transgenic and knockout models mentioned above that can affect every cell within the animal, others have developed technology to allow expression of oncogenes or deletion of tumor suppressors within specific tissue(s). A number of investigators have taken advantage of these systems to develop new mouse models of soft tissue sarcoma driven by tissue specific expression of oncogenes or deletion of tumor suppressors.

The development of site-specific recombinase technology has allowed this to take place. There are two site-specific recombinases commonly used in mammalian systems: *Cre-loxP* and *Flp-FRT*. Both recombinase systems work using the same general principles. The site specific recombinase, *Cre* or *Flp*, recognizes a small sequence within the DNA known as a *loxP* or *FRT* site. When there are two adjacent sites, the recombinase will recognize them and delete DNA between the *loxP* or *FRT* sites. This technology can be used to functionally delete genes by removing key exons (Figure 1A). Others have extended this technology to temporally restrict gene expression by generating knockin mice with transcriptional and translational STOP cassettes between *loxP* sites. This creates a "*Lox-Stop-Lox*" (LSL) cassette, which only allows expression of downstream genes after *Cre* mediated recombination (Figure 1B). Thus, specific expression of downstream genes can be restricted until *Cre* is expressed. Therefore, expression of downstream oncogenes or reporter genes can be regulated in a in a temporally and spatially restricted fashion.

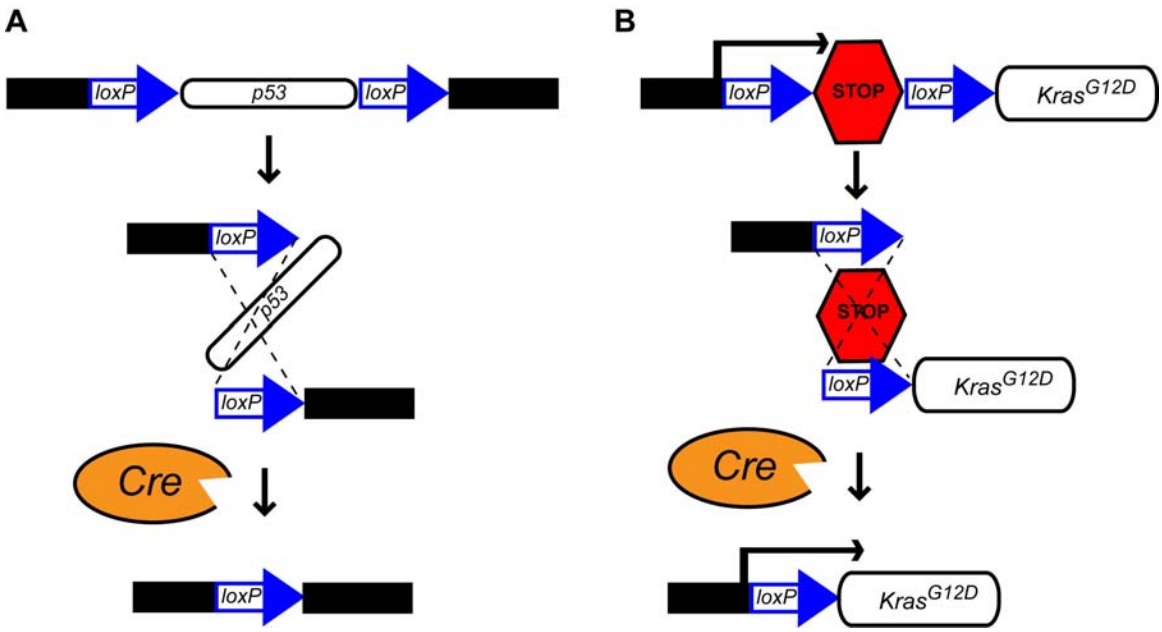

Figure 1: *Cre* Recombinase Mediates Site Specific Recombination

Figure 1: *Cre* recombinase mediates site specific recombination. Cre recombinase recognizes specific 34bp *loxP* sites within the genome and can be used to **(A)** delete genes flanked by *loxP* sites (Flox) or **(B)** delete transcriptional and translational "STOP" cassettes to allow expression of downstream gene(s).

Mouse Models of Translocation Associated Soft Tissue Sarcomas

Alveolar Rhabdomyosarcoma (aRMS) is defined by the presence of the *Pax3:FoxO1* fusion gene. To study this translocation, mice were developed that conditionally express the *Pax3:FoxO1* fusion gene from the endogenous *Pax3* promoter. Using a *Myf6* driven *Cre* to express *Cre* recombinase from *Myf6* expressing cells, *Pax3:FoxO1* is expressed and drives development of aRMS like tumors (1 of 228). The penetrance of aRMS like tumors was greatly enhanced by cooperating mutations in *p53* or *Ink4a/Arf* (3 of 17 and 4 of 14, respectively) [64]. These tumors closely resemble human aRMS both histologically and at the gene expression level [65].

Synovial sarcoma is characterized by an *SYT-SSX* fusion gene between chromosome 18 and the X chromosome and accounts for up to 10% of all soft tissue sarcomas. To generate this mouse, the *SYT-SSX2* fusion gene was cloned into a *Rosa26* targeting vector downstream of a *loxP*-NEO-STOP-*loxP* cassette to prevent *SYT-SSX2* expression in the absence of *Cre*. When bred to *Myf5-Cre* mice, which restricts *Cre* expression to *Myf5* expressing cells, these mice developed synovial sarcomas in 3-5 months that recapitulated the histologic variants (mono- and bi-phasic) and gene expression characteristics of synovial sarcoma [66]. These data suggest that synovial sarcomas that appear to derive from synovial cells may have a myogenic cell of origin.

Mouse Models of Soft Tissue Sarcoma with Complex Karyotypes

Several genes have been implicated in eRMS including *p53*, *Rb1*, and *Ras* [18, 67, 68]. Thorough characterization of muscle lineage cells that give rise to rhabdomyosarcoma has been performed using muscle lineage specific *Cre* drivers. These studies have shown that loss of *p53* and/or one allele of *Ptch1* is sufficient to induce eRMS from *Pax7* satellite cells, *Myf5* or *Myf6* expressing progenitor cells [69], suggesting that the cell of origin for eRMS can arise from a variety of muscle lineage cells.

In contrast to several of the above models, multiple primary mouse models of leiomyosarcoma have been described in the literature. One of the better characterized models uses *Tagln-Cre* combined with *Pten*^{Flox} mice to delete the tumor suppressor *Pten* in smooth muscle cells. This results in aberrant activation of the PI3K cascade and the development of leiomyosarcomas throughout the body in approximately 3 months [70]. Moreover, treatment with the rapamycin analog Everolimus significantly prolongs survival in these mice and prevents activation of AKT, and subsequently mTOR. Another model of leiomyosarcomas limits tumor development to the uterus. Utilizing *p53*^{Flox} and *BRCA1*^{Flox} mice crossed to an *Amh2r-Cre*. Mice in this model develop uterine leiomyosarcomas with a latency of approximately 50 weeks [71]. Together these models are capable of covering a broad spectrum of leiomyosarcomas.

1.7 Study Objectives

Despite the advances of recent years in developing primary mouse models of soft tissue sarcoma, they all have significant weaknesses. First, they all rely upon *Cre* drivers. Thus tumors can arise over a large period of time, and in the case of the *Cre* drivers that are broadly expressed, like *Tagln-Cre* and *Myf5-Cre,* tumors can arise at nearly any site within the body with delayed kinetics (up to 50 weeks) that may not make these models ideal pre-clinical model systems. Thus, generating both temporally and spatially restricted mouse models of soft tissue sarcoma that arise with accelerated kinetics will greatly enhance the pre-clinical utility of these mouse models.

One such model is the *LSL-Kras*^{G12D}*; p53*$^{Flox/Flox}$ mouse (referred to here as *KP* mice) model of soft tissue sarcoma [72]. In *KP* mice, sarcomas are initiated by intramuscular injection of an adenovirus expressing *Cre*-recombinase. Mice develop high grade soft tissue sarcomas at the site of injection in approximately two to three months with 90% penetrance. Much like human patients, approximately 40% of these mice will go onto develop distant lung metastases. For my thesis, I am using this model to: 1) Perform cross species genomic analysis to identify the subtype of soft tissue sarcoma modeled in *KP* mice. 2) Use this model to study local control using intraoperative molecular imaging, and 3) Study the role of miRNAs in the development of distant metastases in *KP* mice.

2. Materials and Methods

2.1 Cross Species Genomic Analysis Comparison of Soft Tissue Sarcomas in KP Mice

Both mouse genotyping and generation of tumors was carried out as described previously [72] in accordance with Duke University and MIT Institutional Animal Care and Use Committee approved protocols. Sarcomas were induced in the left hind limb and allowed to grow until ~300mm^3 in volume. Tumors were then surgically excised via amputation of the limb and animals followed for a minimum of 4 months to determine the metastatic potential of the primary tumor.

RNA Isolation

RNA was extracted from tumors in *KP* mice or normal muscle using TRIzol reagent (Invitrogen) and was purified using RNeasy mini kit (Qiagen).

Microarray Processing and Analysis

Briefly, gene expression was determined using Affymetrix 430A 2.0 arrays (Affymetrix) as described in detail online (http://www.genome.duke.edu/cores/microarray/). .CEL files were processed using the RMA algorithm [73, 74] to normalize the data. Genesets were identified using a signal-to-noise metric.

Human and Mouse datasets [75-77] were downloaded from GEO (GSE6461, GSE6481, GSE2553, and GDS1209), normalized with RMA (when appropriate). Genesets and array data were used in GSEA as described previously [78]. Classes were defined as one soft tissue sarcoma subtype versus controls (other sarcoma or normal muscle) present in their respective datasets.

Database Accession Numbers

Microarray data was generated in conformity to MIAME guidelines and has been deposited in the GEO database under accession number GSE16779.

Oncogenic Pathway Predictors

Human soft tissue sarcoma datasets [76, 77] were combined using ComBat [79] and normal tissue samples removed from the combined dataset. An oncogenic pathway classifier for Ras pathway activity was developed as described previously [80]. This classifier was used to compare UPS samples (n=29) against all other soft tissue sarcomas. Significance was determined using a non-parametric Mann-Whitney test.

Q-RT-PCR

RNA isolated from an independent cohort of tumors and normal muscle samples was isolated using TRIzol (Invitrogen). Reverse transcription reaction was performed using 500μg of total RNA and the iScript cDNA synthesis kit (Biorad) per manufacturer's instructions. Q-RT-PCR was performed using the following primer pairs: Bcat1 5'-CTTTGGAAGGCTTCTTGACG-3' and 5'-ACAGATCGACCAAGAATGGG-3', Ccnb1 5'-GGCTTGGAGAGGGATTATCA-3' and 5'-ACCAGAGGTGGAACTTGCTG-3', Ccnb2 5'-CAGAGAAAGCTTGGCAGAGG-3' and 5'- TGAAACCAGTGCAGATGGAG-3', Cenpa 5'-TCTGCAGGGTCTTGATTTCC-3' and 5'- AGACCCCAAGGAGGAGACC-3', Cenpe 5'-CCTGAAGCACTTTTCTCGAAG-3' and 5'- GGACAACCTGAGAGAAGCCA-3', Lpxn 5'-

TTTGGCTCTTGGACCTCACT-3' and 5'- AAAGACCTTGTCATCGCAGG, Foxm1 5'-CAGACACAGAGTCCTGCCAA-3' and 5'- AGATGAGTTCTGACGGGCTG-3', Marcksl1 5'- GCTTCTCACGTGGCCATT-3' and 5'- GGCAGCCAGAGCTCTAAGG-3', and Melk 5'- CCAGGCGAGTTGTAGTCACA-3' and 5'- GTTCTCACTGCGCTCACAAG-3'. Primers used for Q-RT-PCR of candidate marker genes were selected from the qPrimerDepot database [81]. PCR was performed with POWER SYBR green PCR Master Mix (Applied Biosystems) and the following cycling parameters: 10 mins at 95^{o}C, Forty cycles of 30 secs at 95^{o}C, 15 secs at 58^{o}C, and 30 secs at 72^{o}C on the IQ5 Multicolor Real-Time PCR Detection System (Biorad). Samples were normalized to 18s ribosomal RNA. Relative fold expression was determined to the lowest expressing sample and differential expression was tested using a two-tailed student's T-test.

Histology and Immunohistochemistry and Image Analysis

All human samples were obtained from tissue repositories at Duke and MD Anderson. These samples were used in accordance with Duke and MD Anderson Cancer Center Institutional Review Board (IRB) approved protocols under a waiver of consent. Five micron thick sections were cut from formalin fixed paraffin embedded samples. Samples were subjected to standard hematoyxlin and eosin staining or immunohistochemistry. Immunohistochemistry was performed with the following antibodies: phospho-ERK (Invitrogen 29-2389) and FOXM1 (Abcam ab47808), using the Vectastain ABC Rabbit IgG kit with Vectastain Elite ABC Reagent (Vector Labs).

Brightfield images of slides taken at 40x were used for analysis using Image Pro AMS v6.1. The counting module was trained using both positive and negative nuclear staining for phospho-ERK. A minimum of 3000 nuclei were counted per sample and the ratio between positive and total nuclei was determined using a minimal and maximal area of 100 and 1000 pixels respectively.

Tissue Microarrays

Tissue Microarrays (TMAs) were generated at MD Anderson Cancer Center and contained a clinically annotated set of 214 soft tissue sarcoma samples including: 166 UPS/Unclassified sarcomas, 19 synovial sarcomas, 6 leiomyosarcomas, 8 pleomorphic liposarcomas, 8 myxoid liposarcomas, 6 atypical lipomatous tumors, and 1 dedifferentiated liposarcoma. TMAs were stained as above and scored semiquantitatively on a scale from 0-3+ by a musculoskeletal pathologist blinded to patient outcome. Scores were correlated with both diagnosis and clinical outcome.

Statistical Analysis of Tissue Microarrays

Scoring of TMAs was correlated with diagnosis, and metastasis-free survival. Correlation of immunohistochemical staining with diagnosis was tested for normality using a chi-square test. This did not reach statistical significance, therefore comparison between UPS and other soft tissue sarcomas was performed using the non-parametric Mann-Whitney test.

Metastasis free survival analysis was performed on UPS samples comparing 3+ staining to 0-2+ staining. Survival was determined by Kaplan-Meier analysis.

2.2 Intraoperative Detection and Removal of Microscopic Residual Sarcoma Using Wide-Field Imaging

Microarray Analysis of Cathepsin Expression

Microarray data was downloaded from GEO (GSE16779) and normalized as described above. The mean expression between tumor and normal muscle of cathepsin proteases was identified using the statistical package BRB-arraytools (http://linus.nci.nih.gov/BRB-ArrayTools.html).

Mice and Sarcoma Generation

All mouse work was performed in accordance with Duke University Institutional Animal Care and Use Committee approved protocols. Mouse genotypes used to generate sarcomas include *LSL-Kras*$^{G12D/+}$;*p53*$^{Flox/Flox}$ [72], *Rosa26*^{YFP};*LSL-Kras*$^{G12D/+}$;*p53*$^{Flox/Flox}$ *[82]*, *Braf*$^{Ca/+}$;*p53*$^{Flox/Flox}$ and *Braf*$^{Ca/Ca}$;*p53*$^{Flox/Flox}$ [83]. The *Rosa26*^{YFP} mice were obtained from Jackson Laboratory. Soft tissue sarcomas were generated by intramuscular injection of an adenovirus expressing Cre recombinase as described previously.

Imaging Device

Fluorescence excitation illumination is provided by a 300 W Xenon lamp (Sunoptics) and is transmitted into the device through an optical fiber bundle (Sunoptics). An achromatic doublet lens (Thorlabs) collimates the fiber bundle light output. Input light is reflected 90˚ by a cube-mounted mirror (Thorlabs) towards a band-pass excitation filter (Chroma Technologies) to limit the illumination to a narrow band matching the absorption spectrum of the fluorophore in use. The filtered excitation light is reflected 90˚ towards the specimen by a dichromatic mirror (Chroma Technologies). A lens pair sends collimated illumination into the specimen plane and collects the emission of the excited fluorophores. After passing through the dichromatic mirror, the emission light is filtered by a band-pass optical element (Chroma Technologies). The image is relayed onto a CCD containing over 1.4 million pixels (PixelFly QE; PCO) by an achromatic doublet lens (Thorlabs). The embodiment of the device was built from modular parts from opto-mechanics vendors and several custom-made components. The CCD camera is connected to a desktop computer for image acquisition and display. Data acquisition software was written in LabView (National Instruments). Image analysis was performed using MatLAB (Mathworks) and ImageJ (National Institute of Health).

Device Characterization

Because the level of fluorescence intensity can vary in different tumor samples, the exposure time of the camera may need to be adjusted. To compare two raw images with different exposure times, I adopted an approach described previously [84, 85] where raw pixel counts from each image are normalized by their exposure time to obtain a time-independent parameter with units of pixel counts per second.

To calibrate for intensity levels, 6-µm fluorescent beads with varying fluorescence emission (Invitrogen) were imaged in a flow channel using the device. The nominal fluorescence ranged from 0.4% to 100% (normalized by the brightest beads). Data obtained from microspheres with nominal relative fluorescence of 0.08% or lower were not reported as background noise interfered with the fluorescence signal. The fluorescence emission of fifteen microspheres was measured for each nominal relative fluorescence. The average and standard deviation of the fluorescence emission from the microspheres in a given image was calculated and plotted against the manufacturer's nominal relative intensity, showing a CCD linear response for ~100-fold change in intensity. Because of the linear response of the device to both exposure time and sample intensity, images of different samples can be compared in a straightforward fashion.

The spatial resolution of the device was determined by imaging a US Air Force 1951 standard calibration target. The highest and minimum intensities (I_{max} and $I_{min,}$ respectively) of two consecutive lines for several cycles/mm groups were determined by image analysis with ImageJ. The modulus of the contrast transfer function (CTF) was determined as follows:

$$CTF(f) = \frac{I_{max}(f) - I_{min}(f)}{I_{max}(f) + I_{min}(f)}$$

where f is the spatial frequency in line cycles/mm. Using the Rayleigh resolution criterion, the spatial frequency resolution limit of an optical system is found at the frequency f_{res} where $CTF(f = f_{res})$ = 26.4%. Curve-fitting the data to the CTF function resulted in a horizontal and vertical f_{res} of 62.8 and 63.0 cycles/mm, respectively. Thus, the estimated transverse horizontal and vertical resolutions are approximately 16 μm in both axes.

Quantifying Tumor-to-muscle Signal Fluorescence Intensity Ratio

Mice with primary soft tissue sarcomas were injected with 2 nmol of Prosense 680, Prosense 750, MMPSense 680, Non-Cleavable Prosense 680 Control, Cat K 680 FAST, or VM249 (all from Perkin Elmer/Visen Medical) via the tail vein. Twenty-four hours after injection for Noncleavable Prosense 680 Control, Prosense 680, Prosense 750, MMPsense 680 or 6 hours after Cat K 680 FAST or VM249, sections of the surface, middle and deep portions of the tumor were surgically removed and imaged with the device. The spectral filters used were: 665 ± 20 nm band-pass excitation filter, 680 nm long-pass dichroic and 710 ± 12 nm band-pass emission filter for all imaging agents except Prosense 750 which utilized a 710 ± 32 nm band-pass excitation filter, 750 nm long-pass dichroic, and 810 ± 45 nm band-pass emission filter (all filters from Chroma Technologies). Several samples of muscle or nerve tissue were also resected and imaged with the device. The pixel values of the images were normalized by the corresponding image exposure time. Using ImageJ, the normalized intensity was measured over the region of the image containing tumor, muscle, or nerve, and their ratio was taken to obtain the tumor-to-muscle or nerve-to-muscle signal ratio.

Reproduction of Intraoperative Images for Display

For display purposes, the contrast and brightness of images was adjusted so that the reader can appreciate the differences in fluorescence intensities between tumor and normal tissue. The intensity histogram of the excised tumor image was computed and the brightness and contrast were set according to the maximum and minimum intensities of the tumor histogram. For the same mouse, the contrast and brightness settings from the tumor image were applied to all images from the same mouse.

Flow Cytometry

Rosa26$^{YFP/YFP}$*; LSL-Kras; p53*$^{Flox/Flox}$ mice with YFP-expressing sarcomas were injected with 2 nmols of Prosense 680. Cells from sarcomas were sorted by flow cytometry after the tumor was homogenized with trypsin, collagenase IV, dispase (all from Invitrogen) and passed through a 40 μM filter to separate the tumor aggregate into individual cells and stained with anti-CD11b-PE antibody (ebiosciences). Cells were sorted for YFP using flow cytometry (FACSVantage; Becton Dickinson) and single cell suspensions were stored in phosphate buffered saline (PBS) on ice. Colony initiating efficiency was determined by plating 600 sorted cells into complete media (DMEM+10% FBS).

Tumor Reconstitution

50,000 freshly sorted cells were injected intramuscularly into immunocompromised nude mice to generate sarcomas. Tumors were measured and volume calculated using the following formula: Volume = $(\pi*D_1*D_2*D_3)/6$. The percentage of YFP+ cells in transplanted tumors was determined by flow cytometry as described above.

Fluorescence Intensity Threshold Setting and Intraoperative Tumor Bed Imaging

Twenty-four hours prior to surgery, mice (n=14) with primary soft tissue sarcomas were injected with 2 nmol of Prosense 680 (Visen Medical) via tail vein injection. After induction with isoflurane anesthesia and analgesic treatment, the grossly apparent soft tissue sarcoma was surgically removed. The resected tumor and the exposed tumor bed were imaged with the device and the pixel intensity values were normalized by the exposure time to obtain a time-independent fluorescence emission rate. After imaging, the surgeon biopsied the tumor bed. Hematoxylin and eosin stained sections of the primary tumor and biopsy of the tumor bed were analyzed by a veterinary pathologist blinded to the results from imaging to determine whether the biopsy of the tumor bed contained soft tissue sarcoma cells. Images of the tumor and tumor bed were also analyzed post-surgery using ImageJ. After surgery, wounds were closed and mice were observed for several months for local recurrence. The fluorescence emission rate range of the tumor and the tumor bed image were compared and correlated with the pathological results from the tumor bed biopsies. All tumor beds with residual cancer cells on biopsy had residual fluorescence from Prosense 680 in the tumor bed of 80% or higher than the minimum intensity range of the tumor fluorescence. Thus, I set the positive/negative residual fluorescence threshold in the tumor bed at an intensity level of 80% of the minimum fluorescence emission rate of the tumor for subsequent intraoperative imaging experiments.

Imaging of Yellow Fluorescent Protein in the Tumor Bed of Mice

Rosa26$^{YFP/YFP}$; LSL-Kras; p53$^{Flox/Flox}$ mice with YFP-expressing sarcomas were injected with 2 nmols of Prosense 680, Cat K 680 FAST, or VM249 (Perkin Elmer). Tumors were removed at 6 hour (VM 249 and Cat K 680 FAST) or 24 hours (Prosense 680). The resected tumor was imaged with the device and an automatic software routine calibrated the threshold intensity level normalized by the exposure time for each mouse at a pixel-by-pixel basis. Then, subsequent imaging of the tumor bed was classified as either “positive” or “negative” residual NIR fluorescence based on the threshold calibration and the tumor bed was subsequently imaged with the novel imaging device with filters for YFP.

Detection of Microscopic Residual Sarcoma and Intraoperative Image Guided Surgery

Prior to surgery, mice with primary soft tissue sarcomas were injected intravenously with 2 nmol of Cat K 680 FAST or VM249. After induction with isoflurane anesthesia and analgesic treatment, the grossly apparent soft tissue sarcoma was surgically removed. The resected tumor was imaged with the device and an automatic software routine calibrated the threshold intensity level normalized by the exposure time for each mouse at a pixel-by-pixel basis. Then, all subsequent imaging of this animal was classified as either “positive” or “negative” NIR residual fluorescence based on the threshold calibration. For sarcomas expressing YFP, tumors were also imaged using filters for YFP. Images obtained at the time of surgery were also analyzed after surgery to ensure correct intraoperative diagnosis using ImageJ based on the same threshold setting. The intraoperative classification of residual fluorescence was based solely on the raw pixel counts normalized to exposure time. After surgery and intraoperative imaging of the tumor beds, the wound was closed and mice were observed for several months for local recurrence. Intraoperative imaging and tumor bed assessment took approximately 1-2 minutes to complete. For image guided surgery, the same imaging routine was applied and tissue was resected until tumor beds were cleared of residual NIR fluorescence. Significance of local control according to intraoperative diagnosis was determined by Kaplan-Meier analysis.

2.3 Genotype Dependent Control of miRNA Biogenesis and Metastasis is Mediated Through MAPK Dependent Regulation of Dgcr8

MEK Inhibition and Activation

KP sarcoma cell lines were grown in DMEM (Gibco) in 1% FBS and treated with 20μM PD98059 (Cell Signaling) unless otherwise noted. Media and drugs were replenished at 24 hours. Cells were harvested in RIPA buffer supplemented with protease and phosphatase inhibitors (all Sigma). *In vivo* tumors were generated from *Kras*$^{G12D/+}$*; Ink4a/Arf*$^{Flox/Flox}$ cell lines in nude mice.

Mice with allografts were treated with 5mg/kg of PD325901 daily for 7-8 days. Tumors were harvested and flash frozen in liquid nitrogen prior to dissociation by grinding in liquid nitrogen for downstream assays.

For Mek activation, Phi-NX cells were transfected with pBABE-Puro [86] or pBabe-Puro-MEK-DD [87] using Lipofectamine 2000 (Invitrogen). Virus was harvested after 48 hours and sarcoma cells from *KP* mice were infected in the presence of polybrene. Cells were then selected in DMEM supplemented with 10% FBS and puromycin for 7 days. Cells were grown in DMEM supplemented with 1% FBS for 48 hours prior to harvesting.

Western Blotting

Western blots were performed using the following antibodies: Anti-Dgcr8 (Cell Signaling, 6914), Drosha (Cell Signaling, 3364), Erk1/2 (Cell Signaling, 4695), Phospho-Erk1/2 (Cell Signaling, 4370), Trbp (Abcam, ab42018), Dicer (Cell Signaling, 5362), Rreb1 (Sigma, HPA001756), Gapdh (Sigma, G9545) and Actin (BD, 612656).

Dgcr8 Promoter Analysis

The Dgcr8 promoter was cloned from normal mouse tail DNA into pGL3-basic (Promega). Site directed mutagenesis was performed on the pGL3 clone containing -518 to -100 upstream of Dgcr8. Soft tissue sarcoma cell lines were cotransfected with pGL3 clones and pRL-CMV Renilla control vector (Promega) using Lipofectamine 2000 (Invitrogen). Luciferase activity was assessed 24 hours later using the Dual-Glo Luciferase Assay System (Promega). Firefly luciferase signal was normalized to Renilla signal and reported relative to vector or wild type control. The Dgcr8 Promoter was cloned with the following primers: Forward -1032: 5' - CCA CTT TTC ATG TCC AGC AG - 3'; Forward -518: 5' – CTC CTT TCC TAT CCT CCG CA - 3'; Forward -260: 5'-GAG CGA CAG CCG TTA GAA GT - 3' and Reverse: -100: 5'-CAA TCA CGG CGC ACG GCC TC - 3'. Site directed mutagenesis was performed by mutating the putative Rreb1 binding site in the -518 to -100 reporter construct. Mutations were introduced by PCR and verified by direct sequencing.

Rreb1 Chromatin Immunoprecipitation

Soft tissue sarcoma cell lines were harvested at 90% confluence using a Agarose ChIP kit (Pierce), per manufacturer's suggestions using an anti-Rreb1 (Sigma, HPA001756), isotype control, or anti-RNA Polymerase II antibody. PCR for Rreb1 binding at the Dgcr8 promoter was performed with REDTaq (Sigma) and the following primers: Dgcr8-Rreb1-Fwd: 5'- ATC GGC TCT GCT TCT CCT TC-3', Dgcr8-Rreb1-Rev: 5'-GAT GCG GAG GAT AGG AAA GG-3', Dgcr8-Ctrl-Fwd: 5'-TTT GTC CTC TGC AGT GGT CCT TG-3', and Dgcr8-Ctrl-Rev: 5'-AAA GGT GTT CCC ATC AAA GGT GC-3'

RREB1 Overexpression and Knockdown

pCMV-SPORT6.1-FLAG-Rreb1 [88] was transfected into HEK293T cells using Lipofectamine 2000. Cells were harvested at 36 hours for western blot analysis. pLKO.1-TRC control [89] (Addgene plasmid 10879) or Rreb1 shRNA vectors [88] were transfected into HEK293T cells with psPAX2 and pMD2.G (Addgene plasmid 12260 and 12259, respectively) using lipofectamine 2000. Virus was harvested at 48 hours and *KP* sarcoma cells were infected in the presence of polybrene. Infected cells were subjected to puromycin selection for seven days prior to western blot analysis.

Q-RT-PCR

Cells or tumors were harvested and RNA isolated and reverse transcribed as described above. Q-RT-PCR using Sybr green was performed using the iQ Sybr Green Supermix (Biorad) using the delta-delta-CT method. The following primers were used for Q-RT-PCR: Dgcr8-Fwd: 5' – AGG TCT CTG TGC TCC CAA GAA G – 3', Dgcr8-Rev: 5' – TGG TCA TCA TTG GCT GTA CAC TT – 3', Rreb1-Fwd: 5' – CCA CTT CTG GAG CAC AGG AT – 3', Rreb1-Rev: 5' - CAT CTC TCC TCG TTC TCT CCC - 3', 18S-Fwd: 5' - GAG GCC CTG TAA TTG GAA TGA G - 3', and 18S-Rev: 5' - GCA GCA ACT TTA ATA TAC GCT ATT GG - 3'.

Human *RREB1* and *DGCR8* Correlation

Gene expression data sets were imported from GEO using BRB Array tools [90]. A $\log_2$ transformation was applied to the data, and arrays normalized to the expression of the median array from the following datasets: GDS2201 [91], GDS3312 [92], GDS3262 [93], GDS1064 [94], GDS2947 [95], and GDS1479

[96]. Log_2 intensity values were exported for Dgcr8 (probes 218650_at, 219811_at, 64474_g_at, and 91617_at). The mean expression value of Dgcr8 was compared to the log_2 expression value of Rreb1 (probe 203704_s_at) for correlation and line fit.

Primary-miRNA and Mature miRNA Expression

Cells or tumors were harvested with Trizol reagent, per manufacturer's suggestion. Reverse transcription for pri-miRNA transcripts was performed using iScript cDNA synthesis kit (Biorad) with 300ng of total RNA. Reverse transcription for specific mature miRNAs was performed using the Taqman microRNAs Reverse Transcription kit (Applied Biosystems). Q-PCR was carried out with Taqman probes for their respective targets (Applied Biosystems), pri-miRNA and mature miRNA expression were normalized to 18S and SnoRNA202 expression, respectively using the delta-delta-CT method.

Taqman PCR Arrays for miRNA Expression

Reverse transcription was performed using 1 microgram of total RNA using the Taqman Human or Rodent microRNAs A card v2.0 (Applied Biosystems). Samples were normalized to RNU44 (human) or SnoRNA202 (mouse) expression. Samples were compared in the delta-delta-CT method. Row normalized heatmaps were made using differentially expressed miRNAs based on two-tailed T-test ($p<0.05$) between either sarcomas from: *KP* or *BP* sarcomas, *Dicer-KP* mice or *BP, KP* and *Dicer-BP*, and primary human

Undifferentiated Pleomorphic Sarcomas that subsequently did or did not give rise to distant metastases.

Generation of Soft Tissue Sarcomas

Primary soft tissue sarcomas were generated using the following previously described alleles: *LSL-Kras*^{G12D} [97]; *p53*^{Flox}[98], *Braf*^{Ca} [83], and *Dicer*^{Flox}[99]. Tumors were initiated by injection of an Adenovirus expressing Cre-recombinase as described previously [72]. Rearrangement of *Dicer1* was confirmed using DNA from primary sarcomas as described previously [99].

Histology and Immunohistochemistry

Five micron thick tissue sections from formalin fixed paraffin embedded tissue were subjected to standard hematoxylin and eosin staining. Immunohistochemistry was performed with the following antibodies: pERK1/2 (Cell Signaling), pS6 (Cell Signaling, 9234), Dgcr8 (Sigma), Ki67 (BD Pharmagen) using the Vectastain Elite ABC Reagent (Vector labs). Ki67 staining was quantified as described above.

3. Cross Species Genomic Comparison of Murine Soft Tissue Sarcomas

3.1- Summary

UPS, formally known as Malignant Fibrous Histiocytoma, is one of the most common subtypes of human soft tissue sarcoma. Using cross species genomic analysis, I define a geneset from the *LSL-Kras*^{G12D}*; p53*$^{Flox/Flox}$ mouse model of soft tissue sarcoma that is highly enriched in human UPS. With this mouse geneset as a filter, I identify expression of the RAS target FOXM1 in human UPS. Expression of *Foxm1* is elevated in mouse sarcomas that metastasize to the lung and tissue microarray analysis of human UPS correlates overexpression of FOXM1 with metastasis. These results suggest that genomic alterations present in human UPS are conserved in the *LSL-Kras*^{G12D}*; p53*$^{Flox/Flox}$ mouse model of soft tissue sarcoma and demonstrate the utility of this pre-clinical model.

This work was performed in collaboration with: R. Riedel (oncogenic pathway analysis), L. Dodd (scoring immunohistochemistry), G. Lahat (scoring immunohistochemistry), A. Lazar (scoring immunohistochemistry), R. Dodd (molecular bioglogy), L. Stangenberg (mouse surgeries), W. Eward (mouse surgeries), F. Hornicek (mouse surgeries), B. Brigman (mouse surgeries), and S. Mukherjee (assistance with statistical analysis).

3.2 – Introduction

Malignant Fibrous Histiocytoma was first described in the 1960s and quickly became the most commonly diagnosed adult soft tissue sarcoma [32]. Because these tumors do not appear to arise from histiocytes, the term Malignant Fibrous Histiocytoma has recently fallen out of favor and many pathologists now classify these tumors as UPS. Despite this change in nomenclature, UPS remains one of the most common adult soft tissue sarcomas encountered in the clinic. However, the cell(s) of origin of UPS is unknown. Indeed, some have suggested that UPS is a collection of undifferentiated mesenchymal tumors sharing a common morphology rather than a single clinical entity [33, 100, 101] and recent animal work has suggested a variety of cell types can give rise to UPS [69]. This debate could be clarified by identifying the cell(s) of origin of a mouse model for UPS. Whether UPS describes a cancer that is a single pathogenic entity or an undifferentiated state shared by several sarcoma subtypes, the survival of patients with UPS has not improved for decades. Therefore, identifying a mouse model of UPS may also lead to better treatments for patients with this diagnosis.

Human UPS is characterized by a propensity to metastasize to the lungs and by a range of histologic appearances including spindle and pleomorphic cells. Although these features are recapitulated in a mouse model of soft tissue sarcoma initiated by conditional mutations in *Kras* and *p53* [72], it is not clear whether this model is most similar to human UPS or another soft tissue sarcoma.

Therefore, I sought to more accurately classify the sarcoma subtype for this mouse model using gene expression profiling.

3.3 - Results

Cross-Species Genomic Analysis of the *KP* mouse model of soft tissue sarcoma

I hypothesized that genes most differentially expressed between mouse sarcoma and normal muscle would provide a useful molecular signature to interrogate human sarcoma datasets (Figure 2).

Figure 2: Schematic for Cross Species Genomic Comparison Using Geneset Enrichment Analysis

Figure 2: Schematic for cross species genomic comparison using Geneset Enrichment Analysis. Genes highly expressed in sarcomas from *KP* mice were identified by signal-to-noise metric. This geneset was then inserted into a relevant geneset database and used for Geneset Enrichment Analysis using human soft tissue sarcoma datasets.

To test this approach, I first analyzed published gene expression data from a previously validated mouse model of synovial sarcoma [66]. After identifying a geneset of 100 genes highly overexpressed in synovial sarcoma compared to normal muscle (Appendix A), I used Gene Set Enrichment Analysis (GSEA) [78] to probe gene expression data from three studies of human soft tissue sarcomas [75-77]. There was strong statistical enrichment ($p<0.001$, False Discover Rate [FDR] <0.02) of this geneset in human synovial sarcomas, but not in other subtypes of soft tissue sarcoma (Figure 3A, Table 1). This result is in agreement with GSEA for the mouse model of synovial sarcoma that was previously reported [66].

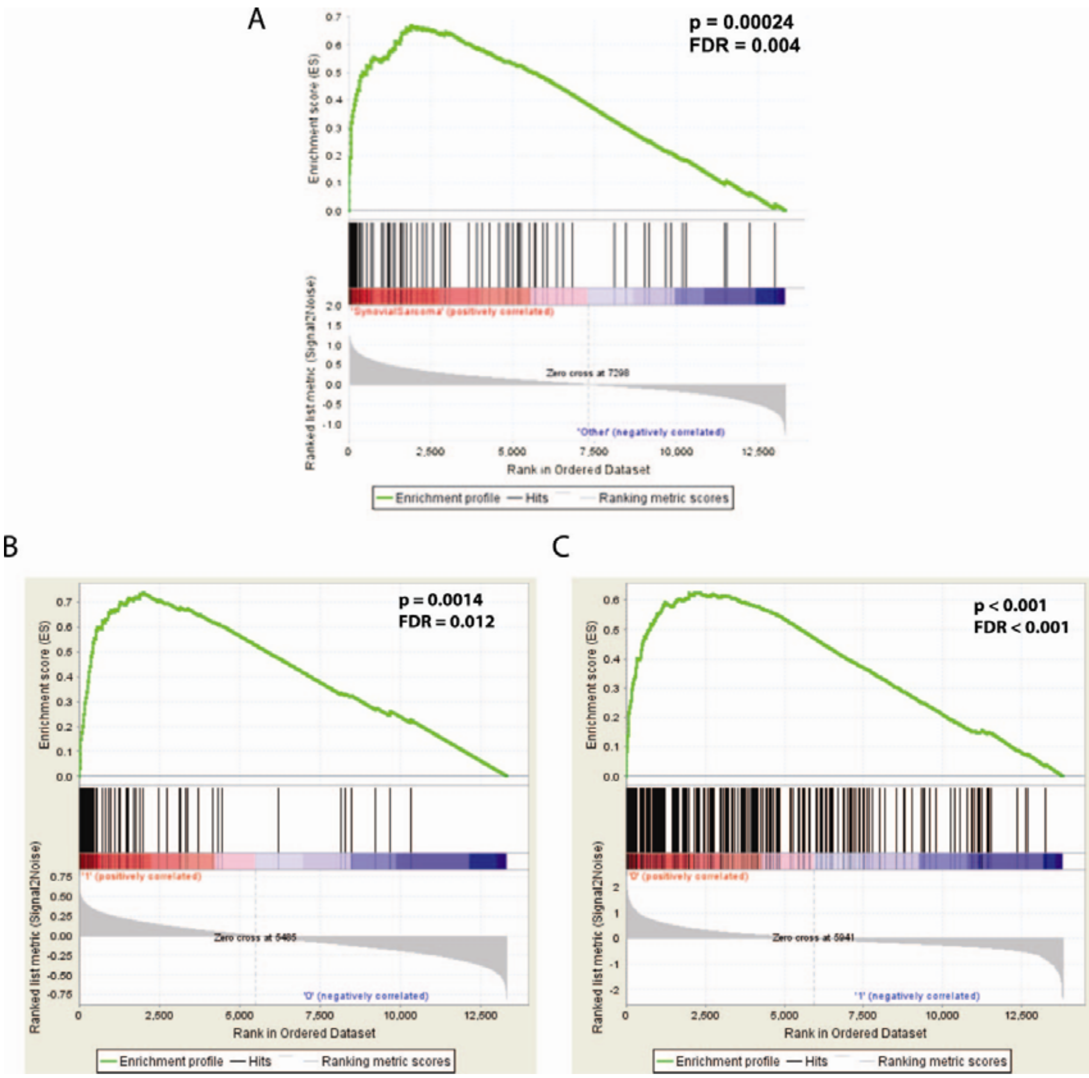

Figure 3: Geneset Enrichment Analysis of Mouse Models of Soft Tissue Sarcoma

Figure 3: Geneset Enrichment Analysis of mouse models of soft tissue sarcoma. (A) The mouse synovial sarcoma geneset (Appendix A) shows strong enrichment for human synovial sarcoma (Enrichment Score [ES] = 0.67, Normalized ES [NES] = 2.21) in a human soft tissue sarcoma dataset (p <0.0005; FDR < 0.01). **(B)** The geneset from sarcoma (Appendix B) in *KP* mice are highly enriched in human UPS (ES = 0.74, NES = 2.09, p = 0.0014, FDR = 0.012). **(C)** Conversely, a human UPS geneset (Appendix C) is strongly enriched in sarcomas from *KP* mice (p<0.001, FDR<0.001, ES=0.637, NES = 2.78).

Table 1: The Mouse Synovial Sarcoma Geneset Enriches for Human Synovial Sarcoma

Table 1: The mouse synovial sarcoma geneset enriches for human synovial sarcoma. The murine synovial sarcoma geneset (Appendix A) was used to examine three datasets [75-77] containing various subtypes of human soft tissue sarcoma. Only synovial sarcoma showed significant enrichment. Table contains p-values with FDR in parentheses. Bolded results note significance with p < 0.05 and FDR < 0.25. DNE = did not enrich, dash marks represent insufficient data points to do comparison

Tumor Type	Nakayama	Detwiller	Baird
UPS	DNE	DNE	DNE
Myxofibrosarcoma	DNE	-	-
Fibrosarcoma	DNE	-	-
Leiomyosarcoma	DNE	DNE	0.655 (0.806)
Synovial Sarcoma	**0.00024 (0.004)**	0.003 (0.371)	0.008 (0.471)
Myxoid Liposarcoma	DNE	-	-
Dedifferentiated Liposarcoma	DNE	-	-
Rhabdomyosarcoma	-	-	0.453 (0.684)
Ewing's Sarcoma	-	-	0.630 (0.921)

Having validated this approach, I identified a geneset of 100 genes highly overexpressed in sarcomas generated in *KP* mice (n=17) compared to normal muscle (n=4) (Appendix B). When this geneset was analyzed in the three human datasets of soft tissue sarcoma [75-77], only UPS samples showed statistical enrichment (p = 0.001; FDR = 0.012) (Table 2, Figure 3B). Enrichment was seen in all three datasets, which represent 325 sarcoma samples and two types of array platforms. Moreover, genesets derived from human UPS (Appendix C) also enriched in the mouse sarcoma data (p < 0.001; FDR < 0.001) (Figure 3C). These data indicate that this mouse sarcoma model and human UPS share common genomic features.

Table 2: Geneset Enrichment Analysis Results for the *KP* Sarcoma Geneset

Table 2: Geneset Enrichment Analysis results for the *KP* sarcoma geneset. The KP sarcoma geneset (Appendix B) was used to examine three human soft tissue sarcoma datasets [75-77]. Only UPS demonstrated statically significant enrichment across all three datasets. Table contains p-values with FDR in parentheses. Bolded results note significance with p < 0.05 and FDR < 0.25. DNE = did not enrich, dash marks represent insufficient data points to do comparison

Tumor Type	Nakayama	Detwiller	Baird
UPS	**0.001 (0.012)**	**0.014 (0.149)**	**0.024 (0.190)**
Myxofibrosarcoma	0.162 (0.559)	-	-
Fibrosarcoma	0.177 (0.326)	0.159 (0.784)	DNE
Leiomyosarcoma	0.262 (0.673)	0.854 (0.981)	0.401 (0.715)
Synovial Sarcoma	DNE	DNE	DNE
Myxoid Liposarcoma	DNE	-	-
Dedifferentiated Liposarcoma	DNE	-	-
Rhabdomyosarcoma	-	-	0.586 (0.781)
Ewing's Sarcoma	-	-	DNE

Ras Pathway Activity is Enriched in Human UPS

The initiating events of human UPS are not well understood. Previous studies have shown mutations in p53 occur in 36% of human UPS [102] while the rate of canonical *RAS* mutations in human UPS varies from 0-50% [103, 104]. I hypothesized that the RAS pathway may be activated in human UPS even in the absence of canonical RAS mutations. To explore a link between UPS and Ras, I utilized previously described oncogenic pathway predictors that correlate with *RAS* activity [80]. The Ras oncogenic signature is enriched in human UPS samples compared to a panel of other soft tissue sarcomas (p = 0.002) (Figure 4).

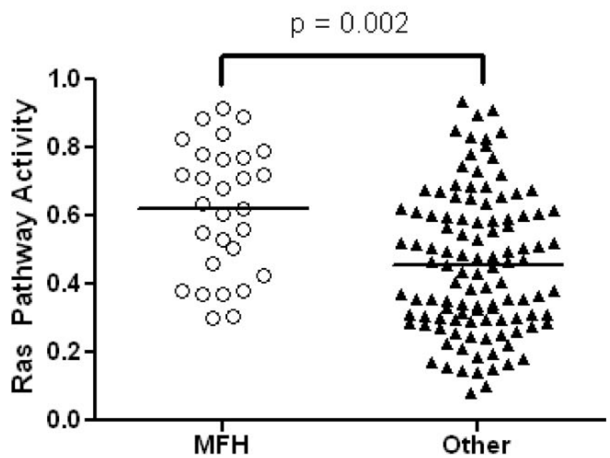

Figure 4: An Oncogenic Ras Signature is Enriched in Human UPS

Figure 4: An oncogenic Ras signature is enriched in human UPS. An oncogenic Ras signature is enriched in human UPS samples compared to other types of soft tissue sarcoma (p = 0.002, non-parametric Mann-Whitney Test)

FoxM1 is a Novel Marker of Metastasis in UPS

Because human UPS and sarcomas generated in *KP* mice share common genomic features, I wanted to determine if these shared features could be used to identify diagnostic or prognostic factors for human UPS. As UPS is considered a diagnosis of exclusion, I initially attempted to identify a marker that is specific to UPS. I identified a panel of 10 candidate biomarkers based on their common upregulation in both human UPS and sarcomas from *KP* mice (Table 3). Expression of 9 of these candidates was validated in an independent cohort of mouse sarcomas by Q-RT-PCR (Figure 5).

Table 3: Candidate Marker Genes for Human UPS

Table 3: Candidate marker genes for human UPS. Candidate marker genes of human UPS were identified using differentially expressed genes between human UPS and other sarcomas (T-test, $p<0.001$). This list of genes was then cross referenced against the soft tissue sarcoma geneset generated from *KP* mice (Appendix B) and ten overlapping genes were identified.

Candidate Markers
BCAT1
CCNB1
CCNB2
CENPA
CENPE
FCGR1
FOXM1
LPXN
MARCKSL1
MELK

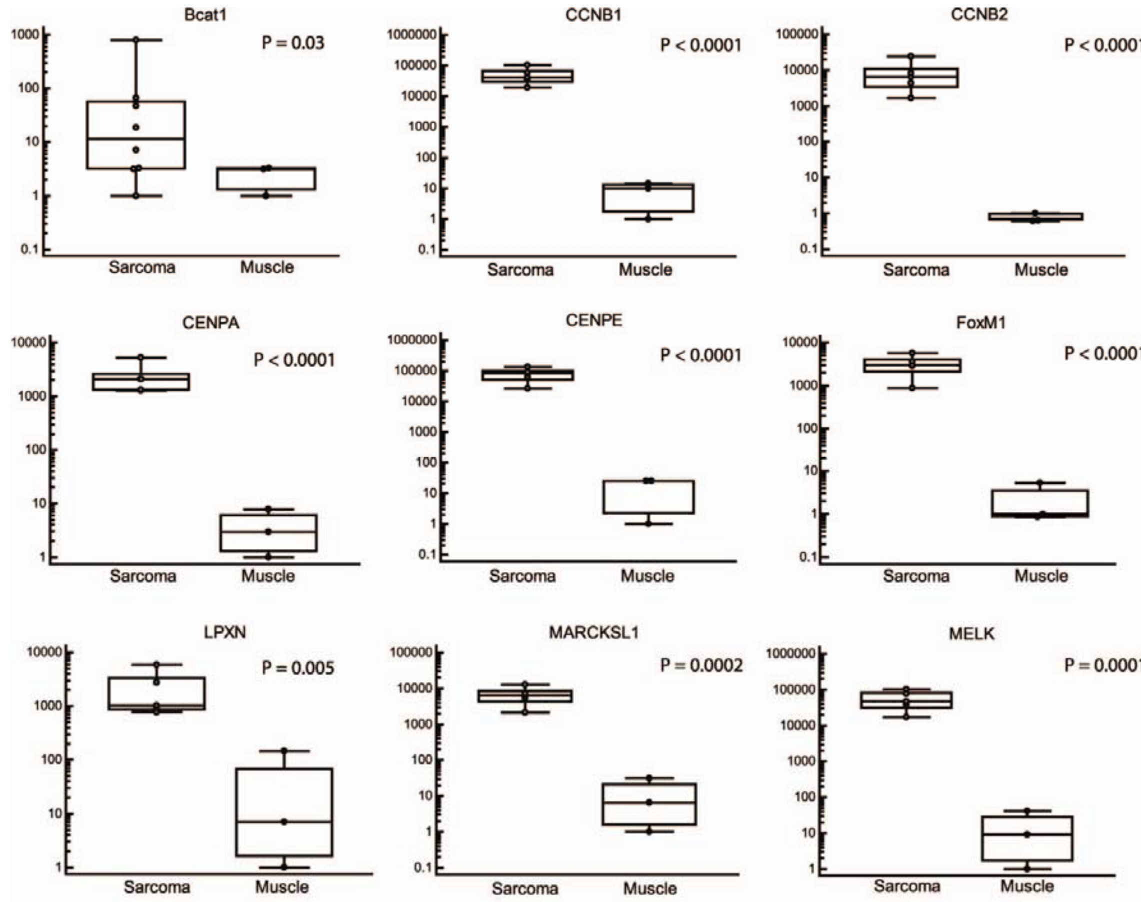

Figure 5: Realtime PCR for Candidate Markers of Human UPS

Figure 5: Realtime PCR for candidate markers of human UPS. Box and whisker plots of nine candidate genes selected for Q-RT-PCR using an independent set of mouse soft tissue sarcomas (n = 5) and normal muscle samples (n = 3). Relative fold expression determined to lowest expressing normal muscle sample. Significance of differentially expressed genes was determined by two-tailed student's T-test.

FOXM1, which is a member of the forkhead transcription factor family that enhances tumorigenesis in other solid tumors [105], was selected for further analysis because it is downstream of *Ras* [106]. I next analyzed the expression of FOXM1 in a clinically annotated tissue microarray (TMA) containing 166 UPS samples and 48 other soft tissue sarcomas. Although 84% of the UPS samples stained positive for FOXM1 ($p = 0.02$, Figure 6), this marker was also expressed, but to a lesser degree, in other sarcoma subtypes. Therefore, a potentially Ras regulated transcription factor, FOXM1, may not be a useful diagnostic marker for human UPS.

Because FOXM1 has previously been shown to regulate the expression of matrix metalloproteases MMP-2 and -9, which are key mediators of cell invasion [107], I hypothesized that high FOXM1 expression may correlate with metastasis. I measured *FoxM1* gene expression in murine soft tissue sarcomas and found a correlation with the development of lung metastases (Figure 7A, $p = 0.01$). Likewise, human UPS with high FOXM1 expression correlated with decreased metastasis-free survival compared to sarcomas with low to no FOXM1 expression (Figure 7B).

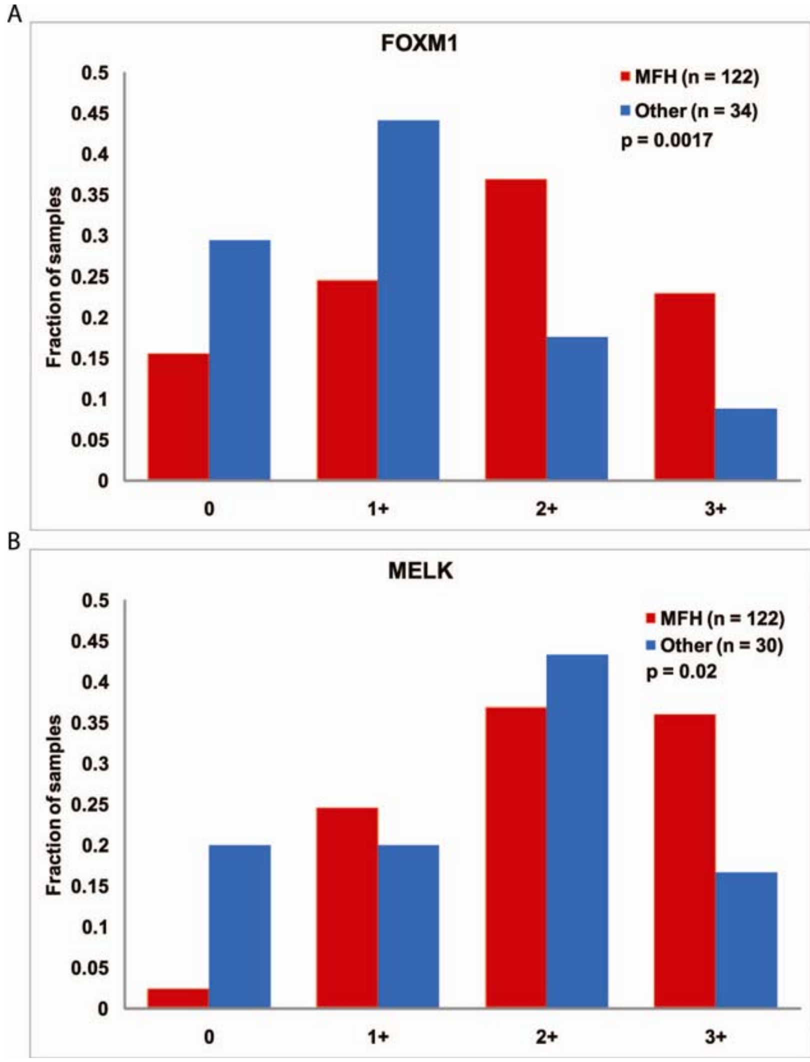

Figure 6: Immunostaining of Tissue Microarrays for FOXM1 and MELK

Figure 6: Immunostaining of tissue microarrays for FOXM1 and MELK. Tissue Microarrays containing 214 soft tissue sarcomas were stained for FOXM1 and scored semi-quantitatively. The degree of staining for **(A)** FOXM1 (p = 0.0017, non-parametric Mann-Whitney test) and **(B)** MELK (p = 0.02, non-parametric Mann-Whitney test) was correlated with UPS.

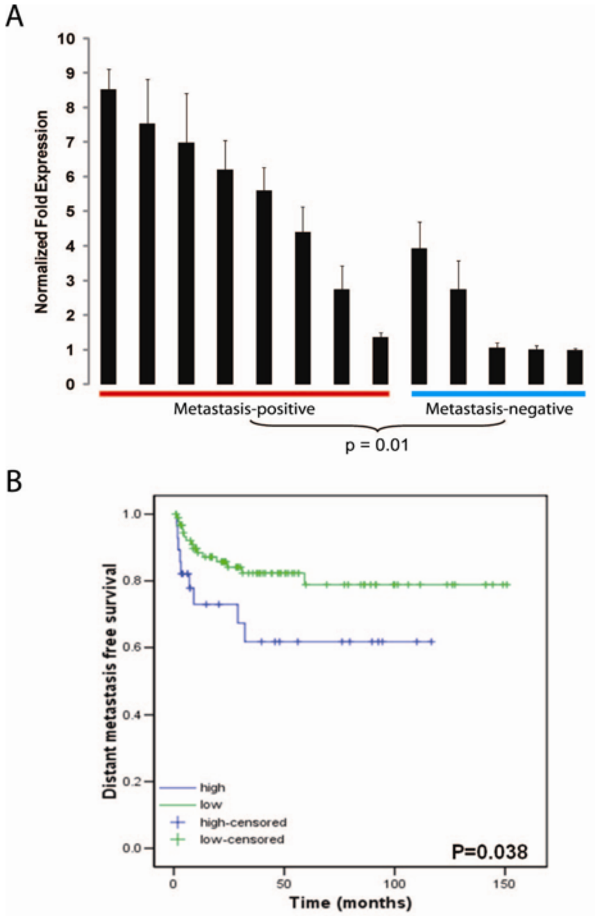

Figure 7: FOXM1 Expression Correlates with Metastatic Progression in Both Mouse and Man.

Figure 7: FOXM1 expression correlates with metastatic progression in both mouse and man. (A) Gene expression of *FoxM1* in sarcomas from *KP* mice, as measured by Q-RT-PCR correlates with metastatic progression in primary tumors (p = 0.01, two-tailed student's T-test, scale bars represent standard deviation from the mean). **(B)** FOXM1 expression in a tissue microarray correlates with metastasis free survival in human UPS (p = 0.038)

3.4 Discussion

I used cross species genomic analysis to determine which human sarcoma subtype is represented by the *KP* mouse model of soft tissue sarcoma. I identified a geneset in the mouse sarcomas that is highly enriched in human UPS. This geneset was not enriched in other human sarcomas, such as fibrosarcoma or leiomyosarcoma, which can be difficult to distinguish from UPS. Furthermore, I have identified enrichment of Ras pathway activity in human UPS compared to other types of soft-tissue sarcoma. Additionally, sarcomas in *KP* mice have a propensity to metastasize to the lungs much like human UPS [72]. Based on this genomic analysis, the pattern of lung metastasis, and the similarity of the mouse sarcomas to human UPS at the histological level, I conclude that this model closely resembles UPS.

I recognize that the diagnosis of UPS has recently been questioned as a distinct clinical entity [33, 100, 101]. My results do not exclude the possibility that UPS is a collection of mesenchymal tumors derived from different cell types that share an undifferentiated state. However, my finding of a sarcoma geneset conserved between mouse sarcomas and human UPS suggests that this subtype of human sarcoma shares an underlying biology beyond a common histologic appearance. Moreover, the use of cross-species analysis to identify FOXM1 as a marker of metastasis-free survival in human UPS supports the use of this mouse model to understand mechanisms of metastasis, to investigate the cell(s) of origin, and to develop novel therapies for human UPS.

4. Intraoperative Detection and Removal of Microscopic Residual Sarcoma Using Wide-Field Imaging.

4.1 Summary

The goal of limb-sparing surgery for a soft tissue sarcoma of the extremity is to remove all malignant cells while preserving limb function. After initial surgery, microscopic residual disease in the tumor bed will cause a local recurrence in approximately one-third of patients with a sarcoma. To help identify these patients, I have collaborated with engineers and MIT to develop a *in vivo* imaging system to investigate the suitability of molecular imaging for intraoperative imaging [108]. Using a primary mouse model of soft tissue sarcoma and a wide field-of-view imaging device, I utilize a series of exogenously administered near-infrared (NIR) fluorescent probes activated by cathepsin proteases for real-time intraoperative imaging and demonstrate that exogenously administered cathepsin-activated probes can be utilized for image-guided surgery to identify microscopic residual NIR fluorescence in the tumor beds of mice. The presence of residual NIR fluorescence correlates with microscopic residual sarcoma and local recurrence. Removal of residual NIR fluorescence improves local control. This technique has the potential to be used for intraoperative image-guided surgery to identify microscopic residual disease in patients with cancer.

This work was performed in collaboration with: J. Ferrer and L. Marshall who helped to design and characterized the imaging device; B. Brigman, W.

Eward, and S. Ramasunder who performed mouse surgeries; C. Lee and R. Dodd who assisted with surgeries and probe validation; and J. Carter who assisted with image analysis.

4.2 Introduction

When surgeons resect a soft tissue sarcoma of the extremity, they attempt to preserve limb function while removing a margin of normal tissue surrounding the tumor so that no malignant cells remain. For soft tissue sarcomas, surgical margin status correlates with local recurrence, development of distant metastases, and disease specific survival [109-111]. The presence of tumor cells at the surgical margin of the resected specimen suggests residual tumor cells may remain in the tumor bed. Margin status of the resected specimen can be evaluated by a pathologist at the time of resection. However, during surgery, time constraints normally limit margin assessment to one or two small areas of the tumor making this analysis prone to sampling error. The remaining excised tissue is fixed in formalin and a more comprehensive assessment of the margin may take days to complete. If tumor cells are identified at the margin, patients may require a repeat surgical resection [112] leading to increased patient morbidity and healthcare costs. Therefore, a method to directly assess the entire tumor bed at the time of surgery has the potential to improve therapy.

Intraoperative margin assessment in cancer patients has been accomplished using radiofrequency spectroscopy [113]. Although initial studies with this technology are encouraging, limitations of this approach include an inability to resolve small clusters of tumor cells and an analysis of excised tissue rather than the surgical bed. An alternative approach for intraoperative tumor bed imaging is microscopy (e.g. confocal). Microscopy in the operative setting requires scanning technology with rigid positioning of the detector relative to the tumor bed to maintain the focal distance. These restrictions can be cumbersome and too time-consuming to scan an entire tumor bed during surgery. More recently, others have proposed using exogenous cancer-labeling NIR imaging agents to guide surgical resection of tumor tissue [114].

I have used optical imaging with epi-illumination during surgery to identify residual cancer with millimeter resolution in mice with primary soft tissue sarcomas [72]. Although this approach has potential drawbacks including limited tissue penetration [115], so that signal deep to the exposed tumor bed may not be detected, I hypothesized that NIR fluorescence with epi-illumination can be utilized to detect microscopic residual disease in a tumor bed after the surgeon removes all grossly apparent sarcoma.

To test this hypothesis, I utilized genetically engineered mice with conditional mutations in *Braf* and *p53* that develop primary sarcomas. In contrast to xenograft models, this primary model has an intact immune system that more closely resembles the tumor microenvironment in human patients. Furthermore, these tumors frequently have poorly defined pseudocapsules and are highly invasive into the adjacent normal muscle [72]. After intravenous injection of NIR fluorescent probes, I performed surgery guided by intraoperative imaging using a wide field-of-view imaging device that can resolve microscopic clusters of tumor cells. Here, I tested the ability of optical imaging with epi-illumination to detect microscopic residual sarcoma during surgery.

4.3 Results

Imaging Device Design and Characterization

To detect microscopic residual cancer, I have collaborated with engineers to develope a wide field-of-view imaging device for direct assessment of a tumor bed at the time of surgery. A schematic of the device's optical layout and the prototype are depicted in Figure 8A-B. The device employs white light for illumination and a set of spectral filters appropriate for the fluorescent imaging agent used. Lenses are used to relay the fluorescence image at no magnification into a charge-coupled device (CCD). By maintaining a 1:1 ratio of the sample with its image, the fluorescence emission of small numbers of cells are mapped onto multiple pixels, which improves sensitivity and signal-to-noise ratio of weak signals. The CCD response to exposure time and intensity was calibrated with methods described previously [84, 85] and found to be linear (Figure 8C-D). The imaging system has a spatial resolution of approximately 16 μm determined using a US Air Force 1951 calibration standard (Figure 8E-F) and a relatively large field of view (9.0 mm x 6.6 mm). Thus, the user can scan a mouse tumor bed of 2 cm x 2 cm in a relatively short time (~1 minute).

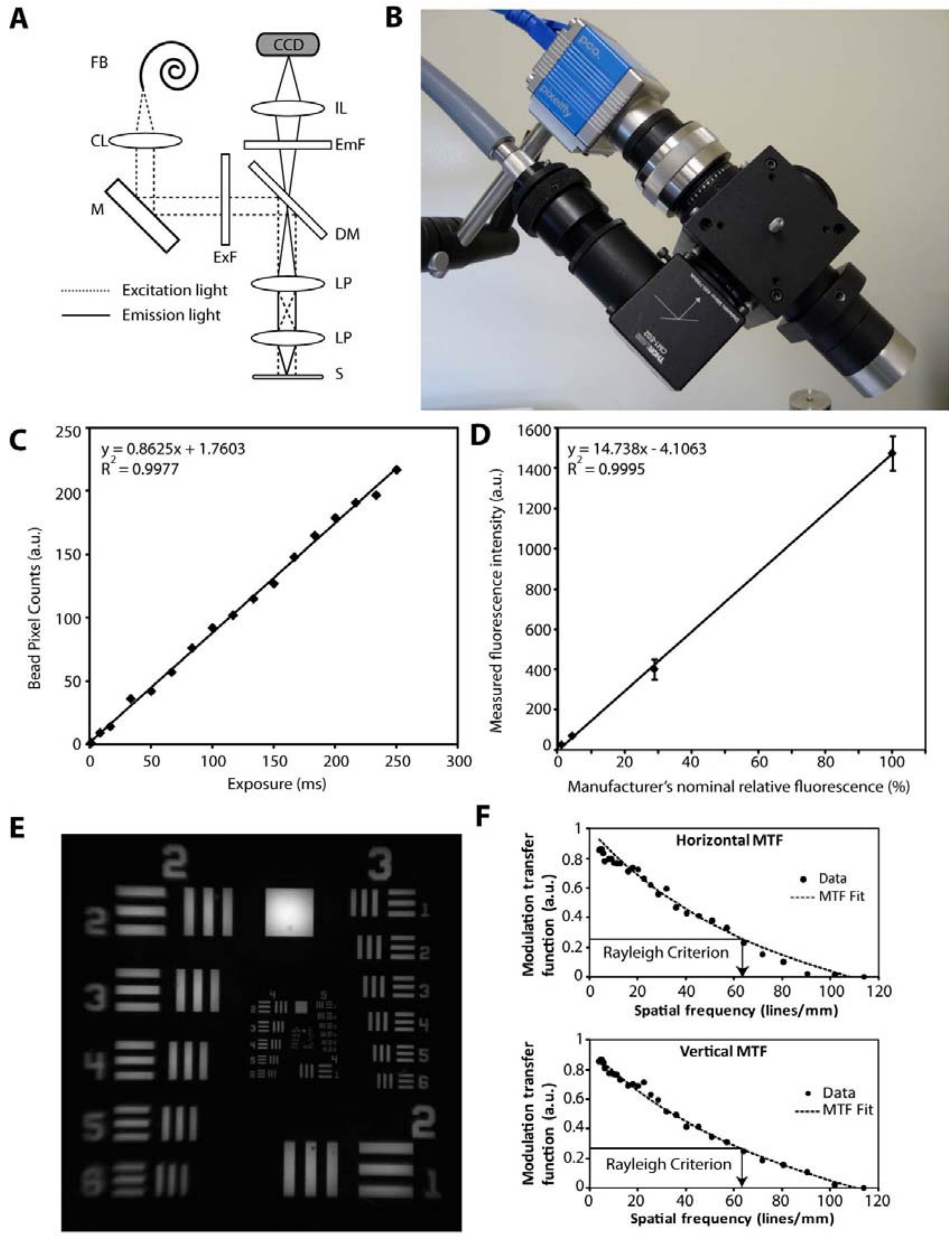

Figure 8: Optical Diagram and Characterization of the Prototype Device

Figure 8: Optical diagram and characterization of the prototype device. (A) Optical representation of the intraoperative imaging device. A fiber bundle (FB) is connected to a light source, and attaches to the device. A collimating lens (CL) collects the input light and a mirror (M) reflects the light towards a band-pass excitation filter (ExF). A long-pass dichroic mirror (DM) reflects the filtered excitation light towards a lens pair (LP) to illuminate the specimen (S). Fluorescence emission from the sample is transmitted through the dichroic mirror and spectrally filtered by a band-pass emission filter (EmF). An imaging lens (IL) focuses the fluorescence emission into a charge-coupled device (CCD). **(B)** Image of the prototype imaging device. **(C)** Pixel intensities acquired from fluorescent microspheres imaged at different exposure times demonstrate a linear response of the device to exposure time (line fit). **(D)** The device was found to have a linear response to 100-fold changes in intensity (line fit). Error bars indicate standard deviation from the mean. **(E)** Image of a standard U.S. Air Force 1951 resolution target was acquired with the imaging device to determine the spatial resolution of the system. **(F)** Horizontal and vertical contrast transfer functions for the imaging system measured with the target image in e. The horizontal and vertical spatial frequency resolution limits are 62.8 and 63.0 cycles/mm, respectively. These correspond to approximately 16 μm of spatial resolution in both axes.

Tumor-to-muscle Fluorescence Signal Ratio

To study intraoperative imaging, I used the primary mouse model of soft tissue sarcoma in *KP* mice. A major challenge to detect microscopic residual cancer *in vivo* is to achieve sufficient contrast between the cancer cells and surrounding normal tissue. Because gene expression analysis shows that the sarcomas in the mouse model overexpress many proteases from the cathepsin family, when compared to normal muscle (Table 4), I used cathepsin-activated imaging agents Prosense 680, Prosense 750 [116] and another imaging agent activated by MMP-2 and MMP-9 proteases, MMPsense 680 [117]. In their nominal, or “inactive”, state, these imaging agents have self-quenched fluorescence which becomes unquenched, or “activated”, upon cleavage of the peptide backbone. 24 hours after intravenous injection, I used the imaging device to measure the tumor-to-muscle fluorescence signal ratio *ex vivo* in samples of sarcoma and normal muscle from the contralateral limb. The average tumor-to-muscle fluorescence signal ratio (±SD) for Prosense 680, Prosense 750 and MMPSense 680 was approximately 12 ± 2.4, 5 ± 1.0, and 8 ± 3.5, respectively (Figure 9A). The other critical non-malignant tissue for resection of extremity soft tissue sarcomas is the neurovascular bundle. Imaging of sarcoma-bearing mice injected with Prosense 680 showed similar fluorescence signal ratio between normal muscle and the neurovascular bundle. To determine the contribution of imaging agent activation from increased cathepsin-activity in the tumor compared to enhanced permeability and retention, I injected sarcoma-bearing mice (n=4) with either Prosense 680 or a non-cleavable Prosense 680 control and harvested tumor and muscle tissues 24 hours after injection. Significant Prosense 680 activation is apparent only in the tumor of the mouse injected with Prosense 680, and not normal muscle from the same animal nor tissue from the animal injected with the non-cleavable version of Prosense 680 (Figure 9B-C).

Table 4: Multiple Cathepsin Proteases are Overexpressed in Primary Soft Tissue Sarcomas in Mice Compared to Normal Muscle.

Table 4: Multiple cathepsin proteases are overexpressed in primary soft tissue sarcomas in mice compared to normal muscle. Fold change represents fold-overexpression in soft tissue sarcomas compared to normal muscle along with corresponding p-values and FDR

Gene	Fold-change	p-value	FDR
Cathepsin A	2.9	< 1e-07	< 1e-07
Cathepsin B	2.5	3.68E-05	9.03E-05
Cathepsin C	4.3	< 1e-07	< 1e-07
Cathepsin E	2.0	0.0074	0.011
Cathepsin H	5.2	< 1e-07	< 1e-07
Cathepsin K	5.9	0.0016	0.0036
Cathepsin L	4.2	< 1e-07	< 1e-07
Cathepsin S	25	< 1e-07	< 1e-07
Cathepsin Z	4.7	< 1e-07	< 1e-07

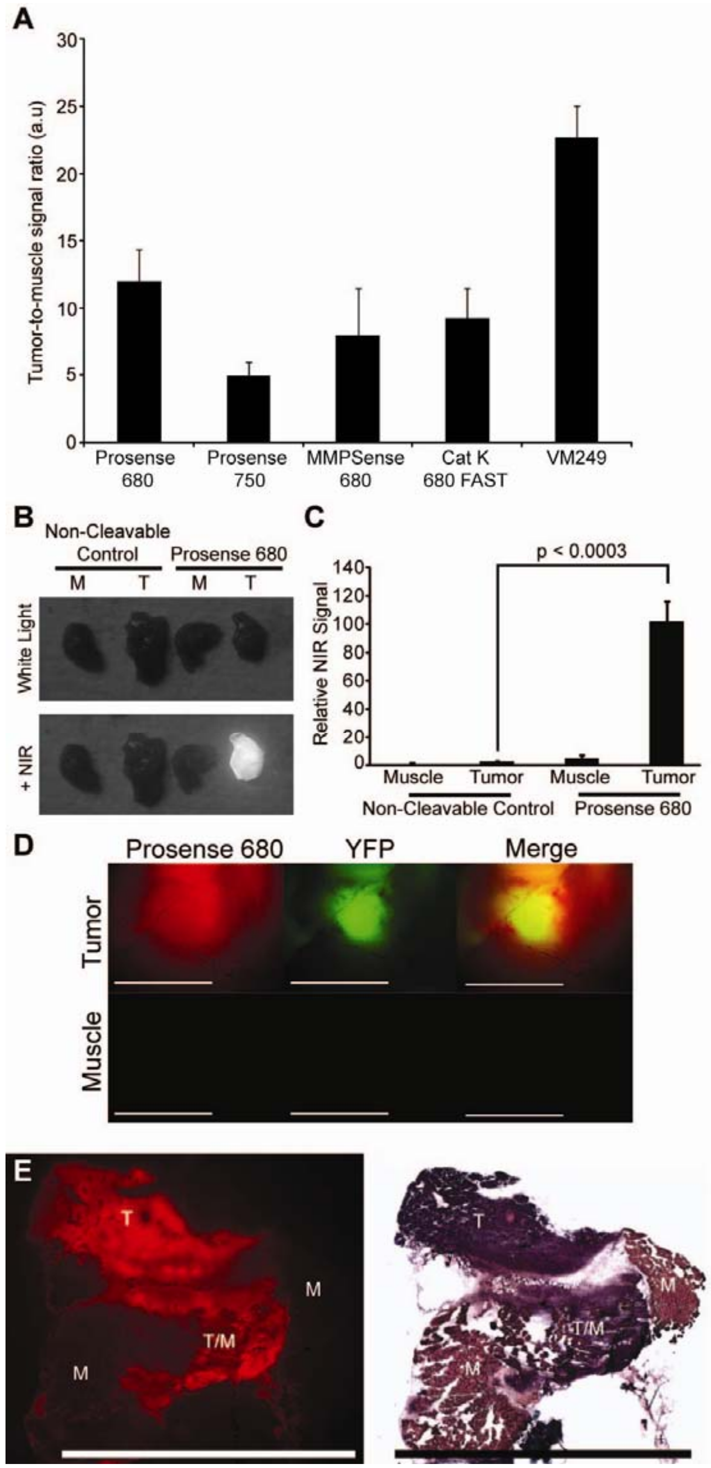

Figure 9: Protease Activation of NIR Imaging Agents in Autochthonous Soft Tissue Sarcomas

Figure 9: Protease activation of NIR imaging agents in autochthonous soft tissue sarcomas. (A) Fluorescence emission from sarcomas in mice injected with different probes (Prosense 680, Prosense 750, MMPSense 680, Cat K 680 FAST and VM249) compared to normal muscle from the same mouse. **(B)** Sarcoma-bearing mice injected with Prosense 680 or a non-cleavable Prosense 680 control shows that signal from the tumor tissue (T), but not normal muscle (M), is observed with Prosense 680 when imaged under NIR. **(C)** Quantification of fluorescence emission from sarcomas and normal muscle of mice injected with Prosense 680 or a non-cleavable Prosense 680 control. **(D)** Fluorescence imaging of a YFP+ sarcoma after Prosense 680 injection shows that Prosense is activated in the sarcoma (tumor), but not normal muscle from the contralateral limb (muscle). **(E)** Comparison of fluorescence from Cat K 680 FAST of a frozen section to the section stained with hematoxylin/eosin confirms the presence of tumor (T) in regions of high NIR fluorescence adjacent to normal muscle (M). Fluoresence imaging also detects areas of tumor invasion into normal muscle (T/M). All scale bars: 5 mm. Error bars represent standard deviation from the mean. Significance determined by two-tailed T-test.

Specificity of Cathepsin-Activated Probes for Tumor Imaging

To determine if Prosense 680 was labeling sarcomas *in vivo*, I used a mouse with a YFP reporter that is activated by Cre recombinase and expressed from the Rosa26 locus (*Rosa26*^{YFP}) [82]. *Rosa26*$^{YFP/YFP}$; *KP* mice that develop sarcomas after Adeno-Cre injection express YFP specifically in tumor cells. Mice with YFP+ primary sarcomas were injected with Prosense 680 24 hours prior to imaging with the device. Soft tissue sarcomas showed significant YFP expression, which co-localized with Prosense 680 (Figure 9D). The NIR signal from Prosense 680 also extended beyond the YFP expressing tumor cells, suggesting that Prosense 680 is activated by cathepsins secreted into the extracellular matrix [118] and/or that Prosense labels non-tumor parenchymal cells, such as tumor-associated macrophages [119, 120]. Conversely, normal muscle from the contralateral limb showed no YFP expression or significant

Prosense 680 activation (Figure 9D). Furthermore, fluorescence signal from the cathepsin-activated imaging agents in frozen sections from sarcoma samples was also imaged with the device and compared to histology. By comparing fluorescence imaging with histology, the imaging agents were seen to have effectively labeled microscopic tumor areas including the invasive edge (T/M in Figure 9E).

Imaging Microscopic Residual Disease

I explored whether Prosense 680 could be used in conjunction with the novel imaging device to detect microscopic cancer in the tumor bed of mice during surgery. I first utilized an initial cohort of sarcoma-bearing mice (n=14) injected with Prosense 680 to establish a metric capable of distinguishing tumor beds with and without microscopic residual sarcoma. For each mouse, the soft tissue sarcoma was grossly resected and the excised tumor was imaged with the hand-held device to determine its fluorescence intensity level normalized by the exposure time to obtain a time-independent quantification of the fluorescence emission rate. Then, the tumor bed was imaged with the imaging device. A biopsy of the tumor bed in the area of highest residual fluorescence was performed for histologic analysis to determine a threshold for image-based classification of the tumor bed. Using these data, a threshold of 80% of the minimum fluorescence emission rate of the primary tumor was established as capable of identifying mice with biopsy-proven microscopic residual disease in the tumor bed (Figure 10A). Moreover, no mice in which the fluorescence of the tumor bed was below this threshold had biopsy-proven microscopic residual disease (Figure 10B). When the entire cohort was followed for local recurrence, the presence of residual fluorescence above this threshold in the tumor bed predicted decreased relapse-free survival (HR: 4.7, p=0.013, Figure 10C).

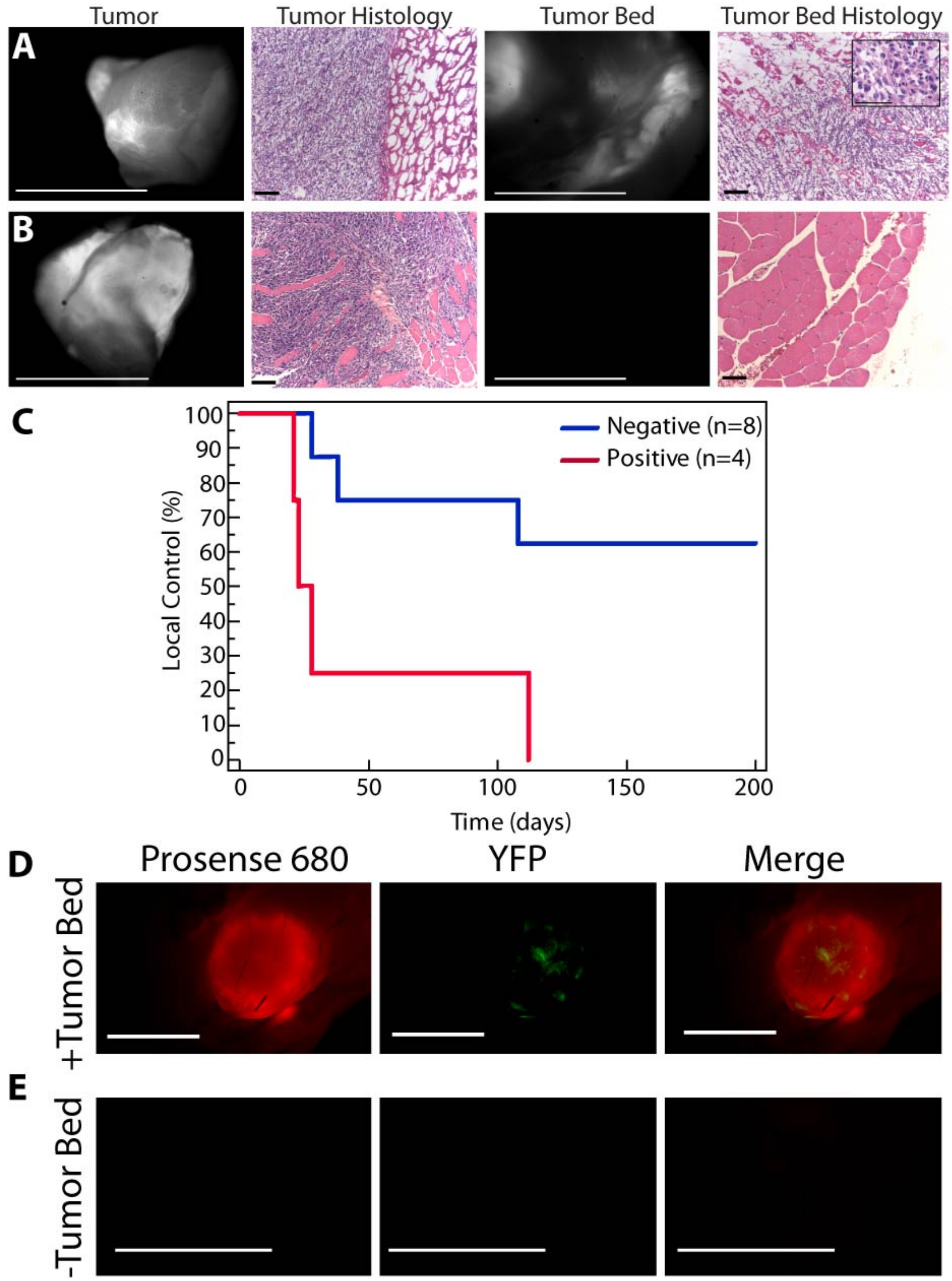

Figure 10: Correlation of Residual Prosense 680 Fluorescence with Microscopic Residual Sarcoma and Local Recurrence

Figure 10: Correlation of residual Prosense 680 fluorescence with microscopic residual sarcoma and local recurrence. (A and B) Primary sarcomas were removed by gross total resection from mice after Prosense 680 injection and the excised tumors were imaged with the device (Tumor), which correlated with the histologic presence of tumor (Tumor Histology). Then, the tumor bed was imaged and residual fluorescence suggested the presence **(A)** or absence **(B)** of residual microscopic sarcoma (Tumor Bed). Hematoxylin and eosin staining of a biopsy of the tumor beds from A and B confirms the presence and absence of residual sarcoma cells in the tumor bed, respectively (Tumor Bed Histology). The inset shows a 100x image of the residual sarcoma cells. **(C)** Post-Hoc image analysis for residual NIR fluorescence in the tumor bed after injection with Prosense 680 can risk-stratify mice for local recurrence (HR: 4.7, p=0.013). Mice with primary sarcomas that express YFP were also injected with Prosense 680 and tumors were resected. In tumor beds with NIR fluorescence above the threshold **(D)**, YFP+ sarcoma cells were identified in the tumor bed, while in tumor beds without residual NIR fluorescence **(E)** there were no YFP+ sarcoma cells. Scale bars: 5 mm fluorescence images in A, B and E, 1 mm for fluorescence images in D, 100 μm for histology in panels A and B, and 50 μm for inset.

To further validate that residual fluorescence in the tumor bed correlates with microscopic residual sarcoma, I injected *Rosa26*$^{YFP/YFP}$; *KP* mice (n=5) with Adeno-Cre to generate sarcomas where YFP is expressed only in sarcoma cells. 24 hours after Prosense 680 injection, all gross tumor was removed and the tumor bed was imaged with the device using filters for NIR and YFP fluorescence. In tumor beds with residual NIR fluorescence above the threshold, YFP expressing tumor cells were observed in the tumor bed (Figure 10D). As observed previously, the Prosense 680 signal appeared to extend beyond the YFP expressing sarcoma cells. In tumor beds without residual fluorescence above the threshold, no YFP+ cells were observed (Figure 10E).

The activation of Prosense 680 in small intestinal polyps in mice is primarily due to cathepsins expressed in inflammatory stromal cells [121]. In order to determine the contribution of imaging agent activation from tumor cells and CD11b+ tumor-associated immune cells, which may contribute to the extension of the Prosense 680 signal beyond the boundaries of the YFP expressing sarcoma cells *in vivo*, YFP+ sarcomas from mice injected with Prosense 680 were isolated and sorted by flow cytometry for YFP, Prosense 680, and CD11b. Approximately two-thirds of Prosense 680+ cells were YFP+ sarcoma cells, while approximately one-third of Prosense 680-labeled cells were YFP-, CD11b+, implying that infiltrating immune cells, such as macrophages, also activate the imaging agent *in vivo* (Figure 11A-B). To confirm that YFP+ cells had significantly more tumor-initiating capacity, *in vitro* colony formation was assessed on freshly sorted cells. YFP+ cells formed approximately 15-fold more colonies compared to YFP- cells (Figure 11C). Colonies initiated from YFP-sorted cells were later found to express YFP (Figure 11D), suggesting that these colonies were derived from mis-sorted YFP+ sarcoma cells. Injection of 50,000 YFP+ or YFP- cells generated sarcomas with 100% penetrance when transplanted into immunocompromised nude mice. Tumors derived from YFP-sorted cells did demonstrate a significant growth delay compared to tumors derived from YFP+ sorted cells (Figure 11E). Similar to results obtained *in vitro*, tumors derived from YFP- sorted cells contained large numbers of YFP+ expressing sarcoma cells (Figure 11F). These data are consistent with previous reports that tumor-associated immune cells activate Prosense *in vivo* [121], but also demonstrate that this molecular imaging agent labels a substantial fraction of tumor cells – showing the utility of cathepsin-activated imaging agents for imaging primary soft tissue sarcomas *in vivo*.

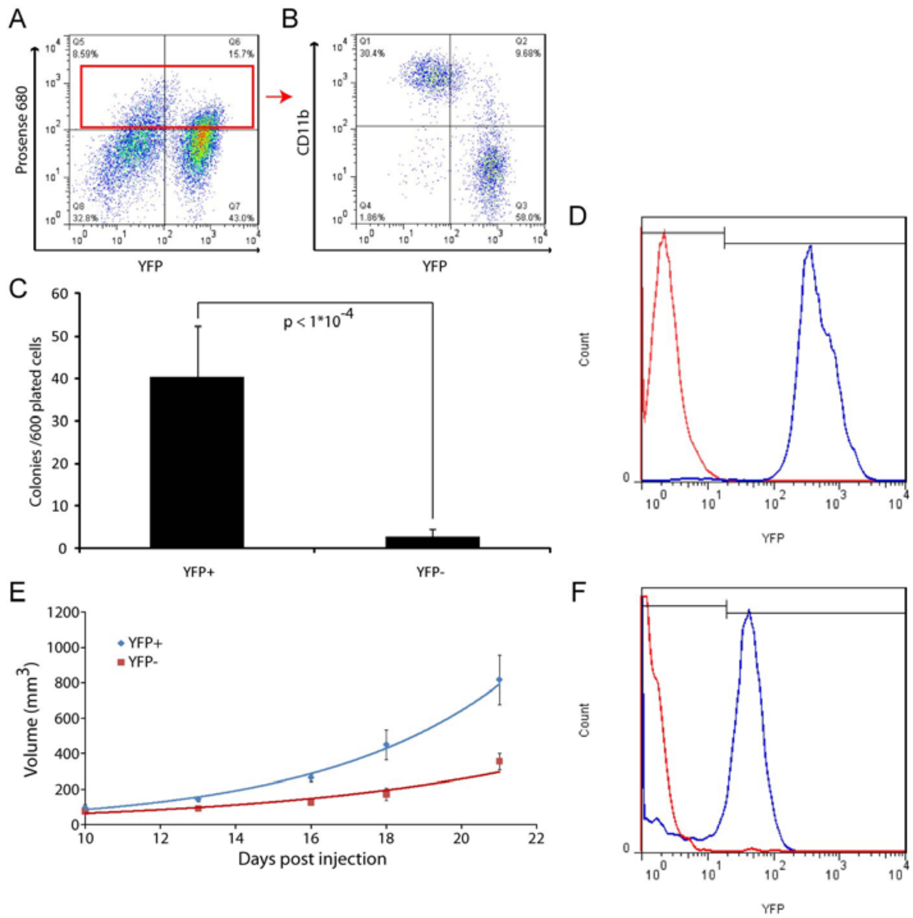

Figure 11: Prosense 680 Labels Tumor Cells and Tumor Associated Immune Cells

Figure 11: Prosense 680 labels tumor cells and tumor associated immune cells. (A) Both YFP+ sarcoma cells and YFP- stromal cells activate Prosense 680 *in vivo*. Sarcoma bearing *Rosa26*$^{YFP/YFP}$*; KP* mice were injected with Prosense 680 and the tumor was removed 24 hours later. Cells from the tumor were stained for CD11b and sorted by flow cytometry. **(B)** Prosense 680 was found to primarily label YFP+ tumor parenchymal cells (~68%) and CD11b+ tumor associated immune cells (~30%). **(C)** YFP+ cells had significantly higher colony initiating efficiency compared to YFP- cells ($p < 1*10^{-4}$). **(D)** The colonies initiated from YFP- sorted cells expressed YFP by flow cytometry (blue line, YFP- control cells in red). **(E)** YFP+ and YFP- sorted cells (50,000) from primary soft tissue sarcomas were injected into immunocompromised nude mice. All mice (n=20) developed soft tissue sarcomas at the site of injection. However, tumor development was delayed in YFP- sorted cells derived. **(F)** Similar to the plated cells, allograft tumors derived from YFP- cells were found to contain YFP expressing sarcoma cells by flow cytometry (blue line, YFP- control cells in red). These results suggest that tumors initiated from the YFP- gated cells were due to YFP+ cells that were mis-sorted.

Intraoperative Imaging for Direct Tumor Bed Examination and Surgical Guidance

Having established a threshold for residual NIR fluorescence using Prosense 680 that correlates with microscopic residual sarcoma and local recurrence, I next tested whether residual fluorescence also correlates with residual sarcoma and local recurrence after injection with other cathepsin-specific imaging agents. Because cathepsin K is overexpressed in sarcomas (Table 4), the cathepsin K specific Cat K 680 FAST probe was tested in addition to a multi-cathepsin imaging agent VM249. Cat K 680 FAST and VM249 are self-quenched imaging agents with an amino acid recognition sequence flanked on both sides by Vivotag S 680; however, VM249's substrate is susceptible to cleavage by cathepsins B, K, L and to a lesser extent S. These new imaging agents have potential advantages over Prosense 680 including a smaller molecular weight, the ability to image tumors several hours, rather than 24 hours, after administration, and for VM249 a higher tumor-to-muscle signal ratio than Prosense 680 (22.7 ± 2.3, Figure 10A). I injected Cat K 680 FAST or VM249 intravenously into mice (n=4 for each probe) with sarcomas expressing YFP and performed marginal surgical resections after six hours. Technical advances in software allowed for real-time imaging at the time of surgery and a more thorough examination of the tumor beds of the subsequent animals in these experiments. Tumor beds were imaged and classified as positive or negative for residual NIR fluorescence, in real-time, based on 80% of the minimum fluorescence emission rate of the primary sarcoma as determined previously with Prosense 680. The presence of residual fluorescence above this threshold correlated with YFP positive cells present in the tumor bed for both Cat K 680 FAST and VM249 (Figure 12A-B). I also injected mice with primary sarcomas with Cat K 680 FAST (n=24) or VM249 (n=26) for intraoperative imaging to determine whether residual NIR fluorescence correlated with local recurrence. For these experiments, no biopsy of the tumor bed was performed to avoid removal of residual sarcoma cells that may alter the rate of local recurrence. Using the established threshold, residual fluorescence in tumor beds after injection with Cat K 680 FAST or VM249 correlated with the development of local recurrence (Figure 12C-D, HR: 3.9, p=0.01 and HR: 11.1, p=0.0001, respectively). These results demonstrate that this imaging approach can detect residual fluorescence in the tumor beds of mice following injection with a NIR imaging agent that not only correlates with microscopic residual sarcoma, but also can risk-stratify tumor beds for local recurrence.

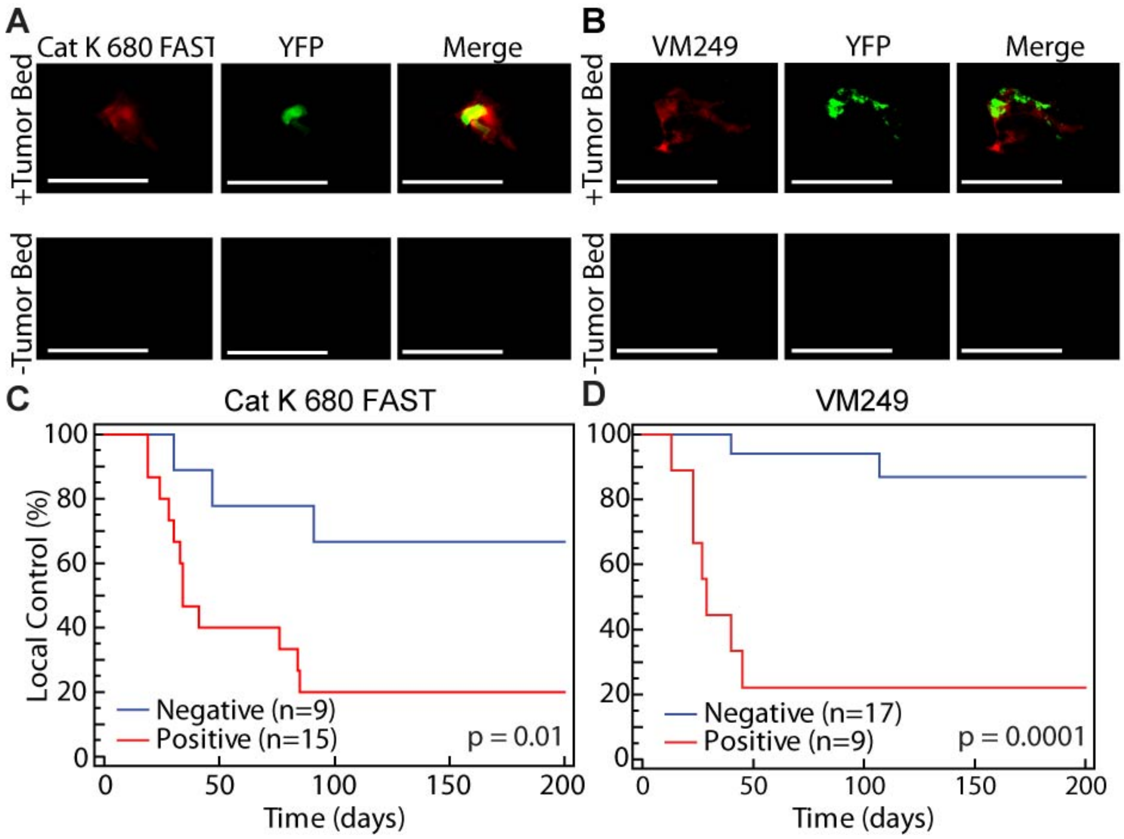

Figure 12: Correlation of Residual Cat K 680 FAST and VM249 Fluorescence with Microscopic Residual Sarcoma and Local Recurrence

Figure 12: Correlation of residual Cat K 680 FAST and VM249 fluorescence with microscopic residual sarcoma and local recurrence. Fluorescence imaging of mice with primary YFP+ sarcomas injected with **(A)** Cat K 680 FAST or **(B)** VM249 shows that the presence of residual NIR fluorescence (+Tumor Bed) in the tumor bed is associated with residual YFP+ tumor cells, while the absence of residual NIR fluorescence (-Tumor Bed) shows no residual YFP+ cells. Real-time imaging of residual fluorescence in the tumor bed after injection with **(C)** Cat K 680 FAST or **(D)** VM249 can risk-stratify mice for local recurrence (HR: 3.9, p=0.01 and HR: 11.2, p=0.0001, respectively). Scale bars: 5 mm.

A proof-of-principle experiment was designed to test the ability of the intraoperative imaging system to guide surgical resection of microscopic residual cancer from the tumor bed. Mice were injected with Cat K 680 FAST (n=13) or VM249 (n=12) 6 hours prior to surgery. The tumor was then removed in a multi-step resection and the device was used to image the tumor bed after each resection to determine when the tumor bed was free of residual fluorescence above the established threshold. Each piece of tissue removed was collected for subsequent histologic analysis. For these mice, multiple resections were necessary to achieve a tumor bed free of residual fluorescence (Figure 13A). In all cases, biopsy of the final surgical bed did not identify residual sarcoma. However, in mice injected with either Cat K 680 FAST or VM249 that had multiple resections, removal of all residual fluorescence significantly improved local control (Figure 13B-C, HR: 2.5, p=0.05 and HR: 3.4, p=0.02). Thus, complete removal of residual fluorescence in one or more resections enhances overall local control compared to tumor beds with residual fluorescence.

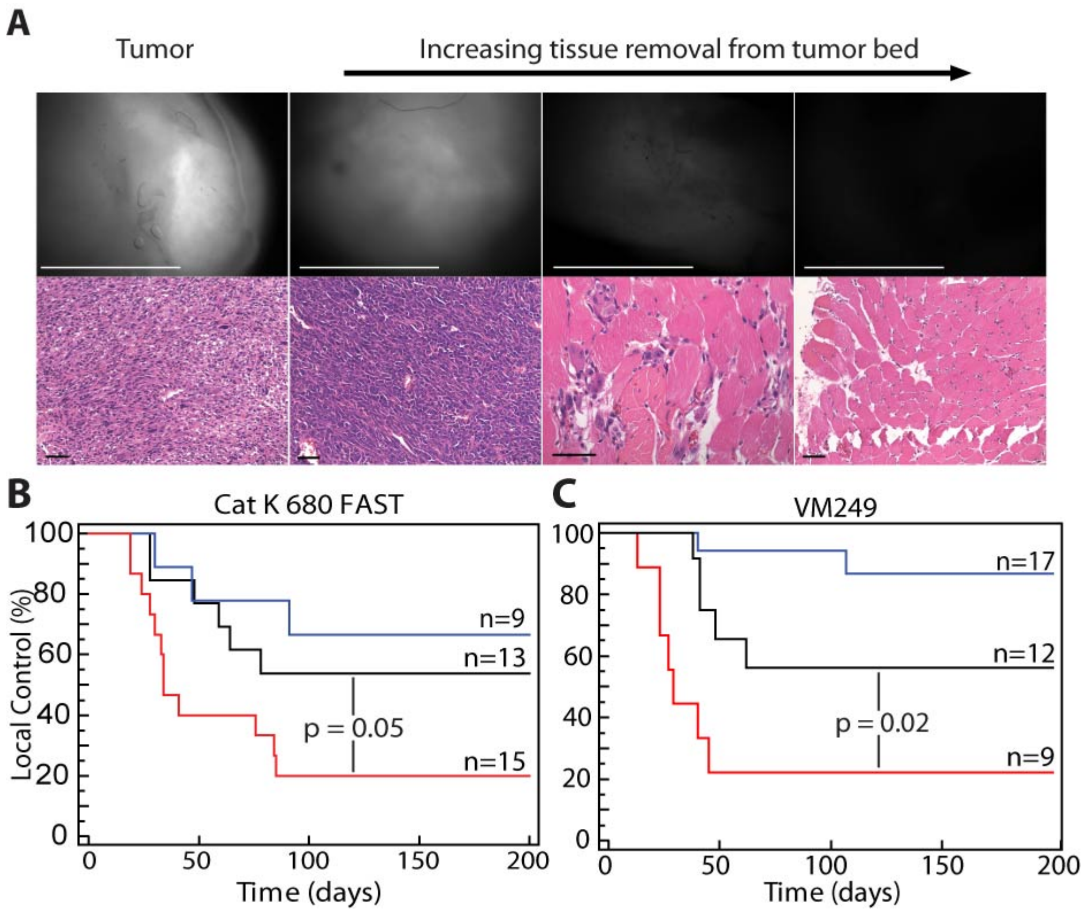

Figure 13: Intraoperative Image-guided Surgery Improves Local Control

Figure 13: Intraoperative image-guided surgery improves local control. (A) Representative histology from removal of tumor using the imaging device. The top row corresponds to fluorescence images of the tumor (first column) and tumor bed after one, two, and three resections. The bottom row shows the corresponding histology of a biopsy of the tumor bed at each step in the surgery. Removal of residual fluorescence from the tumor bed improves local control with either **(B)** Cat K 680 FAST or **(C)** VM249 (HR: 2.5, p=0.05 and HR: 3.4, p=0.02 respectively). Blue lines represent single resections with no residual NIR fluorescence, red lines single resections with residual NIR fluorescence and black lines multiple resections to a tumor bed free of residual NIR fluorescence. Numbers of mice in each cohort are noted above each line. The single positive and single negative cohorts are the same groups as shown in Fig 12C-D. Scale bars: fluorescence images, 5 mm; histology images, 50 μm.

4.4 Discussion

In this study I have shown that the combination of NIR fluorescence with epi-illumination is capable of identifying small clusters of microscopic residual sarcoma cells that have activated a fluorescent imaging agent *in vivo*. Although other groups have performed elegant experiments of image-guided surgery using transplanted tumors with different molecular imaging agents [122-124], in this study of intraoperative imaging I utilized a highly invasive primary mouse model of sarcoma with the clinically relevant end point of local control. When the device identified tumor beds with positive residual fluorescence, this correlated with microscopic residual sarcoma present in a biopsy of the tumor bed when analyzed by histology (Figure 10A), and by direct fluorescence imaging of the tumor bed for YFP expressing sarcoma cells (Figure 10D, 12A-B). Moreover, the presence of residual fluorescence correlated with local recurrence for multiple cathepsin-activated imaging agents (Figure 10C, 12C-D) and image-guided resection of residual fluorescence improved local control (Figure 13B-C).

By using exogenously delivered NIR imaging agents activated by cathepsin proteases, I have been able to detect microscopic residual sarcoma in the tumor bed at the time of surgery. Utilizing imaging agents that label both tumor cells and tumor-infiltrating immune cells allows targeting of both the tumor parenchymal cells as well as a stromal compartment which has been shown to induce and sustain tumor angiogenesis, proliferation, invasion and metastasis [125]. Many of these tumor-infiltrating immune cells will congregate at the margin of the tumors to create a tumor-promoting microenvironment [119]. Furthermore, removal of these cells in animal models can lead to tumor regression [126]. Therefore, the ability to label and remove tumor-associated immune cells in addition to labeled tumor cells at the time of oncologic resection may contribute to improving local control. However, it is important to note that because these imaging agents label immune cells, this may limit the ability of these probes to distinguish malignant tissue from inflammatory conditions. As a result, this approach may be best suited for surgery after a diagnosis of cancer has been established by biopsy and histologic analysis.

This imaging system has several limitations. This approach uses epi-illumination to deliver fluorescence excitation light and allows for straightforward collection of fluorescence emission to generate images of the area of interest. The signal that reaches the detector will depend on the depth in tissue from where the cell emits its signal [127]. Although I have demonstrated that this imaging device has the sensitivity to identify small clusters of tumor cells if microscopic residual cancer is at the surface of the tumor bed, it is likely that this approach will not detect a small number of tumor cells that have migrated beyond the tumor bed surface [115]. Therefore, detection of deep, discontinuous cancer cell clusters is beyond the scope of this system. However, many cancers, including some soft tissue sarcomas, demonstrate collective invasion at the margins [128]. Cancer cells from these tumors will migrate as sheets of cells rather than as discontinuous, single cells [129] and often migrate with tumor-infiltrating immune cells [130]. I anticipate that for many tumors, residual tumor-infiltrating immune cells or cancer cells after resection will be at the tumor bed surface.

Because this technology examines the entire tumor bed in a few minutes, it can provide the surgeon with a comprehensive real-time analysis of the tumor bed. The imaging device was purposely not designed to provide the spatial resolution of a microscope, but rather the sensitivity to detect small numbers of cells after protease activation of the imaging agent. Therefore, the device does not have the resolution to identify cell-cell boundaries – as such a design would preclude the wide field-of-view that makes this device a practical intraoperative tool. A device with an even larger field-of-view would speed up the task of surveying the tumor beds in patients with sarcomas. Recently, several molecular imaging agents have been developed that are useful for imaging cancer. These agents target over-expressed proteolytic enzymes [116, 117], surface markers [124], and changes in intracellular acidity levels [131], to provide high contrast between the fluorescence emission of cancer and normal tissue. To improve specificity and enhance tumor contrast, it may be necessary to utilize a cocktail of these imaging agents that target both tumor cells and the tumor-associated microenvironment. Such a cocktail could be tailored to an individual patient by examining expression of target molecules from a biopsy sample prior to surgery. However, to the best of my knowledge, none of these imaging agents have overcome the significant hurdles that are required to receive regulatory approval for use in humans. Still, early human studies using the near-infrared fluorescence imaging agent indocyanine green (ICG) have been promising for sentinel lymph node mapping [132], as well as for limited use for some tumor types, such as hepatobiliary cancer [133]. Thus, despite the significant time and expense required to develop NIR imaging agents for clinical use, the availability of NIR imaging agents, such as those activated by cathepsin proteases, would greatly improve the outlook for utilizing intraoperative molecular imaging. Regardless of the imaging agent(s) used in the future, clinical implementation of an imaging device-imaging agent system would be one example of utilizing molecular imaging as a promising treatment tool [134].

In summary, I have combined a wide field-of-view imaging device with a series of NIR cathepsin protease-activated imaging probes to detect microscopic residual sarcoma in mice *in vivo.* I have observed that the presence of residual NIR fluorescence can risk-stratify animals for local recurrence, and demonstrate the feasibility of this approach for intraoperative image-guided surgery to direct additional surgical resection that removes residual sarcoma and improves outcomes. To my knowledge, this is the first time that a primary tumor model system, in the absence of tumor transplantation, has been utilized for intraoperative imaging studies with local control as the endpoint. These results demonstrate the power of molecular imaging for intraoperative imaging and provide a pre-clinical platform to test new imaging agents and systems. Before this technology can be translated to human trials, it will be important to optimize the imaging system with an even larger field-of-view to more easily image large tumor beds and to complete pre-clinical toxicity testing of a NIR imaging agent.

5. Genotype Dependent Control of miRNA Biogenesis and Metastasis is Mediated Through MAPK Dependent Regulation of Dgcr8

5.1 – Summary

MicroRNAs are a class of small RNAs that post-transcriptionally regulate gene expression. Global alterations in miRNAs are frequently observed in cancer. However, the mechanism controlling changes in miRNA expression remain unclear as few mutations have been identified in components of the miRNA biogenesis pathway. miRNA biogenesis is a multistep process which involves initial cleavage of primary miRNA transcripts into shorter pre-miRNA by Drosha and the RNA binding protein Dgcr8. Cleavage by Dicer yields the final mature miRNA, which can suppress the expression of target mRNAs. To study mitogen-activated protein kinase (MAPK) regulation of miRNA biogenesis in cancer, I used primary sarcomas expressing either *Braf*^{V600E} or *Kras*^{G12D} and Dicer haploinsufficiency. I find that *Braf*^{V600E} mutant tumors, which have increased MAPK signaling and Dgcr8 levels, suppress Dicer haploinsufficiency from promoting metastasis. Here I show that one of the key proteins involved in miRNA processing, Dgcr8, is regulated by MAPK signaling. Dgcr8 levels are increased by activated MAPK. Conversely, MEK inhibition leads to decreased Dgcr8 and mature miRNAs, with accumulation of primary miRNA transcripts. I identify the MAPK target, Ras Responsive Element Binding Protein1 (Rreb1), as a key regulator of Dgcr8.

This work was performed in collaboration with: M Sachdeva and H. Min who assisted with validation of Rreb1 dependent regulation of Dgcr8, M. Javid who assisted with MEK-DD overexpression experiments, R. Dodd who performed *in vivo* allograft experiments, Y. Ma who performed IHC, J. Carter and B. Brigman who performed animal surgeries and L. Dodd who reviewed histology and IHC.

5.2 – Introduction

miRNAs are small ~22nt RNAs capable of post-transcriptional gene regulation. Primary miRNA transcripts (pri-miRNA) are transcribed in a canonical fashion by RNA polymerase II [135]. Pri-miRNAs form extended hairpin structures that are recognized by the microprocessor, which is composed of the ribonuclease Drosha and the double stranded RNA binding protein Dgcr8 [136]. The microprocessor cleaves these pri-miRNAs to shorter ~70nt pre-miRNA within the nucleus [137]. Upon export into the cytoplasm through an Exportin 5 mediated process [138], pre-miRNAs are further processed into their mature form by Dicer and its binding partner Trbp (Figure 14) [139]. These ~22nt mature miRNAs are then loaded into a complex with Ago proteins to form the RNA-induced silencing complex, where miRNAs function as post-transcriptional regulators of gene expression through direct base pairing with target mRNAs [140].

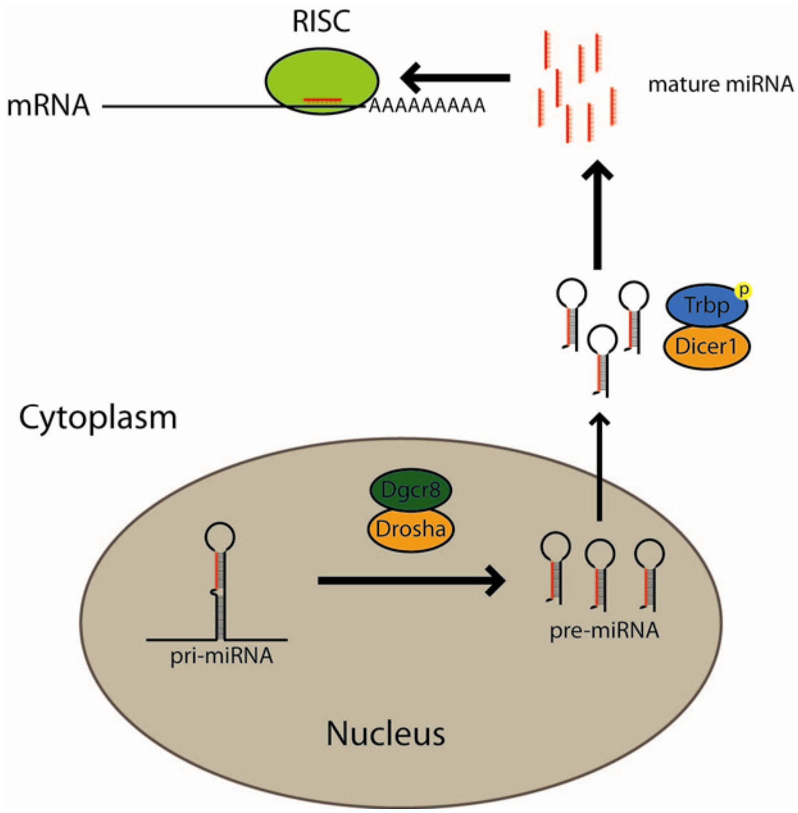

Figure 14: miRNA Biogenesis is a Multistep Process

Figure 14: miRNA biogenesis is a multistep process. Pri-miRNAs are transcribed from the host genome. Recognition of stem-loop RNAs pri-miRNAs by Dgcr8. Dgcr8 then recruits Drosha to cleave the pri-miRNA into ~70 bp pre-miRNAs. Pre-miRNAs are then exported from to the cytoplasm where they are cleaved into mature miRNAs by Dicer with its binding partner Trbp. Mature miRNAs can then be incorporated in to the RNA induced silencing complex (RISC), where they often act to suppress target mRNAs to suppress gene expression.

Widespread loss of miRNA expression has been found in many cancers when compared to normal tissue [141]. Loss of mature miRNA expression has been correlated to tumor progression and the development of distant metastases [142, 143]. Some have hypothesized that loss of mature miRNA expression could be caused by defects in miRNA processing [144], but how miRNA biogenesis is regulated in cancer remains to be fully defined.

Mutations in a number of enzymes that process pri-miRNA transcripts into mature miRNAs have been identified in human cancer. For example, *DICER* is mutated in ovarian cancer and soft tissue sarcomas [145, 146]. In addition, mutations in *EXPORTIN 5* and *TRBP* have been reported in mismatch repair deficient colorectal cancer [147, 148]. In some human tumors, altered expression of enzymes that perform miRNA processing have been correlated to clinical outcomes in a tumor type dependent manner. For instance, decreased DICER or DROSHA levels are associated with worse outcomes in ovarian cancer and neuroblastoma [149, 150]. Conversely, overexpression of DICER has been linked to worse outcome in colorectal and prostate cancer [151, 152].

miRNA biogenesis has also been reported to be regulated by the MAPK pathway [153]. Activation of the MAPK pathway is a common feature of a diverse set of human tumors. Mutations in growth factor receptors, Ras, or within the MAPK pathway itself can activate the MAPK pathway leading to cell proliferation [154-156]. MAPK signaling has been reported to regulate miRNA biogenesis in cells *in vitro* through phosphorylation of Trbp, the binding partner of Dicer, which can enhance both Dicer stability and miRNA biogenesis [153]. Here I show that MAPK signaling can regulate miRNA biogenesis in tumors *in vivo*. Using complementary primary mouse models of soft tissue sarcoma, I find that tumors initiated by *Braf*^{V600E}, compared to tumors expressing *Kras*^{G12D}, have increased pERK, Dgcr8 expression, and expression of mature miRNAs. Although sarcomas expressing *Kras*^{G12D} with Dicer haploinsufficiency have increased metastasis, deletion of one allele of *Dicer* in *Braf*^{V600E} driven tumors does not increase metastasis. I further show that the MAPK pathway can regulate miRNA biogenesis at the level of the microprocessor by controlling expression of Dgcr8 through Rreb1. These results indicate that in cancer the consequences of a mutation in a component of the miRNA biogenesis machinery depends on specific oncogenic mutations in the MAPK pathway.

5.3 – Results

MAPK Signaling can Alter miRNA Biogenesis *in vivo*

Others have shown that MAPK signaling regulates miRNA processing *in vitro* [153]. To test the functional significance of the MAPK pathway on tumor progression *in vivo*, I generated primary mouse soft tissue sarcomas initiated by oncogenic *Braf*^{V600E} and loss of *p53* or oncogenic *Kras*^{G12D} and loss of *p53*. Because mutations in upstream receptor tyrosine kinases and *Kras*^{G12D}, but not *Braf*^{V600E}, induce Sprouty and other suppressors of MAPK signaling [157], I hypothesized that *Braf*^{V600E} mutant sarcomas would have increased MAPK signaling compared to *Kras*^{G12D} mutant sarcomas. Intramuscular injection of an adenovirus expressing Cre recombinase into *Braf*$^{Ca/+}$; *p53*$^{Flox/Flox}$ mice (referred to here as *BP* mice) [83], results in Cre dependent activation of the mutant *Braf*^{V600E} allele and deletion of *p53,* causing soft tissue sarcomas. Sarcomas in *BP* mice developed in approximately 55 days (median time to tumor), which is approximately 20 days faster than sarcomas in *KP* mice (Figure 15A, $p<0.03$). Sarcomas in *BP* mice have similar histology to sarcomas from *KP* mice (Figure 15B). However, in contrast to the sarcomas in *KP* mice, which I have described previously [72], sarcomas in *BP* mice have significantly higher levels of steady state MAPK signaling (Figure 15C) compared to their Kras driven counterparts. Conversely, downstream Ras targets of the PI3K pathway were not consistently different (Figure 15D).

Consistent with a model where MAPK signaling regulates miRNA biogenesis *in vivo*, miRNA profiling of soft tissue sarcomas from *BP* and *KP* mice demonstrates that sarcomas with increased MAPK signaling, such as those in *BP* mice, also have increased expression of mature miRNAs (Figure 15E, and Appendix D). In order to determine if processing of pri-miRNAs is more efficient in *Braf*^{V600E} sarcomas, I selected 6 miRNAs implicated in tumor progression to measure levels of pri-miRNA and mature miRNA in the primary sarcomas from *BP* and *KP* mice. I found an increased ratio of mature:pri-miRNA in the *Braf*^{V600E} mutant sarcomas (Figure 15F). This suggests that sarcomas in *BP* mice have more efficient processing of pri-miRNAs compared to sarcomas in *KP* mice in a manner independent of pri-miRNA expression. Together these data suggest that pri-miRNA processing in primary sarcomas is regulated by MAPK signaling in a genotype dependent manner.

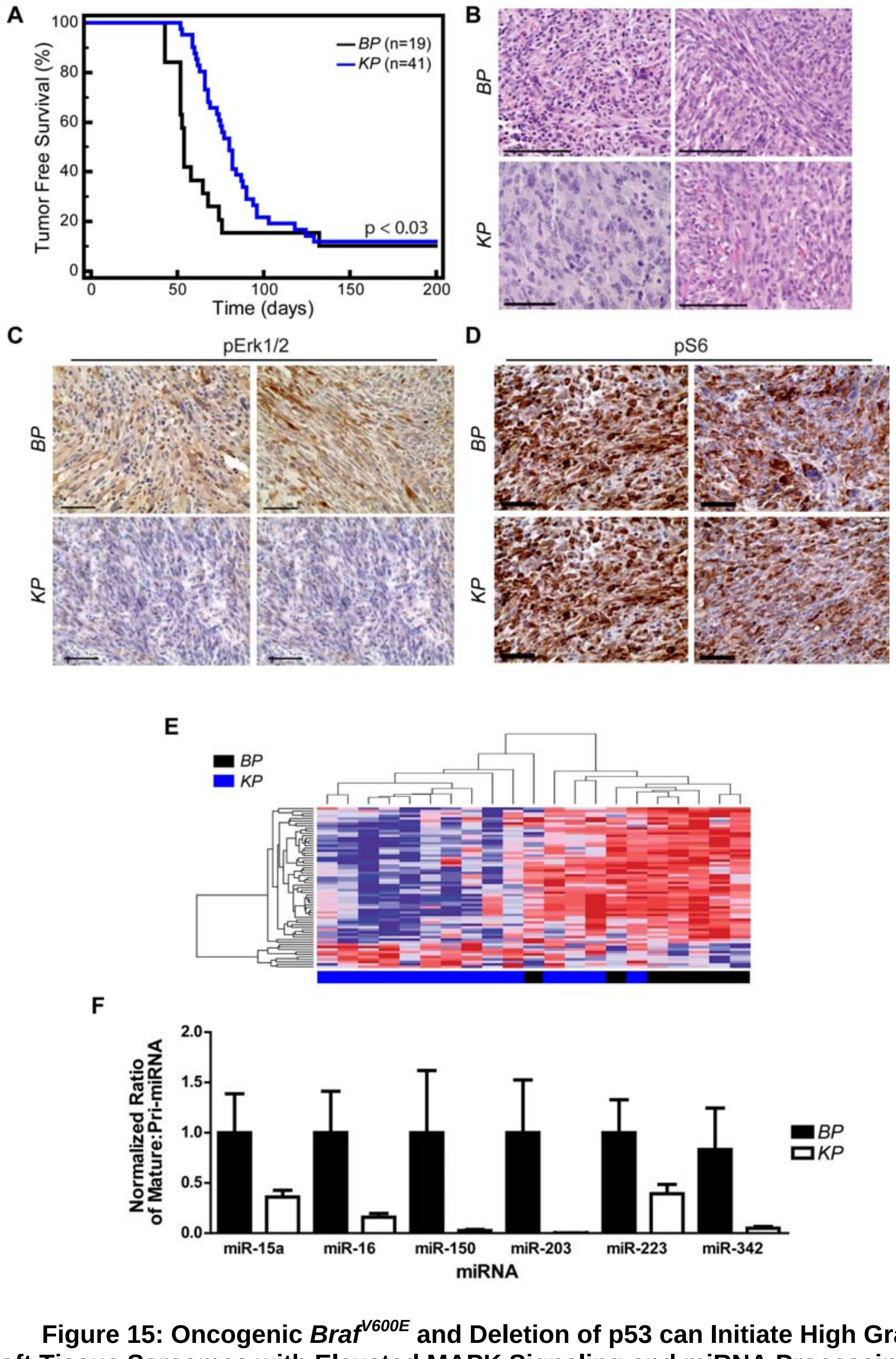

Figure 15: Oncogenic *Braf*^{V600E} and Deletion of p53 can Initiate High Grade Soft Tissue Sarcomas with Elevated MAPK Signaling and miRNA Processing

Figure 15: Oncogenic *Braf*^{V600E} and deletion of p53 can initiate high grade soft tissue sarcomas with elevated MAPK signaling and miRNA processing. (A) *Braf*^{V600E} sarcomas develop in *BP* mice with accelerated kinetics compared to *Kras*^{G12D} sarcomas in *KP* mice ($p<0.03$). **(B)** *Braf*^{V600E} initiated soft tissue sarcomas share similar histologic appearance to *Kras* initiated sarcomas. **(C)** Higher levels of pERK1/2 were consistently detected by IHC in *Braf* mutant sarcomas (n=8) compared to *Kras* driven sarcomas (n=8). **(D)** Conversely, no significant alterations were observed downstream of other Ras effectors, such as pS6. **(E)** *Braf*^{V600E} mutant soft tissue sarcomas have increased mature miRNAs, measured by Taqman PCR arrays. **(F)** *Braf*^{V600E} sarcomas have increased efficiency of miRNA processing compared to *Kras*^{G12D} mutant sarcomas as measured by the ratio of mature to pri-miRNA levels. Scale bars represent 100 microns, error bars represent standard error from the mean (SEM).

Dicer Haploinsufficiency Enhances Tumor Proliferation in a Genotype Dependent Manner

Having demonstrated that sarcomas in *BP* mice have increased MAPK signaling and elevated pri-miRNA processing, I next tested the functional significance of these findings in cancer by generating primary sarcomas with Dicer haploinsufficiency. Dicer haploinsufficiency has been observed in a number of human cancers, and specific mutations in Dicer have been identified in several subtypes of soft tissue sarcoma [145, 146, 158]. In *KP* mice, Dicer acts as a haploinsufficient tumor suppressor [159]. Therefore, I crossed *Dicer*^{Flox} mice to *KP* and *BP* mice to generate: *LSL-Kras*$^{G12D/+}$*; p53*$^{Flox/Flox}$*; Dicer*$^{Fl/+}$ and *Braf*$^{Ca/+}$*; p53*$^{Flox/Flox}$*; Dicer*$^{Flox/+}$ mice (referred to here as *Dicer-KP* and *Dicer-BP* mice, respectively). These mice developed soft tissue sarcomas at the site of Adeno-Cre injection with similar kinetics to their littermate controls with wildtype Dicer (Figure 16A-B). Western blot analysis of sarcoma cell lines derived from *Dicer-KP* and *Dicer-BP* mice showed decreased Dicer protein levels compared to sarcomas from *KP* and *BP* mice (Figure 16C). I also confirmed that recombination of the *Dicer*^{Flox} allele occurred in all sarcomas examined by PCR genotyping of genomic DNA from primary tumors (Figure 16D).

Previous studies have suggested that decreased miRNA expression from knockdown of Dicer or other components of the miRNA biogenesis machinery enhances tumor cell proliferation both *in vitro* and *in vivo* [160]. Therefore, I examined hematoxylin and eosin stained sections of sarcomas from *KP*, *Dicer-KP*, *BP* and *Dicer-BP* mice and scored the frequency of mitotic figures. I found a significant increase in mitoses per field in *Dicer-KP* mutant sarcomas compared to *KP* littermate controls (Figure 16E-F). In contrast, no increase in mitotic rate was observed in sarcomas from *Dicer-BP* mice compared to *BP* littermate controls. Interestingly, the mitotic rate in the sarcomas from *BP* and *Dicer-BP* mice was similar to *KP* mice with wildtype Dicer. In an independent assay to assess proliferation in these sarcomas, I performed immunohistochemistry for the proliferation marker *Ki67*, and quantified the data through automated counting. Similar to the results from scoring mitoses, sarcomas from *Dicer-KP* mice had a significantly higher *Ki67* index compared to sarcomas from *KP*, *BP* or *Dicer-BP* mice (Figure 16G-H).

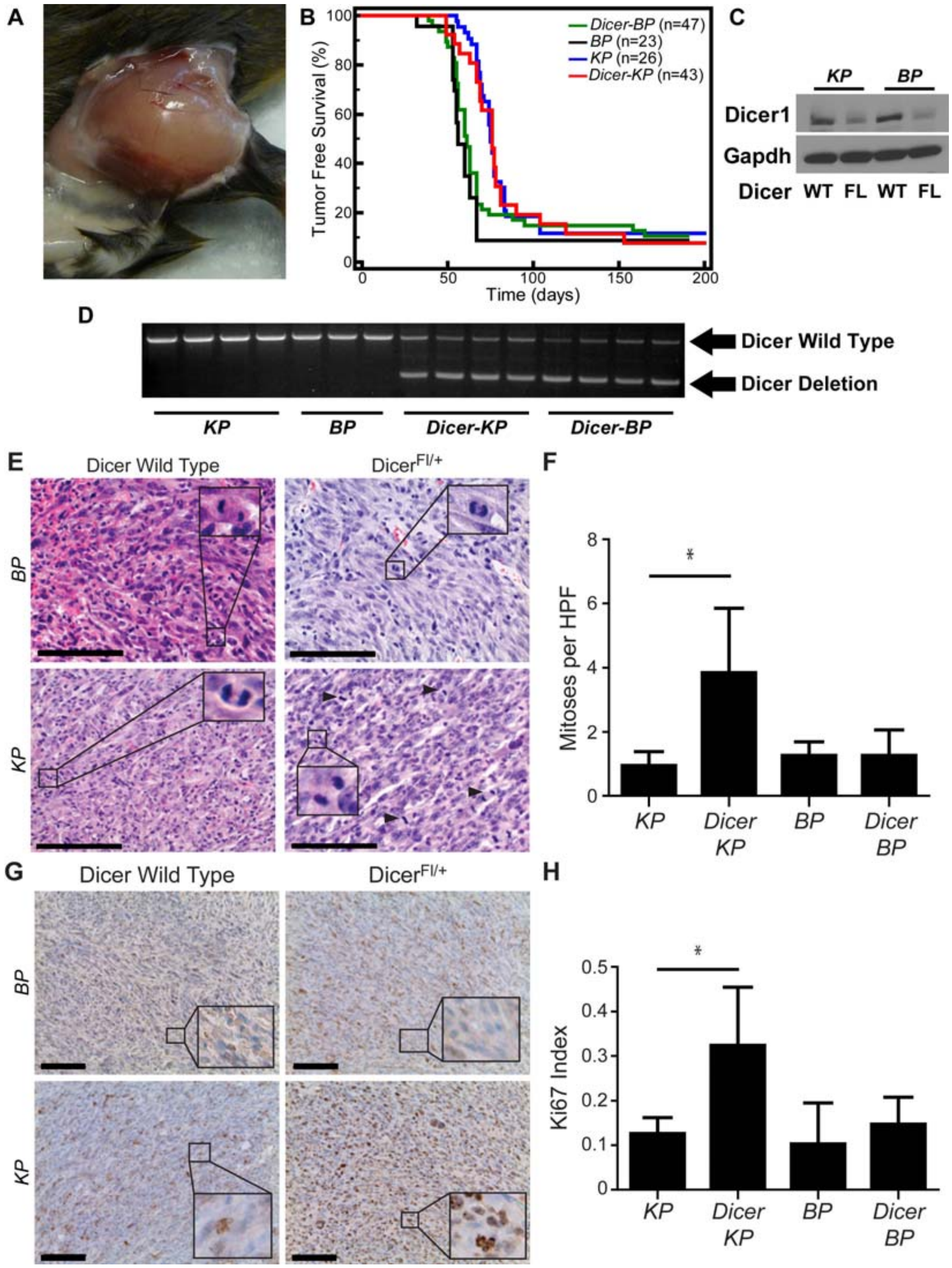

Figure 16: Deletion of One Allele of Dicer Alters Tumor Proliferation in a Genotype Dependent Manner.

Figure 16: Deletion of one allele of Dicer alters tumor proliferation in a genotype dependent manner. *Dicer-KP* and *Dicer-BP* mice develop **(A)** sarcomas at the site of injection with **(B)** similar kinetics to *KP* and *BP* littermate controls. **(C)** Decreased Dicer protein levels in sarcoma cells derived from primary tumors from $Dicer^{Fl/+}$ mice. **(D)** $Dicer^{Fl/+}$ allele is efficiently recombined in sarcomas by PCR genotyping of genomic DNA from primary tumors. **(E-F)** Proliferation of sarcomas as measured by mitoses per high powered field (**E,** arrowheads denote additional mitotic figures in a field) was increased in sarcomas from *Dicer-KP* mice, but proliferation was not increased in sarcomas from *Dicer-BP* mice. **(G-H)** Similarly, staining for the proliferation marker Ki67 showed increased proliferation only in sarcomas from *Dicer-KP* mice (n=6, each genotype). Scale bars represent 100 microns, error bars represent SEM, * represent $p \leq 0.01$ by two-tailed T-test.

Dicer Haploinsufficiency Enhances Metastasis and Decreases Mature miRNA Expression in a Genotype Dependent Manner

Increased tumor proliferation has been linked to worse outcomes in a number of human tumor types including soft tissue sarcomas [161]. Thus, I hypothesized that sarcomas in *Dicer-KP* mice may have increased rates of distant metastases, which are the most common cause of death in sarcoma patients. To test this hypothesis, a cohort of compound conditional mutant *Dicer-KP* and *Dicer-BP* mice and their littermate *KP* and *BP* controls were used to generate primary tumors in the distal hind limb. When sarcomas reached approximately 500 mm^3 in volume, they were removed by transfemoral amputation. These mice were then followed for a minimum of 6 months for the development of distant metastases, which occurred most frequently in the lungs (Fig 17A), but also to the body wall and soft tissues (Figure 17B, Table 5). Cellular morphology was maintained between primary (Figure 17C) and metastatic lesions (Figure 17D).

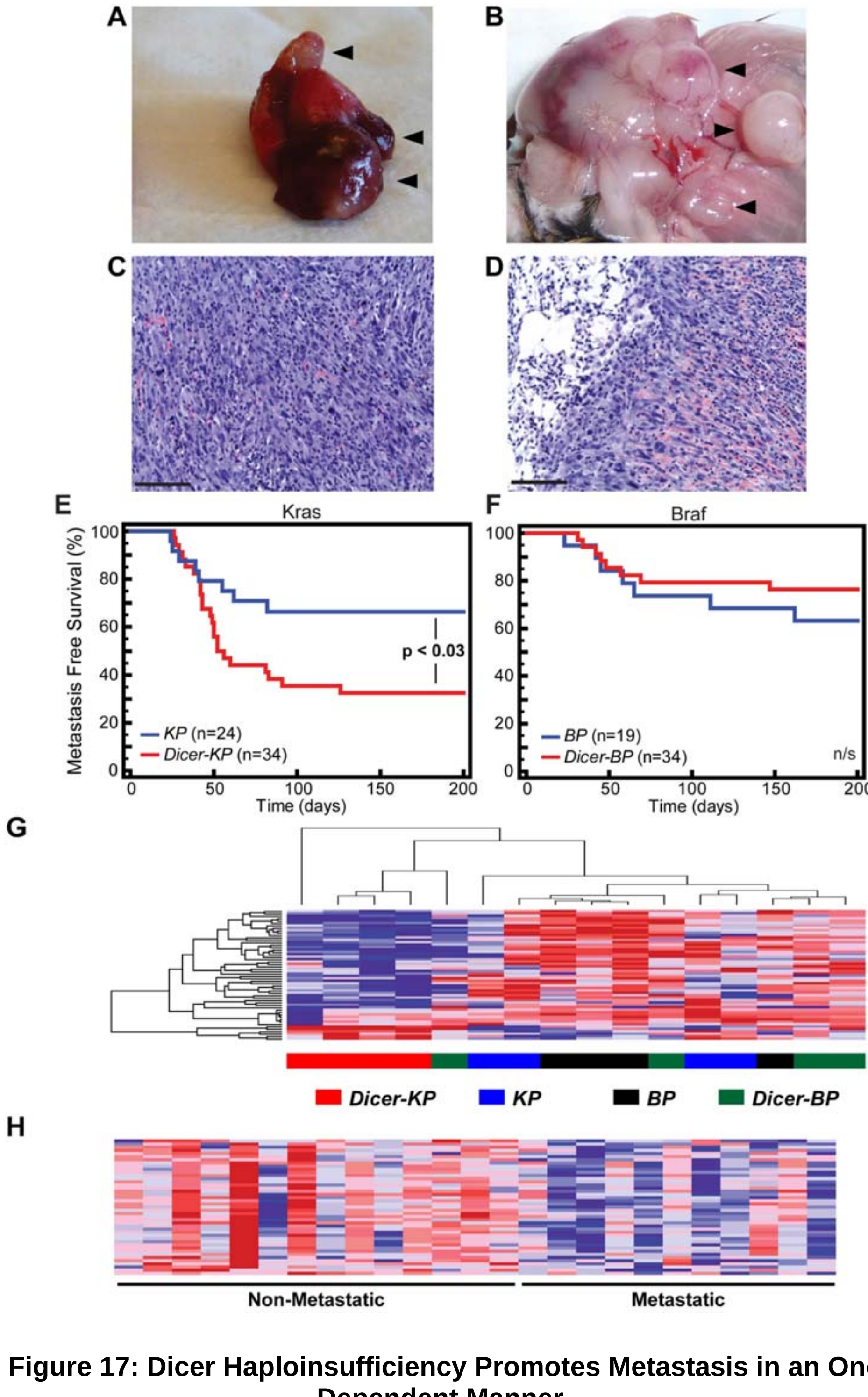

Figure 17: Dicer Haploinsufficiency Promotes Metastasis in an Oncogene Dependent Manner

Figure 17: Dicer haploinsufficiency promotes metastasis in an oncogene dependent manner. Sarcomas from *Dicer-KP* and *Dicer-BP* mice develop distant metastases to both the **(A)** lung and **(B)** body wall (metastases noted by arrow head), while the morphology of **(C)** primary sarcomas is maintained in **(D)** distant metastases. **(E)** Dicer haploinsufficiency enhances metastatic spread of $Kras^{G12D}$ mutant tumors with low MAPK signaling, while **(F)** $Braf^{V600E}$ mutant tumors with high MAPK signaling were protected from Dicer haploinsufficiency promoting metastasis. **(G)** Significant loss of miRNA expression was only observed in sarcomas from *Dicer-KP* mice ($p \leq 0.05$). **(H)** Loss of miRNA expression in human UPS is associated with the development of distant metastases.

Table 5: Primary Sarcomas in *Dicer-KP* Mice Metastasize to More Varied Locations than Sarcomas in *KP*, *BP*, or *Dicer-BP* Mice

Table 5: Primary sarcomas in *Dicer-KP* mice metastasize to more varied locations than sarcomas in *KP*, *BP*, or *Dicer-BP* mice. Metastases to multiple sites within a mouse were included. Intraperitoneal metastases include those to the liver or spleen. Soft tissue metastases included those to the thoracic body wall. Fractions represent number of mice with lesions to the metastatic site over all mice of the specified genotype with distant metastasis.

			Metastatic Site		
Mouse Genotype	Total # of mice	Total # of Mice with Metastases	Lung	Soft Tissue	Intraperitoneal
KP	*24*	*8*	7/8	1/8	1/8
Dicer-KP	*34*	*22*	18/22	5/22	11/22
BP	*19*	*7*	7/7	0/7	0/7
Dicer-BP	*34*	*8*	8/8	0/8	1/8

Sarcomas in *Dicer-KP* mice had a significant increase in the rate of metastatic progression compared to their littermate *KP* controls (Figure 17E, $p < 0.03$). In contrast, the rate of distant metastasis in *Dicer-BP* mice was similar to the rate of metastasis in *BP* mice (Figure 17F). Therefore, Dicer haploinsufficiency enhances metastasis in a genotype dependent manner. To explore the mechanism through which *Dicer-KP* mice are at increased risk for the development of distant metastases, I isolated RNA from primary tumors and profiled the expression of mature miRNAs from *Dicer-KP, KP, Dicer-BP* and *BP* mice. miRNA profiling revealed significant loss of miRNA expression in *Dicer-KP* mice compared to the other genotypes (Figure 17G and Appendix E, $p \leq 0.05$). Taken together, these results suggest that oncogene dependent alterations in MAPK signaling can regulate miRNA biogenesis to promote the development of distant metastases.

Decreased miRNA Expression is Associated With the Development of Distant Metastases in Human Sarcoma

Because the sarcomas that develop in *KP* mice are similar to human UPS [162] and loss of miRNA expression through Dicer haploinsufficiency can promote the development of metastases from sarcomas in *KP* mice, I used Taqman PCR arrays to examine the expression of miRNAs in primary human UPS with known metastatic outcome. Similar to my observations in the *KP* mouse model of UPS, human UPS exhibited loss of mature miRNA expression in primary tumors that subsequently developed distant metastases (Figure 17H,

Appendix F). These results indicate that loss of miRNA expression is associated with the development of distant metastases in human soft tissue sarcomas.

MAPK Signaling Regulates miRNA Processing Through Dgcr8

To study the mechanism through which MAPK signaling regulates miRNA biogenesis *in vivo*, I examined the expression of components of the miRNA biogenesis machinery in sarcomas from *KP* and *BP* mice and found increased Dgcr8 expression in sarcomas from *BP* mice (Figure 18A). To determine if the changes in Dgcr8 levels were MAPK specific, I used sarcoma cell lines derived from *KP* mice and infected them with a retrovirus that expressed a constitutively active MEK. Overexpression of activated MEK resulted in increased levels of Dgcr8, but little change to its binding partner Drosha (Figure 18B). In addition, I treated sarcoma cells derived from *KP* mice with the MEK inhibitor PD98059 and measured the expression of various proteins involved in miRNA biogenesis including: Dgcr8, Drosha, Trbp and Dicer. Inhibition of MEK resulted in decreased levels of Dgcr8 protein (Figure 18C). Additionally, in this system, MEK inhibition did not significantly alter levels of Dicer or its binding partner Trbp (Figure 18D). Treatment of allograft soft tissue sarcomas derived from $Kras^{G12D}$; $Ink4/Arf^{Flox/Flox}$ mice using a different MEK inhibitor with *in vivo* activity, PD325901, resulted in significant decreases in Dgcr8 protein levels *in vivo* (Figure 18E). To investigate the mechanism through which MEK inhibition decreases Dgcr8 protein, I performed Q-RT-PCR for Dgcr8 in sarcoma cells and allograft tumors. I found that treatment with the MEK inhibitors decreased levels of Dgcr8 mRNA (Figure 18F).

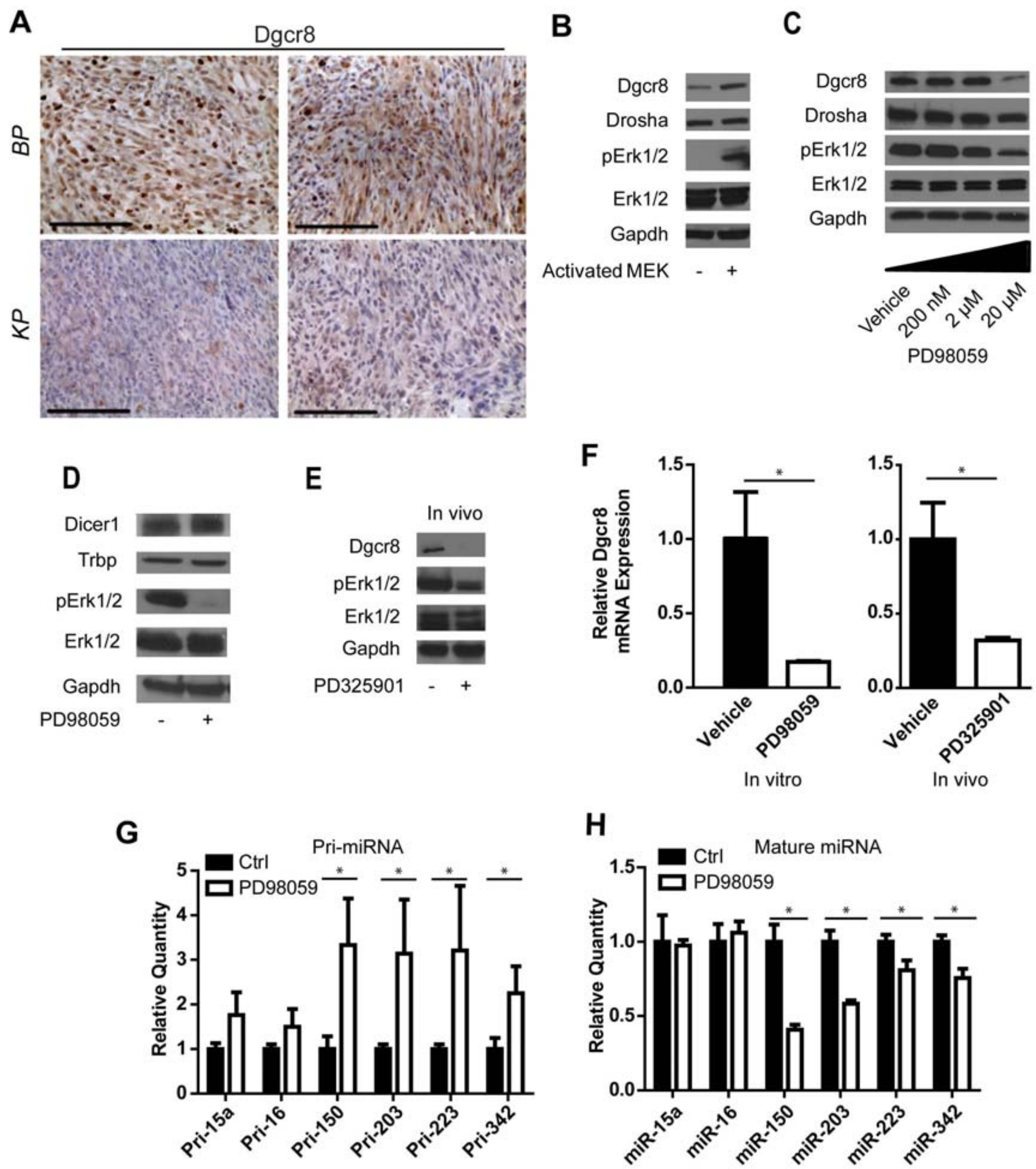

Figure 18: MAPK Signaling Regulates Dgcr8 Expression

Figure 18: MAPK signaling regulates Dgcr8 expression. (A) Elevated Dgcr8 expression was consistently detected by IHC in Braf mutant sarcomas compared to Kras driven sarcomas. **(B)** Expression of a constitutively active MEK increases steady state levels of Dgcr8 in sarcoma cell lines from *KP* mice. MEK inhibition decreases Dgcr8 expression in **(C)** sarcoma cells *in vitro,* but does not alter levels of **(D)** Trbp or Dicer. **(E)** Similarly, in primary sarcoma allografts *in vivo*, Dgcr8 is decreased by MEK inhibition (Drosha was not detected in tumor samples in **E**). **(F)** Inhibition of MAPK signaling decreases levels of Dgcr8 mRNA both *in vitro* and *in vivo*. In a number of pri-miRNA and mature miRNAs pairs, inhibition of MEK leads to **(G)** accumulation of pri-miRNA transcripts and **(H)** decreased mature miRNAs. Error bars represent SD from the mean, * denotes significance with $p \leq 0.05$ by two-tailed T-test. All cell line experiments represent results from at least 3 independent sarcoma cell lines.

To determine if MEK inhibition altered pri-miRNA processing through effects on the microprocessor, I again studied six miRNAs, which have been implicated in tumor progression, by measuring levels of pri-miRNAs and their mature miRNAs products. In a number of the miRNAs screened, MEK inhibition significantly increased the level of pri-miRNAs (Figure 18G) and decreased the levels of mature miRNAs (Figure 18H), thereby altering the ratio of mature to pri-miRNA. This observation implies that MEK inhibition reduces miRNA processing efficiency. Taken together, these results suggest that MAPK dependent transcriptional regulation of Dgcr8 controls the efficiency of the microprocessor to regulate miRNA biogenesis.

Rreb1 Mediates MAPK Dependent Expression of Dgcr8

In order to identify potential mediators of MAPK signaling responsible for Dgcr8 expression, I cloned a segment of the Dgcr8 promoter into a luciferase reporter vector. Deletional analysis of the Dgcr8 promoter indicated that transcriptional activity was regulated by a region approximately 260-518 bps upstream of the transcriptional start site of Dgcr8 (Figure 19A). Analysis of this region identified several potential MAPK regulated transcription factor binding sites. In order to screen for potential regulators, I performed Q-RT-PCR on a panel of primary soft tissue sarcomas from *KP* mice to correlate the expression of Dgcr8 with candidate transcription factors and found Rreb1 mRNA expression to be highly correlated with Dgcr8 mRNA levels in primary sarcomas (Figure 19B, $p < 0.0001$). To investigate whether Rreb1 may regulate the Dgcr8 promoter, I performed site directed mutagenesis of the putative Rreb1 binding site and transfected the mutant and wildtype luciferase reporters into the mouse sarcoma cells. Mutation of the Rreb1 binding site led to decreased luciferase activity (Figure 19C-D, $p < 0.01$). Moreover, in sarcoma cells from *KP* mice, chromatin immunoprecipitation of endogenous Rreb1 showed specific binding of Rreb1 at the Dgcr8 promoter (Figure 19E). To test if there is a functional relationship between Rreb1 and Dgcr8, I overexpressed Rreb1 in HEK293T cells, which resulted in increased levels of DGCR8 (Figure 19F). In addition, knockdown of endogenous Rreb1 in sarcoma cells from *KP* mice resulted in reduced levels of Dgcr8 (Figure 18G). These results suggest a direct link between MAPK signaling and Dgcr8 levels through Rreb1.

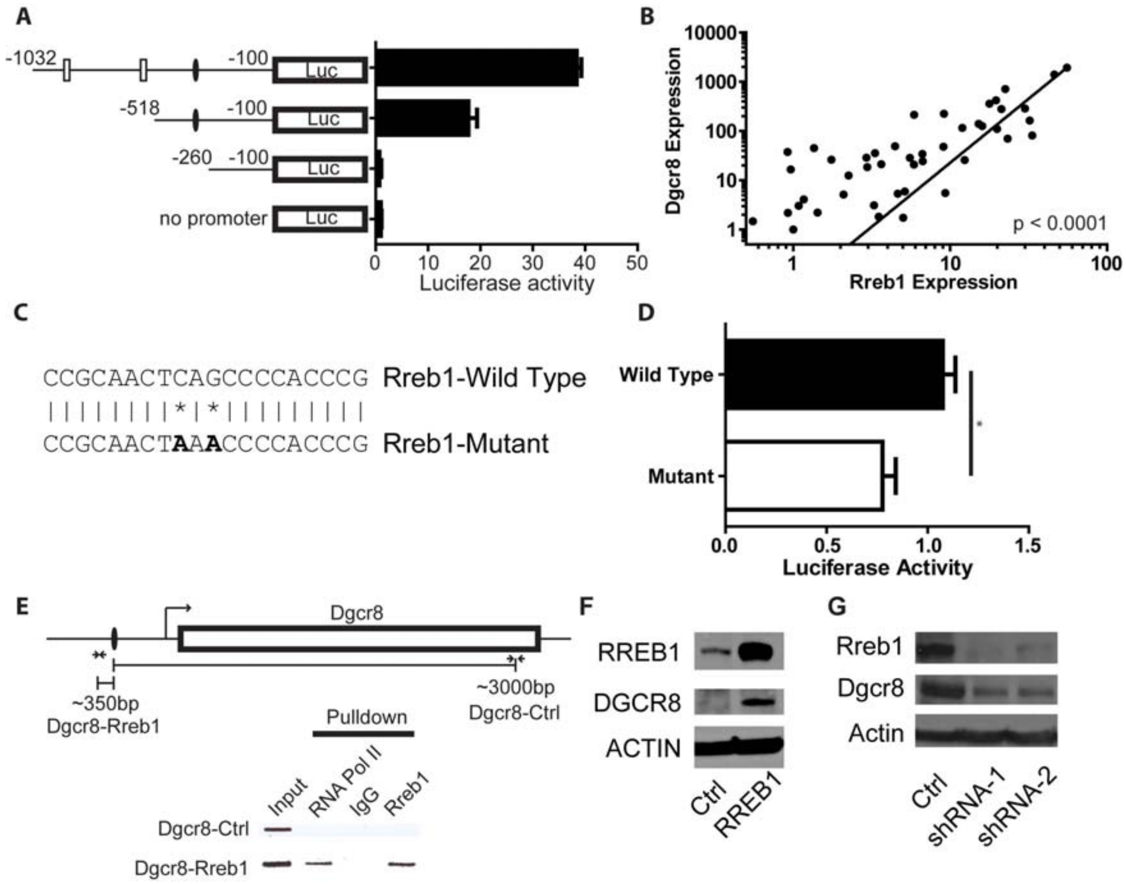

Figure 19: RREB1 is a Transcriptional Activator of Dgcr8.

Figure 19: RREB1 is a transcriptional activator of Dgcr8. (A) Promoter analysis of the Dgcr8 promoter using luciferase assay identified a small ~250 bp region upstream of Dgcr8 that regulates luciferase expression in sarcoma cell lines (black oval represents canonical Rreb1 site, white rectangles represent non-canonical Rreb1 sites). **(B)** Expression of Rreb1 is highly correlated with Dgcr8 expression in a panel of primary mouse sarcomas from *KP* mice (circles represent individual tumors, n=45, p < 0.0001). **(C-D)** Site directed mutagenesis of a putative Rreb1 binding site (black oval in A) in the -518 to -100 Dgcr8 promoter construct decreases Luciferase reporter activity. **(E)** Chromatin immunoprecipitation of endogenous Rreb1 from mouse sarcoma cells showed specific binding to the Dgcr8 promoter (Dgcr8-Rreb1) compared to isotype control (IgG) and compared to downstream control primers (Dgcr8-Ctrl). **(F)** Overexpression of Rreb1 in HEK293T cells results in increased levels of DGCR8, while **(G)** knockdown of endogenous Rreb1 in sarcoma cells from *KP* mice resulted in decreased Dgcr8 protein. * represents p $\leq$ 0.01 by two-tailed T-test. Line fit in **(B)** represents log-log line fit.

5.4 – Discussion

The mechanisms underlying the regulation of proteins that control miRNA processing are slowly being unraveled. To date, relatively little is known about the regulation of Dgcr8. Dgcr8 has been shown to be critical for the processing of pri-miRNAs [136] along with the ribonuclease Drosha [163]. Studies of human tumor samples with elevated levels of Drosha only showed significant increases in one miRNA (miR-31) [164], suggesting that levels of Drosha may not be rate limiting for miRNA biogenesis. Others have suggested that Dgcr8 acts in higher order complexes with pri-miRNAs to recruit Drosha to cleave pri-miRNAs [165]. Thus, Dgcr8 may be rate limiting for miRNA biogenesis and excess Dgcr8 in the setting of tumor cells may increase miRNA processing.

MAPK Dependent Regulation of Dgcr8

I have demonstrated that MAPK signaling regulates Dgcr8 through the Ras effecter Rreb1. Inhibition of MAPK signaling resulted in decreased levels of Dgcr8, and decreased pri-miRNA processing by the microprocessor. Others have identified Rreb1 as a negative regulator of miR-143/145, which can feedback to inhibit Ras signaling [88]. In addition, Rreb1 can inhibit the *Ink4a/ARF* tumor suppressor [166], suggesting that Rreb1 acts as an oncogene. Conversely, others have shown that Rreb1 can induce p53 in response to DNA damage, suggesting that in this context Rreb1 may also have a role as a tumor suppressor [167]. My data indicate that elevated MAPK signaling can act through Rreb1 to promote pri-miRNA processing through direct transcriptional control of Dgcr8 (Figure 18-19). Increased levels of Dgcr8 increase pri-miRNA processing by providing additional Dgcr8 that can counteract the effects of loss of function mutations in other components of the miRNA biogenesis machinery.

Oncogenic Mutations Can Cooperate to Alter miRNA Biogenesis

I have described one mechanism that regulates the levels of Dgcr8 protein through MAPK-Rreb1 dependent regulation of Dgcr8 transcription. My results in a primary mouse model of soft tissue sarcoma show that mutations in components of the miRNA biogenesis machinery can alter the natural history of tumors by increasing cell proliferation and the development of distant metastases in a genotype dependent manner. In human cancers, decreased levels of mature miRNAs have been linked to tumorgenesis [141] as well as the development of metastases in hepatocellular carcinoma [143]. I have also found decreased miRNA expression in human soft tissue sarcomas that subsequently metastasize (Figure 17H, Appendix F). My data suggest that decreases in miRNA levels between tumor types can be partially suppressed through enhanced MAPK signaling. For instance, this increased signaling can be provided by oncogenic mutations that strongly activate the MAPK cascade such as mutations in *Braf*, which are less susceptible to feedback inhibition from downstream Sprouty and other proteins [157]. Conversely, tumors with relatively lower levels of MAPK signaling, such as those with *Kras* mutation, have lower basal miRNA processing activity as well as decreased steady state levels of mature miRNAs. Therefore, as I have observed in primary sarcomas in mice, *Kras* mutant tumors may be more susceptible to mutations in other components of the miRNA biogenesis pathway, such as Dicer, resulting in decreases in miRNA levels to promote tumor proliferation and metastasis.

The ability of mutations in Dicer to increase cell proliferation and metastasis are likely due to the combined downregulation of a number of miRNAs rather than loss of a specific miRNA. Indeed, my data show that several miRNAs are downregulated by Dicer haploinsufficiency in sarcomas from *Dicer-KP* mice (Figure 17G and Appendix E). Moreover, the downregulated miRNAs that are most important for increasing proliferation and promoting metastasis may vary between tumors depending on the specific gene mutations that are driving cancer growth. For instance, miR-146a has been shown to suppress cancer cell invasion by targeting NF-KappaB and IRAK-1 [168]. Therefore, decreased miR-146a expression may be particularly important for promoting tumor progression in cancers with NF-KappaB pathway mutations.

A Model for MAPK Dependent Regulation of miRNA Biogenesis

miRNA expression is frequently altered in a number of disease states, including cancer [169]. Understanding the regulatory framework for miRNA expression may have important implications for therapeutic interventions that target specific signaling pathways. Based on my data, I suggest a model where increased MAPK signaling can promote miRNA processing at multiple steps. My data show that in soft tissue sarcomas, the MAPK pathway target Rreb1 can directly bind to the Dgcr8 promoter to increase Dgcr8 expression, which can promote miRNA biogenesis at the level of the microprocessor. Although I did not observe changes in the levels of endogenous Trbp and Dicer after MEK inhibition in sarcoma cells (Figure 18D), others have described Trbp as a MAPK target that promotes miRNA biogenesis by stabilizing its binding partner Dicer [153]. These data suggest that, depending on the cellular context, MAPK signaling can regulate both the initial entry into the miRNA biogenesis pathway by increasing Dgcr8 levels and the final cleavage through direct phosphorylation and stabilization of the Trbp/Dicer complex to generate mature miRNAs (Figure 20). Remarkably, I find that in tumors with relatively low MAPK signaling, and less efficient miRNA processing, mutation in Dicer lowers the level of mature miRNAs below a critical threshold to increase tumor proliferation and the development of distant metastases. Because increased MAPK signaling can suppress Dicer haploinsufficiency from promoting metastasis, mutation of one allele of Dicer may only have a modest effect on miRNA biogenesis when Dicer mutation occurs in tumors with high levels of MAPK signaling as a result of increased miRNA processing through Trbp and/or the microprocessor.

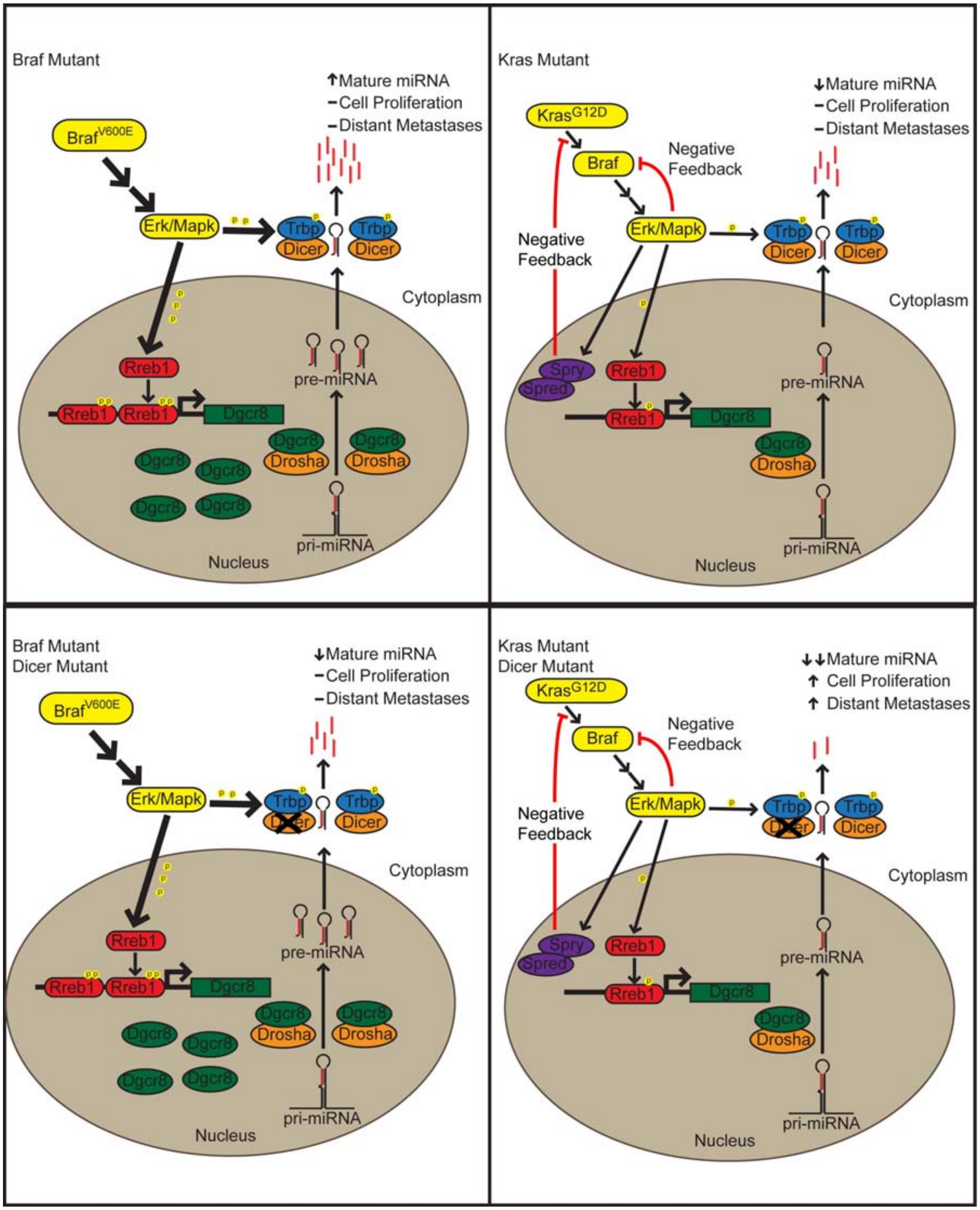

Figure 20: A Model of MAPK Dependent Regulation of miRNA Biogenesis

Finally, my data may have important prognostic and therapeutic implications for cancer. I have observed that loss of miRNA expression in primary sarcomas is linked to the subsequent development of distant metastases. If this finding is replicated in other data sets, then miRNA downregulation may help identify sarcomas at high risk for metastasis. In addition, as MEK inhibitors are being tested in the clinic, my results raise the possibility that if tumors with specific gene mutations are treated with MEK inhibitors, miRNA expression could decrease below a threshold that promotes metastasis. Therefore, additional studies are warranted to study the effects of therapeutic targeting of the MAPK pathway on miRNA processing and how this effects tumor progression.

6. Conclusion

The mouse is one of the best model systems to investigate cancer biology. Our understanding of both the human and mouse genomes has allowed the development of genetically engineered mouse models to study cancer biology *in vivo*. By developing genetically engineered mouse models of cancers, it is possible to fill the gap between patient samples and cell culture reagents for pre-clinical development of compounds and new therapies for rare cancers such as soft tissue sarcoma.

However, there are still limitations to using genetically engineered mouse models of cancer. Primary tumors that develop in genetically engineered mouse models generally take longer to develop compared to allograft or xenograft tumors. Additionally, primary tumors develop in an asynchronous fashion such that enrolling a large number of mice in any study often requires several months to accrue a sufficient number of animals. Furthermore, although the animals all have the same initiating mutations, tumors rapidly diverge and give rise to significant tumor heterogeneity within and between tumors. This is most powerfully illustrated by the development of distant metastases from sarcomas in *KP* mice, which occur in approximately 40% of mice (Figure 17). Although mutations that are made at the time of tumor initiation, such as those in *Dicer*, can certainly affect tumor progression by enhancing tumor proliferation (Figure 17), even these mutations lead to variable outcomes as not all sarcomas in *Dicer-KP* mice give rise to distant metastases. Still, even with these limitations, genetically engineered mouse models offer advantages to xenograft systems that make them compelling model systems.

Perhaps the most obvious advantage of genetically engineered mouse models is the presence of an intact immune systems. Our understanding of the microenvironment's influence on tumorgenesis and progression has increased dramatically in the past ten years [170]. The ability to generate tumors in their native microenvironment provides an ideal system to study early events in tumor initiation that are not possible with xenograft systems. Furthermore, interaction between the microenvironment and tumor parenchymal cells can be examined. Indeed, recent studies have begun to identify oncogenic mutations within stromal cells [171] suggesting that the tumor and stromal cells evolve in tandem. The opportunity to study this evolution *in vivo* is a significant advance. Moreover, with recent advances in dual-recombinase technology [172], it will also be possible to modify the microenvironment *in vivo* by initiating tumors using one recombinase system, such as *Flp/FRT*, and altering genes within the microenvironment using *Cre/loxP* technology.

In this dissertation, I have characterized a mouse model of soft tissue sarcoma generated by conditional mutations in *Kras* and the tumor suppressor *p53*. This model has several advantages over many others animal models described in the introduction. When I examined the molecular features of these tumors using gene expression data, tumors in *KP* mice most closely resemble human UPS. As UPS is one of the most common soft tissue sarcomas of adulthood, this model will likely have broad applicability to study soft tissue sarcoma biology. Additionally, the ability to spatially and temporally restrict sarcoma development makes this an ideal system to perform preclinical studies. As I have demonstrated, these are particularly advantageous traits for developing a mouse model for testing intraoperative imaging techniques. Because these mice have an immune system, in the future we may be able to take advantage of the immune system to treat cancer, such as enhancing tumor labeling with specific molecular imaging agents. Furthermore, due to its propensity to metastasize to a single metastatic site, this model is ideal for studying all the events involved in metastasis including miRNA mediated metastatic progression. With the use of reporter alleles, such as the *Rosa26*^{YFP} mice, one may be able to study all steps in metastatic spread including local invasion, hematogenous dissemination, arrest, extravasation and growth in a distant site and the molecular mechanisms underlying them. Furthermore, in the future, utilizing dual recombinase technology will allow others to modify the tumor microenvironment to dissect mechanisms underlying metastasis and treatment response to targeted therapies in both soft tissue sarcomas and other autochthonous mouse models of cancer.

Appendix A: Mouse Synovial Sarcoma Geneset

2610039C10Rik	*Cpt1a*	*Gsta4*	*Ngfrap1*	*Sh3bgrl2*
5830411G16Rik	*Ctbp2*	*Hmgn3*	*Nipsnap1*	*Slc12a7*
9630031F12Rik	*Cyp51a1*	*Igsf4*	*Nlgn2*	*Slc39a6*
Aldh18a1	*Dna2l*	*Il17rc*	*Nme7*	*Smo*
Aplp1	*Dtx3*	*Inadl*	*Nr2f1*	*Tjp2*
Aw146242	*Efna3*	*Kcnk1*	*Nt5dc2*	*Tle3*
Bcl11a	*Ephb2*	*Kif23*	*Pbk*	*Tmem132a*
Bmp7	*Ephb3*	*Lhx1*	*Pcdhb3*	*Tmem30b*
Cachd1	*Evl*	*Lhx8*	*Pde9a*	*Tmsb10*
Cacna1g	*Fkbp10*	*Limd2*	*Prim1*	*Tnc*
Cbx4	*Fkbp1b*	*LOC630539*	*Ptprk*	*Trim37*
Ccna2	*Fndc4*	*LOC673890*	*Ptprs*	*Trim46*
Ccnd1	*Gad1*	*Man2c1*	*Purg*	*Trip6*
Cdc7	*Gcs1*	*Mdk*	*Rad18*	*Ttc3*
Cdk4	*Gli2*	*Melk*	*Rasl11b*	*Tuba3*
Cdk4	*Gmcl1*	*Mfap2*	*Rbbp8*	*Tubb*
Chst2	*Gmpr2*	*Msh6*	*Rfc5*	*Wbp5*
Clcn5	*Gpm6b*	*Msx1*	*Rgs19*	*Wnt5a*
Col16a1	*Gprasp1*	*Nfatc4*	*Sall2*	*Zfp90*
Col18a1	*Grik5*	*Ngfr*	*Scube2*	*Zic5*

Appendix B: Soft Tissue Sarcoma Geneset from *KP* Mice

2700099C18Rik	*Ccr1*	*Dbf4*	*Lhx8*	*Plscr1*
2810417H13Rik	*Ccr2*	*Depdc1a*	*LOC630539*	*Plscr2*
2810433K01Rik	*Ccr5*	*Dtl*	*Lpxn*	*Pmaip1*
9030408N13Rik	*Cd109*	*Ect2*	*Marcksl1*	*Prc1*
Agtr2	*Cdc2a*	*Edil3*	*Mcm5*	*Psat1*
Ai504432	*Cdc6*	*Ereg*	*Mcm6*	*Rbp1*
Aif1	*Cdca1*	*Esm1*	*Melk*	*Rin1*
Anln	*Cdca5*	*Fcgr1*	*Mki67*	*Rrm2*
Bcat1	*Cdh11*	*Fignl1*	*Mmp13*	*Shcbp1*
Birc5	*Cdkn2a*	*Foxm1*	*Mmp3*	*Slc25a24*
Bub1	*Cenpa*	*Gp49a*	*Ms4a11*	*Smc2*
C130076O07Rik	*Cenpe*	*Gpr34*	*Ms4a6d*	*Tfpi2*
C1qtnf3	*Cep55*	*Gpr65*	*Ms4a7*	*Timp1*
C79407	*Cks2*	*Gsg2*	*Nef3*	*Top2a*
Ccdc99	*Clec4n*	*Hells*	*Nefl*	*Tpbg*
Ccl12	*Crabp1*	*Hmga2*	*Nusap1*	*Trip13*
Ccl2	*Crabp2*	*Hmgb2*	*Pbk*	*Ttk*
Ccna2	*Cx3cr1*	*Ifi44*	*Phgdh*	*Tyms*
Ccnb1	*Cxcl10*	*Iqgap3*	*Plk4*	*Zfp7*
Ccnb2	*Cybb*	*Kif20a*	*Plscr1*	*Zwilch*

Appendix C: Human UPS Geneset

ABL2	*CDC2*	*FOSL1*	*LOC146909*	*PLOD2*	*SIAH2*
ACTR3	*CDC20*	*FOXM1*	*LPXN*	*POLR2K*	*SMC4*
ADAM12	*CDC45L*	*GLRX*	*LRRC59*	*POMP*	*SMS*
ADRM1	*CDCA8*	*GLRX2*	*M6PR*	*PPP2CA*	*SNRPA1*
AHCYL1	*CDR2*	*GMNN*	*M6PRBP1*	*PRDX1*	*SRM*
AKR1B1	*CEBPB*	*GNG5*	*MAD2L1*	*PSMA1*	*STK17A*
ALG3	*CENPA*	*GOLT1B*	*MAGOH*	*PSMA2*	*STK17B*
ANXA2	*CENPE*	*GPSM2*	*MAPK1*	*PSMA5*	*TAF10*
ANXA2P2	*CEP55*	*GSPT1*	*MAPRE1*	*PSMB2*	*TAGLN2*
ANXA5	*CFL1*	*GSTO1*	*MCM4*	*PSMC2*	*TARS*
ANXA7	*CGGBP1*	*H2AFZ*	*MELK*	*PSMD11*	*TFG*
AP2M1	*CKS2*	*HDGF*	*MICAL2*	*PSMD14*	*TFRC*
ARFGAP3	*CLIC1*	*HLA-DPA1*	*MICAL-L1*	*PSMD2*	*THOC7*
ARPC2	*CMPK*	*HMMR*	*MICB*	*PTP4A2*	*TMCO1*
ARPC5	*COMT*	*HNRPAB*	*MIF*	*PTTG1*	*TMEM50A*
ASPM	*COPG*	*HPRT1*	*MKI67*	*RAB27A*	*TNFRSF12A*
ATP6V0B	*CORO1C*	*HSPA1A*	*MME*	*RAN*	*TPMT*
ATP6V0C	*CREB3L1*	*HSPA1B*	*MRPL3*	*RANBP1*	*TPX2*
AURKA	*CRKL*	*HSPC171*	*MSN*	*RER1*	*TRAM2*
BAG3	*CYCS*	*IBRDC3*	*MYBL2*	*RIPK2*	*TTK*
BIRC5	*D15WSU75E*	*ICMT*	*MYH9*	*RPN1*	*TXNL2*
BUB3	*DAP*	*IMPAD1*	*NANS*	*RPP38*	*UBE2C*
C1ORF144	*DEK*	*JOSD1*	*NCAPG*	*RPRC1*	*UBE2L3*
C20ORF24	*DEPDC1*	*JTV1*	*NOLA3*	*RRAS2*	*UCK2*
C6ORF79	*DR1*	*K-ALPHA-1*	*NRBF2*	*RRM1*	*UFD1L*
CALU	*DRAP1*	*KCMF1*	*NUP37*	*RRM2*	*UGCG*
CAP1	*EEF1E1*	*KDELR2*	*P4HA2*	*S100A11*	*USP39*
CAPZB	*EFHD2*	*KDELR3*	*PDE4DIP*	*S100A6*	*VDAC1*
CCDC109B	*EIF2S2*	*KIAA0101*	*PFN1*	*SDC4*	*YARS*
CCNA2	*ENO1*	*KIF2C*	*PGK1*	*SDF2L1*	*YBX1*
CCNB1	*ENPP1*	*KIF4A*	*PHC2*	*SERP1*	
CCNB2	*EVI2A*	*KPNA1*	*PIGT*	*SERPINB8*	
CCNH	*FEN1*	*LDHA*	*PKM2*	*SH3BGRL3*	
CD58	*FLOT1*	*LGALS1*	*PLAU*	*SH3GLB1*	

Appendix D: Sarcomas in *BP* mice Express Higher Levels of miRNAs than Sarcomas in *KP* Mice

MicroRNA	Fold-change	p-value	FDR
mmu-miR-615-5p	16.69	0.0395	0.045
mmu-miR-429	14.16	0.0004	0.0043
mmu-miR-200a	13.66	0.0021	0.0106
mmu-miR-433	12.11	0.0249	0.0372
mmu-miR-431	11.59	0.0338	0.0447
mmu-miR-184	10.12	0.0034	0.012
mmu-miR-323-3p	9.3	0.0156	0.0295
mmu-miR-511	8.45	0.0214	0.0357
mmu-miR-146b	8.17	0.00004	0.002
mmu-miR-150	7.44	0.0009	0.0076
mmu-miR-218	7.33	0.0019	0.0102
mmu-miR-211	6.24	0.0382	0.045
mmu-miR-409-3p	5.98	0.0248	0.0372
mmu-miR-339-3p	5.93	0.0206	0.0352
mmu-miR-200b	5.04	0.0018	0.0102
mmu-miR-191	4.9	0.00006	0.002
mmu-miR-223	4.85	0.0034	0.012
mmu-miR-342-3p	4.77	0.0002	0.0043
mmu-miR-187	4.7	0.0234	0.0364
mmu-miR-369-5p	4.7	0.0424	0.045
mmu-miR-146a	4.57	0.0128	0.0255
mmu-miR-539	4.56	0.0363	0.045
mmu-miR-380-5p	4.52	0.0427	0.045
mmu-miR-434-3p	4.46	0.0105	0.023
mmu-miR-155	4.33	0.0004	0.0043
mmu-miR-200c	4.1	0.0043	0.0141
mmu-miR-138	3.78	0.038	0.045
mmu-miR-294	3.6	0.0411	0.045
mmu-miR-196b	3.5	0.0337	0.0447
mmu-miR-339-3p	3.38	0.0049	0.0141

MicroRNA	Fold-change	p-value	FDR
mmu-miR-126-3p	3.35	0.0031	0.012
mmu-miR-574-3p	3.22	0.0049	0.0141
mmu-miR-148a	2.89	0.0122	0.0251
mmu-miR-425	2.66	0.005	0.0141
mmu-miR-31	2.65	0.0004	0.0043
mmu-miR-186	2.61	0.0093	0.0217
mmu-miR-34b-3p	2.5	0.0029	0.012
mmu-miR-125a-5p	2.47	0.0047	0.0141
mmu-miR-148a	2.89	0.0122	0.0251
mmu-miR-425	2.66	0.005	0.0141
mmu-miR-31	2.65	0.0004	0.0043
mmu-miR-186	2.61	0.0093	0.0217
mmu-miR-34b-3p	2.5	0.0029	0.012
mmu-miR-125a-5p	2.47	0.0047	0.0141
mmu-miR-10a	2.44	0.0183	0.0335
mmu-miR-16	2.41	0.0097	0.0219
mmu-miR-340-3p	2.37	0.0299	0.0427
mmu-miR-214	2.28	0.0226	0.0359
mmu-miR-203	2.24	0.0222	0.0359
mmu-miR-222	2.18	0.0018	0.0102
mmu-miR-199a-3p	2.18	0.0444	0.045
mmu-miR-196c	2.15	0.0439	0.045
mmu-miR-20b	2.1	0.0347	0.0449
mmu-miR-30a	2.05	0.0034	0.012
mmu-miR-30d	1.99	0.0087	0.0217
mmu-miR-194	1.9	0.0092	0.0217
mmu-miR-674	1.88	0.0425	0.045
mmu-miR-30b	1.72	0.0109	0.023
mmu-miR-484	1.72	0.0417	0.045
mmu-miR-491	1.62	0.0409	0.045
mmu-miR-148b	1.59	0.0355	0.045
mmu-miR-192	1.52	0.0432	0.045
mmu-miR-30c	1.49	0.04	0.045
mmu-let-7d	1.46	0.0483	0.0483
mmu-miR-23b	0.55	0.0025	0.0115
mmu-miR-27b	0.52	0.001	0.0076

MicroRNA	Fold-change	p-value	FDR
mmu-miR-328	0.48	0.0017	0.0102
mmu-miR-486	0.44	0.0263	0.0383
mmu-miR-128a	0.4	0.0187	0.0335
mmu-miR-532-5p	0.33	0.0327	0.0447
mmu-miR-335-3p	0.29	0.0153	0.0295
mmu-miR-582-5p	0.2	0.0191	0.0335
mmu-miR-741	0.19	0.0059	0.0152
mmu-miR-298	0.18	0.0056	0.0152
mmu-miR-675-3p	0.16	0.0316	0.0442
mmu-miR-296-5p	0.15	0.0004	0.0043

Appendix D: Sarcomas in *BP* mice express higher levels of miRNAs than sarcomas in *KP* mice by Taqman PCR array. Fold-change represents the ratio of expression between tumors from *BP* and *KP* mice. P-value was determined by two tailed T-test. Significance was determined by $p < 0.05$ and FDR < 0.25.

Appendix E: Sarcomas from *Dicer-KP* Mice Have Significantly Lower Levels of Mature miRNAs

MicroRNA	Fold-change	p-value	FDR
mmu-miR-298	47.15	0.016647	0.154
mmu-miR-685	36.83	0.014079	0.154
mmu-miR-680	7.84	0.045983	0.233
mmu-miR-296-5p	6.04	0.016104	0.154
mmu-miR-207	5.77	0.039073	0.233
mmu-miR-532-5p	3.87	0.046963	0.233
mmu-miR-331-3p	0.65	0.021164	0.17
mmu-miR-92a	0.61	0.032118	0.206
mmu-miR-126-5p	0.6	0.045003	0.233
mmu-let-7f	0.58	0.020162	0.168
mmu-let-7a	0.55	0.009702	0.154
mmu-miR-151-3p	0.55	0.011331	0.154
mmu-miR-214	0.55	0.016764	0.154
mmu-miR-221	0.54	0.028577	0.193
mmu-miR-20b	0.51	0.020233	0.168
mmu-miR-125a-5p	0.49	0.005672	0.133
mmu-miR-320	0.48	0.041889	0.233
mmu-miR-186	0.47	0.030028	0.198
mmu-miR-126-3p	0.44	0.008679	0.154
mmu-miR-484	0.44	0.008864	0.154
mmu-miR-142-3p	0.44	0.014746	0.154
mmu-miR-196c	0.44	0.042665	0.233
mmu-miR-337-5p	0.42	0.049747	0.236
mmu-miR-340-3p	0.4	0.001127	0.0483
mmu-miR-337-3p	0.38	0.009039	0.154
mmu-miR-34b-3p	0.37	0.008639	0.154
mmu-miR-339-3p	0.34	0.010458	0.154
mmu-miR-138	0.34	0.028487	0.193

MicroRNA	Fold-change	p-value	FDR
mmu-miR-574-3p	0.32	0.022861	0.178
mmu-miR-2227	0.31	0.000313	0.0412
mmu-miR-191	0.3	0.013363	0.154
mmu-miR-339-3p	0.3	0.014983	0.154
mmu-miR-495	0.3	0.015139	0.154
mmu-miR-134	0.27	0.024936	0.188
mmu-miR-146a	0.25	0.004103	0.105
mmu-miR-615-5p	0.21	0.013136	0.154
mmu-miR-150	0.21	0.026572	0.191
mmu-miR-223	0.2	0.000747	0.0449
mmu-miR-129	0.17	0.000358	0.0412

Appendix E: Sarcomas from *Dicer-KP* mice have significantly lower levels of mature miRNAs compared to sarcomas from *KP*, *BP*, and *Dicer-BP* mice by Taqman PCR array. Fold-change represents the ratio of expression between Dicer-KP tumors and KP, BP and Dicer-BP tumors. P-value was determined by two tailed T-test. Significance was determined by $p < 0.05$ and FDR < 0.25.

Appendix F: Human Soft Tissue Sarcomas that Give Rise to Distant Metastases Lose Expression of Mature miRNAs

MicroRNA	Fold-change	p-value	FDR
hsa-miR-518b	0.12	0.009	0.151
hsa-miR-511	0.13	0.003	0.151
hsa-miR-629	0.17	0.006	0.151
hsa-miR-150	0.19	0.015	0.151
hsa-miR-146a	0.2	0.005	0.151
hsa-miR-519a	0.2	0.008	0.151
hsa-miR-223	0.2	0.013	0.151
hsa-miR-107	0.23	0.02	0.167
hsa-miR-627	0.24	0.007	0.151
hsa-miR-125a-3p	0.24	0.023	0.172
hsa-miR-140-3p	0.26	0.005	0.151
hsa-miR-126	0.26	0.015	0.151
hsa-miR-545	0.29	0.012	0.151
hsa-miR-489	0.29	0.035	0.206
hsa-miR-142-3p	0.3	0.01	0.151
hsa-miR-16	0.3	0.016	0.151
hsa-miR-21	0.3	0.019	0.164
hsa-miR-222	0.33	0.016	0.151
hsa-miR-148b	0.33	0.028	0.184
hsa-miR-196b	0.33	0.045	0.249
hsa-miR-454	0.34	0.014	0.151
hsa-miR-185	0.34	0.03	0.19
hsa-miR-342-3p	0.35	0.013	0.151
hsa-miR-191	0.35	0.014	0.151
hsa-miR-423-5p	0.35	0.028	0.184
hsa-miR-190	0.35	0.043	0.244
hsa-miR-29a	0.36	0.004	0.151
hsa-miR-103	0.37	0.006	0.151
hsa-miR-339-3p	0.37	0.026	0.184
hsa-miR-320	0.37	0.034	0.205

MicroRNA	Fold-change	p-value	FDR
hsa-miR-152	0.38	0.019	0.164
hsa-miR-197	0.39	0.002	0.151
hsa-miR-28-3p	0.39	0.013	0.151
hsa-miR-340	0.39	0.027	0.184
hsa-miR-186	0.4	0.011	0.151
hsa-miR-590-5p	0.41	0.023	0.172
hsa-miR-484	0.42	0.032	0.198
hsa-miR-125a-5p	0.44	0.011	0.151
hsa-miR-24	0.45	0.021	0.172
hsa-miR-374a	0.46	0.037	0.215
hsa-miR-574-3p	0.48	0.023	0.172

Appendix F: Human soft tissue sarcomas that give rise to distant metastases lose expression of mature miRNAs. Fold-change represents ratio of expression between metastatic and non-Metastatic primary soft tissue sarcomas. P-value was determined by two tailed T-test. Significance was determined by $p < 0.05$ and FDR < 0.25.

References

1. Siegel R, Naishadham D, & Jemal A (2012) Cancer statistics, 2012. *CA Cancer J Clin* 62(1):10-29.

2. Wibmer C, Leithner A, Zielonke N, Sperl M, & Windhager R (2010) Increasing incidence rates of soft tissue sarcomas? A population-based epidemiologic study and literature review. *Ann Oncol* 21(5):1106-1111.

3. Lawrence W, Jr., *et al.* (1987) Adult soft tissue sarcomas. A pattern of care survey of the American College of Surgeons. *Ann Surg* 205(4):349-359.

4. Suit HD*, et al.* (1988) Treatment of the patient with stage M0 soft tissue sarcoma. *J Clin Oncol* 6(5):854-862.

5. Helman LJ & Meltzer P (2003) Mechanisms of sarcoma development. *Nat Rev Cancer* 3(9):685-694.

6. Christopher D.M. Fletcher KKU, and Fredrik Mertens ed (2002) *Pathology and Genetics of Tumours of Soft Tissue and Bone* (IARCPress, Lyon, France).

7. Rangdaeng S & Truong LD (1991) Comparative immunohistochemical staining for desmin and muscle-specific actin. A study of 576 cases. *Am J Clin Pathol* 96(1):32-45.

8. Kumar S, Perlman E, Harris CA, Raffeld M, & Tsokos M (2000) Myogenin is a specific marker for rhabdomyosarcoma: an immunohistochemical study in paraffin-embedded tissues. *Mod Pathol* 13(9):988-993.

9. Hirose T*, et al.* (1992) Malignant peripheral nerve sheath tumors: an immunohistochemical study in relation to ultrastructural features. *Hum Pathol* 23(8):865-870.

10. Smith TA, Machen SK, Fisher C, & Goldblum JR (1999) Usefulness of cytokeratin subsets for distinguishing monophasic synovial sarcoma from malignant peripheral nerve sheath tumor. *Am J Clin Pathol* 112(5):641-648.

11. Guillou L*, et al.* (1997) Comparative study of the National Cancer Institute and French Federation of Cancer Centers Sarcoma Group grading systems in a population of 410 adult patients with soft tissue sarcoma. *J Clin Oncol* 15(1):350-362.

12. Coindre JM*, et al.* (2003) Should molecular testing be required for diagnosing synovial sarcoma? A prospective study of 204 cases. *Cancer* 98(12):2700-2707.

13. Grobmyer SR*, et al.* (2004) Neo-adjuvant chemotherapy for primary high-grade extremity soft tissue sarcoma. *Ann Oncol* 15(11):1667-1672.

14. Gortzak E*, et al.* (2001) A randomised phase II study on neo-adjuvant chemotherapy for 'high-risk' adult soft-tissue sarcoma. *Eur J Cancer* 37(9):1096-1103.

15. Mackintosh C, Madoz-Gurpide J, Ordonez JL, Osuna D, & Herrero-Martin D (2010) The molecular pathogenesis of Ewing's sarcoma. *Cancer Biol Ther* 9(9):655-667.

16. Sheppard DG & Libshitz HI (2001) Post-radiation sarcomas: a review of the clinical and imaging features in 63 cases. *Clin Radiol* 56(1):22-29.

17. Virtanen A, Pukkala E, & Auvinen A (2006) Incidence of bone and soft tissue sarcoma after radiotherapy: a cohort study of 295,712 Finnish cancer patients. *Int J Cancer* 118(4):1017-1021.

18. Kleihues P, Schauble B, zur Hausen A, Esteve J, & Ohgaki H (1997) Tumors associated with p53 germline mutations: a synopsis of 91 families. *Am J Pathol* 150(1):1-13.

19. Wallace MR*, et al.* (1990) Type 1 neurofibromatosis gene: identification of a large transcript disrupted in three NF1 patients. *Science* 249(4965):181-186.

20. May WA*, et al.* (1993) Ewing sarcoma 11;22 translocation produces a chimeric transcription factor that requires the DNA-binding domain encoded by FLI1 for transformation. *Proc Natl Acad Sci U S A* 90(12):5752-5756.

21. Fukuma M, Okita H, Hata J, & Umezawa A (2003) Upregulation of Id2, an oncogenic helix-loop-helix protein, is mediated by the chimeric EWS/ets protein in Ewing sarcoma. *Oncogene* 22(1):1-9.

22. Fuchs B, Inwards C, Scully SP, & Janknecht R (2004) hTERT Is highly expressed in Ewing's sarcoma and activated by EWS-ETS oncoproteins. *Clin Orthop Relat Res* (426):64-68.

23. Nakatani F*, et al.* (2003) Identification of p21WAF1/CIP1 as a direct target of EWS-Fli1 oncogenic fusion protein. *J Biol Chem* 278(17):15105-15115.

24. Caillaud JM*, et al.* (1989) Histopathological classification of childhood rhabdomyosarcoma: a report from the International Society of Pediatric Oncology pathology panel. *Med Pediatr Oncol* 17(5):391-400.

25. Galili N*, et al.* (1993) Fusion of a fork head domain gene to PAX3 in the solid tumour alveolar rhabdomyosarcoma. *Nat Genet* 5(3):230-235.

26. Davis RJ, D'Cruz CM, Lovell MA, Biegel JA, & Barr FG (1994) Fusion of PAX7 to FKHR by the variant t(1;13)(p36;q14) translocation in alveolar rhabdomyosarcoma. *Cancer Res* 54(11):2869-2872.

27. Barr FG (2001) Gene fusions involving PAX and FOX family members in alveolar rhabdomyosarcoma. *Oncogene* 20(40):5736-5746.

28. Crew AJ*, et al.* (1995) Fusion of SYT to two genes, SSX1 and SSX2, encoding proteins with homology to the Kruppel-associated box in human synovial sarcoma. *EMBO J* 14(10):2333-2340.

29. Skytting B, *et al.* (1999) A novel fusion gene, SYT-SSX4, in synovial sarcoma. *J Natl Cancer Inst* 91(11):974-975.

30. Wurl P, *et al.* (1999) Clinical relevance of pRb and p53 co-overexpression in soft tissue sarcomas. *Cancer Lett* 139(2):159-165.

31. Coindre JM, *et al.* (2001) Predictive value of grade for metastasis development in the main histologic types of adult soft tissue sarcomas: a study of 1240 patients from the French Federation of Cancer Centers Sarcoma Group. *Cancer* 91(10):1914-1926.

32. Ozzello L, Stout AP, & Murray MR (1963) Cultural characteristics of malignant histiocytomas and fibrous xanthomas. *Cancer* 16:331-344.

33. Fletcher CD, Gustafson P, Rydholm A, Willen H, & Akerman M (2001) Clinicopathologic re-evaluation of 100 malignant fibrous histiocytomas: prognostic relevance of subclassification. *J Clin Oncol* 19(12):3045-3050.

34. Rao UN, Finkelstein SD, & Jones MW (1999) Comparative immunohistochemical and molecular analysis of uterine and extrauterine leiomyosarcomas. *Mod Pathol* 12(11):1001-1009.

35. Gibault L, *et al.* (2011) New insights in sarcoma oncogenesis: a comprehensive analysis of a large series of 160 soft tissue sarcomas with complex genomics. *J Pathol* 223(1):64-71.

36. Setsu N, *et al.* (2012) The Akt/mammalian target of rapamycin pathway is activated and associated with adverse prognosis in soft tissue leiomyosarcomas. *Cancer* 118(6):1637-1648.

37. Newton WA, Jr., *et al.* (1995) Classification of rhabdomyosarcomas and related sarcomas. Pathologic aspects and proposal for a new classification--an Intergroup Rhabdomyosarcoma Study. *Cancer* 76(6):1073-1085.

38. Williamson D, *et al.* (2010) Fusion gene-negative alveolar rhabdomyosarcoma is clinically and molecularly indistinguishable from embryonal rhabdomyosarcoma. *J Clin Oncol* 28(13):2151-2158.

39. Shukla N, *et al.* (2012) Oncogene mutation profiling of pediatric solid tumors reveals significant subsets of embryonal rhabdomyosarcoma and neuroblastoma with mutated genes in growth signaling pathways. *Clin Cancer Res* 18(3):748-757.

40. Skovronsky DM & Oberholtzer JC (2004) Pathologic classification of peripheral nerve tumors. *Neurosurg Clin N Am* 15(2):157-166.

41. Baehring JM, Betensky RA, & Batchelor TT (2003) Malignant peripheral nerve sheath tumor: the clinical spectrum and outcome of treatment. *Neurology* 61(5):696-698.

42. Ferner RE & Gutmann DH (2002) International consensus statement on malignant peripheral nerve sheath tumors in neurofibromatosis. *Cancer Res* 62(5):1573-1577.

43. Canter RJ, *et al.* (2010) Interaction of histologic subtype and histologic grade in predicting survival for soft-tissue sarcomas. *J Am Coll Surg* 210(2):191-198 e192.

44. Tanabe KK, *et al.* (1994) Influence of surgical margins on outcome in patients with preoperatively irradiated extremity soft tissue sarcomas. *Cancer* 73(6):1652-1659.

45. Yang JC, *et al.* (1998) Randomized prospective study of the benefit of adjuvant radiation therapy in the treatment of soft tissue sarcomas of the extremity. *J Clin Oncol* 16(1):197-203.

46. Cheng EY, Dusenbery KE, Winters MR, & Thompson RC (1996) Soft tissue sarcomas: preoperative versus postoperative radiotherapy. *J Surg Oncol* 61(2):90-99.

47. Pisters PW, Leung DH, Woodruff J, Shi W, & Brennan MF (1996) Analysis of prognostic factors in 1,041 patients with localized soft tissue sarcomas of the extremities. *J Clin Oncol* 14(5):1679-1689.

48. Billingsley KG*, et al.* (1999) Pulmonary metastases from soft tissue sarcoma: analysis of patterns of diseases and postmetastasis survival. *Ann Surg* 229(5):602-610; discussion 610-602.

49. Van Glabbeke M*, et al.* (1999) Prognostic factors for the outcome of chemotherapy in advanced soft tissue sarcoma: an analysis of 2,185 patients treated with anthracycline-containing first-line regimens--a European Organization for Research and Treatment of Cancer Soft Tissue and Bone Sarcoma Group Study. *J Clin Oncol* 17(1):150-157.

50. Antman K*, et al.* (1998) A Southwest Oncology Group and Cancer and Leukemia Group B phase II study of doxorubicin, dacarbazine, ifosfamide, and mesna in adults with advanced osteosarcoma, Ewing's sarcoma, and rhabdomyosarcoma. *Cancer* 82(7):1288-1295.

51. Bramwell V*, et al.* (1994) Adjuvant CYVADIC chemotherapy for adult soft tissue sarcoma--reduced local recurrence but no improvement in survival: a study of the European Organization for Research and Treatment of Cancer Soft Tissue and Bone Sarcoma Group. *J Clin Oncol* 12(6):1137-1149.

52. Jelic S*, et al.* (1997) Randomised study of high-dose epirubicin versus high-dose epirubicin-cisplatin chemotherapy for advanced soft tissue sarcoma. *Eur J Cancer* 33(2):220-225.

53. Dodd RD, Mito JK, & Kirsch DG (2010) Animal models of soft-tissue sarcoma. *Dis Model Mech* 3(9-10):557-566.

54. Zhang L & Hill RP (2007) Hypoxia enhances metastatic efficiency in HT1080 fibrosarcoma cells by increasing cell survival in lungs, not cell adhesion and invasion. *Cancer Res* 67(16):7789-7797.

55. Taylor JGt, *et al.* (2009) Identification of FGFR4-activating mutations in human rhabdomyosarcomas that promote metastasis in xenotransplanted models. *J Clin Invest* 119(11):3395-3407.

56. Nanni P, *et al.* (2010) High metastatic efficiency of human sarcoma cells in Rag2/gammac double knockout mice provides a powerful test system for antimetastatic targeted therapy. *Eur J Cancer* 46(3):659-668.

57. List K, *et al.* (2005) Deregulated matriptase causes ras-independent multistage carcinogenesis and promotes ras-mediated malignant transformation. *Genes Dev* 19(16):1934-1950.

58. Karnoub AE, *et al.* (2007) Mesenchymal stem cells within tumour stroma promote breast cancer metastasis. *Nature* 449(7162):557-563.

59. Meads MB, Gatenby RA, & Dalton WS (2009) Environment-mediated drug resistance: a major contributor to minimal residual disease. *Nat Rev Cancer* 9(9):665-674.

60. Donehower LA, *et al.* (1992) Mice deficient for p53 are developmentally normal but susceptible to spontaneous tumours. *Nature* 356(6366):215-221.

61. Shen MH, Harper PS, & Upadhyaya M (1996) Molecular genetics of neurofibromatosis type 1 (NF1). *J Med Genet* 33(1):2-17.

62. Jacks T, *et al.* (1994) Tumour predisposition in mice heterozygous for a targeted mutation in Nf1. *Nat Genet* 7(3):353-361.

63. Cichowski K, *et al.* (1999) Mouse models of tumor development in neurofibromatosis type 1. *Science* 286(5447):2172-2176.

64. Keller C, *et al.* (2004) Alveolar rhabdomyosarcomas in conditional Pax3:Fkhr mice: cooperativity of Ink4a/ARF and Trp53 loss of function. *Genes Dev* 18(21):2614-2626.

65. Nishijo K, *et al.* (2009) Credentialing a preclinical mouse model of alveolar rhabdomyosarcoma. *Cancer Res* 69(7):2902-2911.

66. Haldar M, Hancock JD, Coffin CM, Lessnick SL, & Capecchi MR (2007) A conditional mouse model of synovial sarcoma: insights into a myogenic origin. *Cancer Cell* 11(4):375-388.

67. Kohashi K, *et al.* (2008) Alterations of RB1 gene in embryonal and alveolar rhabdomyosarcoma: special reference to utility of pRB immunoreactivity in differential diagnosis of rhabdomyosarcoma subtype. *J Cancer Res Clin Oncol* 134(10):1097-1103.

68. Langenau DM, *et al.* (2007) Effects of RAS on the genesis of embryonal rhabdomyosarcoma. *Genes Dev* 21(11):1382-1395.

69. Rubin BP, *et al.* (2011) Evidence for an unanticipated relationship between undifferentiated pleomorphic sarcoma and embryonal rhabdomyosarcoma. *Cancer Cell* 19(2):177-191.

70. Hernando E, *et al.* (2007) The AKT-mTOR pathway plays a critical role in the development of leiomyosarcomas. *Nat Med* 13(6):748-753.

71. Xing D, *et al.* (2009) A role for BRCA1 in uterine leiomyosarcoma. *Cancer Res* 69(21):8231-8235.

72. Kirsch DG, *et al.* (2007) A spatially and temporally restricted mouse model of soft tissue sarcoma. *Nat Med* 13(8):992-997.

73. Bolstad BM, Irizarry RA, Astrand M, & Speed TP (2003) A comparison of normalization methods for high density oligonucleotide array data based on variance and bias. *Bioinformatics* 19(2):185-193.

74. Irizarry RA, *et al.* (2003) Exploration, normalization, and summaries of high density oligonucleotide array probe level data. *Biostatistics* 4(2):249-264.

75. Baird K, *et al.* (2005) Gene expression profiling of human sarcomas: insights into sarcoma biology. *Cancer Res* 65(20):9226-9235.

76. Detwiller KY, *et al.* (2005) Analysis of hypoxia-related gene expression in sarcomas and effect of hypoxia on RNA interference of vascular endothelial cell growth factor A. *Cancer Res* 65(13):5881-5889.

77. Nakayama R, *et al.* (2007) Gene expression analysis of soft tissue sarcomas: characterization and reclassification of malignant fibrous histiocytoma. *Mod Pathol* 20(7):749-759.

78. Subramanian A, *et al.* (2005) Gene set enrichment analysis: a knowledge-based approach for interpreting genome-wide expression profiles. *Proc Natl Acad Sci U S A* 102(43):15545-15550.

79. Johnson WE, Li C, & Rabinovic A (2007) Adjusting batch effects in microarray expression data using empirical Bayes methods. *Biostatistics* 8(1):118-127.

80. Bild AH, *et al.* (2006) Oncogenic pathway signatures in human cancers as a guide to targeted therapies. *Nature* 439(7074):353-357.

81. Cui W, Taub DD, & Gardner K (2007) qPrimerDepot: a primer database for quantitative real time PCR. *Nucleic Acids Res* 35(Database issue):D805-809.

82. Srinivas S, *et al.* (2001) Cre reporter strains produced by targeted insertion of EYFP and ECFP into the ROSA26 locus. *BMC Dev Biol* 1:4.

83. Dankort D, *et al.* (2007) A new mouse model to explore the initiation, progression, and therapy of BRAFV600E-induced lung tumors. *Genes Dev* 21(4):379-384.

84. Sheth RA, Upadhyay R, Weissleder R, & Mahmood U (2007) Real-time multichannel imaging framework for endoscopy, catheters, and fixed geometry intraoperative systems. *Mol Imaging* 6(3):147-155.

85. Upadhyay R, Sheth RA, Weissleder R, & Mahmood U (2007) Quantitative real-time catheter-based fluorescence molecular imaging in mice. *Radiology* 245(2):523-531.

86. Morgenstern JP & Land H (1990) Advanced mammalian gene transfer: high titre retroviral vectors with multiple drug selection markers and a complementary helper-free packaging cell line. *Nucleic Acids Res* 18(12):3587-3596.

87. Boehm JS, *et al.* (2007) Integrative genomic approaches identify IKBKE as a breast cancer oncogene. *Cell* 129(6):1065-1079.

88. Kent OA, *et al.* (2010) Repression of the miR-143/145 cluster by oncogenic Ras initiates a tumor-promoting feed-forward pathway. *Genes Dev* 24(24):2754-2759.

89. Moffat J, *et al.* (2006) A lentiviral RNAi library for human and mouse genes applied to an arrayed viral high-content screen. *Cell* 124(6):1283-1298.

90. Simon R, *et al.* (2007) Analysis of gene expression data using BRB-ArrayTools. *Cancer Inform* 3:11-17.

91. Laiho P, *et al.* (2007) Serrated carcinomas form a subclass of colorectal cancer with distinct molecular basis. *Oncogene* 26(2):312-320.

92. Metzeler KH, *et al.* (2008) An 86-probe-set gene-expression signature predicts survival in cytogenetically normal acute myeloid leukemia. *Blood* 112(10):4193-4201.

93. Palmer RD, *et al.* (2008) Pediatric malignant germ cell tumors show characteristic transcriptome profiles. *Cancer Res* 68(11):4239-4247.

94. Gutierrez NC, *et al.* (2005) Gene expression profile reveals deregulation of genes with relevant functions in the different subclasses of acute myeloid leukemia. *Leukemia* 19(3):402-409.

95. Sabates-Bellver J, *et al.* (2007) Transcriptome profile of human colorectal adenomas. *Mol Cancer Res* 5(12):1263-1275.

96. Dyrskjot L, *et al.* (2004) Gene expression in the urinary bladder: a common carcinoma in situ gene expression signature exists disregarding histopathological classification. *Cancer Res* 64(11):4040-4048.

97. Jackson EL, *et al.* (2001) Analysis of lung tumor initiation and progression using conditional expression of oncogenic K-ras. *Genes Dev* 15(24):3243-3248.

98. Jonkers J, *et al.* (2001) Synergistic tumor suppressor activity of BRCA2 and p53 in a conditional mouse model for breast cancer. *Nat Genet* 29(4):418-425.

99. Harfe BD, McManus MT, Mansfield JH, Hornstein E, & Tabin CJ (2005) The RNaseIII enzyme Dicer is required for morphogenesis but not patterning of the vertebrate limb. *Proc Natl Acad Sci U S A* 102(31):10898-10903.

100. Fletcher CD (1992) Pleomorphic malignant fibrous histiocytoma: fact or fiction? A critical reappraisal based on 159 tumors diagnosed as pleomorphic sarcoma. *Am J Surg Pathol* 16(3):213-228.

101. Hollowood K & Fletcher CD (1995) Malignant fibrous histiocytoma: morphologic pattern or pathologic entity? *Semin Diagn Pathol* 12(3):210-220.

102. Leach FS, *et al.* (1993) p53 Mutation and MDM2 amplification in human soft tissue sarcomas. *Cancer Res* 53(10 Suppl):2231-2234.

103. Yoo J & Robinson RA (1999) H-ras and K-ras mutations in soft tissue sarcoma: comparative studies of sarcomas from Korean and American patients. *Cancer* 86(1):58-63.

104. Yoo J, Robinson RA, & Lee JY (1999) H-ras and K-ras gene mutations in primary human soft tissue sarcoma: concomitant mutations of the ras genes. *Mod Pathol* 12(8):775-780.

105. Liu M*, et al.* (2006) FoxM1B is overexpressed in human glioblastomas and critically regulates the tumorigenicity of glioma cells. *Cancer Res* 66(7):3593-3602.

106. Ma RY*, et al.* (2005) Raf/MEK/MAPK signaling stimulates the nuclear translocation and transactivating activity of FOXM1c. *J Cell Sci* 118(Pt 4):795-806.

107. Wang IC*, et al.* (2008) FoxM1 regulates transcription of JNK1 to promote the G1/S transition and tumor cell invasiveness. *J Biol Chem* 283(30):20770-20778.

108. Mito JK*, et al.* (2012) Intraoperative detection and removal of microscopic residual sarcoma using wide-field imaging. *Cancer*.

109. Lewis JJ*, et al.* (1999) Multifactorial analysis of long-term follow-up (more than 5 years) of primary extremity sarcoma. *Arch Surg* 134(2):190-194.

110. Sabolch A*, et al.* (2011) Adjuvant and definitive radiotherapy for adrenocortical carcinoma. *Int J Radiat Oncol Biol Phys* 80(5):1477-1484.

111. Sadoski C, Suit HD, Rosenberg A, Mankin H, & Efird J (1993) Preoperative radiation, surgical margins, and local control of extremity sarcomas of soft tissues. *J Surg Oncol* 52(4):223-230.

112. Lewis JJ, Leung D, Espat J, Woodruff JM, & Brennan MF (2000) Effect of reresection in extremity soft tissue sarcoma. *Ann Surg* 231(5):655-663.

113. Allweis TM*, et al.* (2008) A prospective, randomized, controlled, multicenter study of a real-time, intraoperative probe for positive margin detection in breast-conserving surgery. *Am J Surg* 196(4):483-489.

114. Weissleder R & Pittet MJ (2008) Imaging in the era of molecular oncology. *Nature* 452(7187):580-589.

115. Thurber GM, Figueiredo JL, & Weissleder R (2010) Detection limits of intraoperative near infrared imaging for tumor resection. *J Surg Oncol* 102(7):758-764.

116. Weissleder R, Tung CH, Mahmood U, & Bogdanov A, Jr. (1999) In vivo imaging of tumors with protease-activated near-infrared fluorescent probes. *Nat Biotechnol* 17(4):375-378.

117. Bremer C, Tung CH, & Weissleder R (2001) In vivo molecular target assessment of matrix metalloproteinase inhibition. *Nat Med* 7(6):743-748.

118. Roshy S, Sloane BF, & Moin K (2003) Pericellular cathepsin B and malignant progression. *Cancer Metastasis Rev* 22(2-3):271-286.

119. Gocheva V*, et al.* (2010) IL-4 induces cathepsin protease activity in tumor-associated macrophages to promote cancer growth and invasion. *Genes Dev* 24(3):241-255.

120. Jaffer FA*, et al.* (2007) Optical visualization of cathepsin K activity in atherosclerosis with a novel, protease-activatable fluorescence sensor. *Circulation* 115(17):2292-2298.

121. Gounaris E*, et al.* (2008) Live imaging of cysteine-cathepsin activity reveals dynamics of focal inflammation, angiogenesis, and polyp growth. *PLoS One* 3(8):e2916.

122. Mohs AM*, et al.* (2010) Hand-held Spectroscopic Device for In Vivo and Intraoperative Tumor Detection: Contrast Enhancement, Detection Sensitivity, and Tissue Penetration. *Anal Chem*.

123. Nguyen QT*, et al.* (2010) Surgery with molecular fluorescence imaging using activatable cell-penetrating peptides decreases residual cancer and improves survival. *Proc Natl Acad Sci U S A* 107(9):4317-4322.

124. Themelis G*, et al.* (2011) Enhancing surgical vision by using real-time imaging of alphavbeta3-integrin targeted near-infrared fluorescent agent. *Ann Surg Oncol* 18(12):3506-3513.

125. Qian BZ & Pollard JW (2010) Macrophage diversity enhances tumor progression and metastasis. *Cell* 141(1):39-51.

126. Lin EY, Nguyen AV, Russell RG, & Pollard JW (2001) Colony-stimulating factor 1 promotes progression of mammary tumors to malignancy. *J Exp Med* 193(6):727-740.

127. Ntziachristos V, Ripoll J, & Weissleder R (2002) Would near-infrared fluorescence signals propagate through large human organs for clinical studies? Errata. *Opt Lett* 27(18):1652.

128. Wolf K*, et al.* (2007) Multi-step pericellular proteolysis controls the transition from individual to collective cancer cell invasion. *Nat Cell Biol* 9(8):893-904.

129. Friedl P & Gilmour D (2009) Collective cell migration in morphogenesis, regeneration and cancer. *Nat Rev Mol Cell Biol* 10(7):445-457.

130. Condeelis J & Pollard JW (2006) Macrophages: obligate partners for tumor cell migration, invasion, and metastasis. *Cell* 124(2):263-266.

131. Ogawa M, Kosaka N, Choyke PL, & Kobayashi H (2009) In vivo molecular imaging of cancer with a quenching near-infrared fluorescent probe using conjugates of monoclonal antibodies and indocyanine green. *Cancer Res* 69(4):1268-1272.

132. Kitai T, Inomoto T, Miwa M, & Shikayama T (2005) Fluorescence navigation with indocyanine green for detecting sentinel lymph nodes in breast cancer. *Breast Cancer* 12(3):211-215.

133. Ishizawa T*, et al.* (2009) Real-time identification of liver cancers by using indocyanine green fluorescent imaging. *Cancer* 115(11):2491-2504.

134. Frangioni JV (2008) New technologies for human cancer imaging. *J Clin Oncol* 26(24):4012-4021.

135. Lee Y*, et al.* (2004) MicroRNA genes are transcribed by RNA polymerase II. *EMBO J* 23(20):4051-4060.

136. Gregory RI*, et al.* (2004) The Microprocessor complex mediates the genesis of microRNAs. *Nature* 432(7014):235-240.

137. Lee Y, Jeon K, Lee JT, Kim S, & Kim VN (2002) MicroRNA maturation: stepwise processing and subcellular localization. *EMBO J* 21(17):4663-4670.

138. Lund E, Guttinger S, Calado A, Dahlberg JE, & Kutay U (2004) Nuclear export of microRNA precursors. *Science* 303(5654):95-98.

139. Chendrimada TP*, et al.* (2005) TRBP recruits the Dicer complex to Ago2 for microRNA processing and gene silencing. *Nature* 436(7051):740-744.

140. Bartel DP (2009) MicroRNAs: target recognition and regulatory functions. *Cell* 136(2):215-233.

141. Lu J*, et al.* (2005) MicroRNA expression profiles classify human cancers. *Nature* 435(7043):834-838.

142. Heinzelmann J*, et al.* (2011) Specific miRNA signatures are associated with metastasis and poor prognosis in clear cell renal cell carcinoma. *World J Urol* 29(3):367-373.

143. Wong CM*, et al.* (2011) Sequential alterations of miRNA expression in hepatocellular carcinoma development and venous metastasis. *Hepatology*.

144. van Kouwenhove M, Kedde M, & Agami R (2011) MicroRNA regulation by RNA-binding proteins and its implications for cancer. *Nat Rev Cancer* 11(9):644-656.

145. Dehner LP, Jarzembowski JA, & Hill DA (2011) Embryonal rhabdomyosarcoma of the uterine cervix: a report of 14 cases and a discussion of its unusual clinicopathological associations. *Mod Pathol*.

146. Heravi-Moussavi A*, et al.* (2012) Recurrent somatic DICER1 mutations in nonepithelial ovarian cancers. *N Engl J Med* 366(3):234-242.

147. Melo SA*, et al.* (2010) A genetic defect in exportin-5 traps precursor microRNAs in the nucleus of cancer cells. *Cancer Cell* 18(4):303-315.

148. Melo SA*, et al.* (2009) A TARBP2 mutation in human cancer impairs microRNA processing and DICER1 function. *Nat Genet* 41(3):365-370.

149. Merritt WM*, et al.* (2008) Dicer, Drosha, and outcomes in patients with ovarian cancer. *N Engl J Med* 359(25):2641-2650.

150. Lin RJ*, et al.* (2010) microRNA signature and expression of Dicer and Drosha can predict prognosis and delineate risk groups in neuroblastoma. *Cancer Res* 70(20):7841-7850.

151. Faber C, Horst D, Hlubek F, & Kirchner T (2011) Overexpression of Dicer predicts poor survival in colorectal cancer. *Eur J Cancer* 47(9):1414-1419.

152. Chiosea S*, et al.* (2006) Up-regulation of dicer, a component of the MicroRNA machinery, in prostate adenocarcinoma. *Am J Pathol* 169(5):1812-1820.

153. Paroo Z, Ye X, Chen S, & Liu Q (2009) Phosphorylation of the human microRNA-generating complex mediates MAPK/Erk signaling. *Cell* 139(1):112-122.

154. Davies H*, et al.* (2002) Mutations of the BRAF gene in human cancer. *Nature* 417(6892):949-954.

155. Pylayeva-Gupta Y, Grabocka E, & Bar-Sagi D (2011) RAS oncogenes: weaving a tumorigenic web. *Nat Rev Cancer* 11(11):761-774.

156. Sharma SV, Bell DW, Settleman J, & Haber DA (2007) Epidermal growth factor receptor mutations in lung cancer. *Nat Rev Cancer* 7(3):169-181.

157. Pratilas CA*, et al.* (2009) (V600E)BRAF is associated with disabled feedback inhibition of RAF-MEK signaling and elevated transcriptional output of the pathway. *Proc Natl Acad Sci U S A* 106(11):4519-4524.

158. Foulkes WD*, et al.* (2011) Extending the phenotypes associated with DICER1 mutations. *Hum Mutat* 32(12):1381-1384.

159. Kumar MS*, et al.* (2009) Dicer1 functions as a haploinsufficient tumor suppressor. *Genes Dev* 23(23):2700-2704.

160. Kumar MS, Lu J, Mercer KL, Golub TR, & Jacks T (2007) Impaired microRNA processing enhances cellular transformation and tumorigenesis. *Nat Genet* 39(5):673-677.

161. Drobnjak M*, et al.* (1994) Prognostic implications of p53 nuclear overexpression and high proliferation index of Ki-67 in adult soft-tissue sarcomas. *J Natl Cancer Inst* 86(7):549-554.

162. Mito JK*, et al.* (2009) Cross species genomic analysis identifies a mouse model as undifferentiated pleomorphic sarcoma/malignant fibrous histiocytoma. *PLoS One* 4(11):e8075.

163. Lee Y*, et al.* (2003) The nuclear RNase III Drosha initiates microRNA processing. *Nature* 425(6956):415-419.

164. Muralidhar B*, et al.* (2007) Global microRNA profiles in cervical squamous cell carcinoma depend on Drosha expression levels. *J Pathol* 212(4):368-377.

165. Faller M*, et al.* (2010) DGCR8 recognizes primary transcripts of microRNAs through highly cooperative binding and formation of higher-order structures. *RNA* 16(8):1570-1583.

166. Zhang S, *et al.* (2003) p16 INK4a gene promoter variation and differential binding of a repressor, the ras-responsive zinc-finger transcription factor, RREB. *Oncogene* 22(15):2285-2295.

167. Liu H, *et al.* (2009) DNA damage signalling recruits RREB-1 to the p53 tumour suppressor promoter. *Biochem J* 422(3):543-551.

168. Li Y, *et al.* (2010) miR-146a suppresses invasion of pancreatic cancer cells. *Cancer Res* 70(4):1486-1495.

169. Esteller M (2011) Non-coding RNAs in human disease. *Nat Rev Genet* 12(12):861-874.

170. Hanahan D & Weinberg RA (2011) Hallmarks of cancer: the next generation. *Cell* 144(5):646-674.

171. Kurose K, *et al.* (2002) Frequent somatic mutations in PTEN and TP53 are mutually exclusive in the stroma of breast carcinomas. *Nat Genet* 32(3):355-357.

172. Lee CL, *et al.* (2012) Generation of primary tumors with Flp recombinase in FRT-flanked p53 mice. *Dis Model Mech*.

Biography

Date and Place of Birth: June 22, 1982 - Edmonds, Washington, U.S.A.

Education:

2007-Present	Duke University; Graduate School, Program in Molecular Cancer Biology
2005-Present	Duke University; School of Medicine
2000-2004	Princeton University; B.A., Major: Molecular Biology, Magna Cum Laude

Previous Positions:

Summers 2002, 2003	Summer Research Intern, Fred Hutchinson Cancer Research Center. Warren Lab, Program in Immunology, Division of Clinical Research.
2004-2005	Research Associate, Fred Hutchinson Cancer Research Center. Warren Lab, Program in Immunology, Division of Clinical Research.

Professional Societies:

2008 – Present, Associate Member, American Association for Cancer Research

Elected 2000, Associate Member, Sigma Xi Research Society

Honors and Awards:

2011, Radiation Oncology and Imaging Program Retreat, Duke University Medical Center, Best Poster.

2010, Days of Molecular Medicine: System Biology Approaches to Cancer and Metabolic Disease, Stockholm Sweden, Conference Travel Award.

Poster Presentations

1: “Dissecting Molecular Mechanisms of Metastasis in a Primary Mouse Model of Soft Tissue Sarcoma”. **Mito JK**, Dodd RD, Brigman BE, Eward WC, Li Z, Mukherjee S, and Kirsch DG. Presented at Days of Molecular Medicine, Stockholm, Sweden. May 20-22, 2010.

2: “A novel wide field-of-view imaging device for real-time, intra-operative tumor bed assessment” **Mito JK,** Ferrer JM, Brigman BE, Lee CL, Dodd RD, Eward WC, Marshall LF, Dankort D, McMahon M, Kim Y, Lee WD, Griffith LG, Bawendi MG, and Kirsch DG. Presented at AACR 101st annual meeting. Washington DC, United States. April 17-21, 2010.

Publications

1: **Mito JK**, Sachdeva M, Min HD, Javid M, Dodd RD, Ma Y, Cater JE, Brigman BE, Dodd L, Dankort D, McMahon M, Lev D, Kirsch DG. Genotype Dependent Control of miRNA Biogenesis and Metastasis is Mediated Through MAPK Regulation of Dgcr8 (Submitted).

2: **Mito JK**, Ferrer JM, Brigman BE, Lee CL, Dodd RD, Eward WC, Marshall LF, Cuneo KC, Carter JE, Ramasunder S, Kim Y, Lee WD, Griffith LG, Bawendi MG, Kirsch DG. Intraoperative detection and removal of microscopic residual sarcoma using wide-field imaging. Cancer. 2012 Mar 21. [Epub ahead of print] PubMed PMID: 22437667.

3: Dodd RD, **Mito JK**, Kirsch DG. Animal models of soft tissue sarcoma. Disease Models and Mechanisms. 2010 Sep-Oct; 3(9-10):557-66 Review.

4: Kang Y, Chen BJ, Deoliveira D, **Mito J**, Chao NJ. Selective enhancement of donor hematopoietic cell engraftment by the CXCR4 antagonist AMD3100 in a mouse transplantation model. PLoS One. 2010 Jun 28;5(6):e11316.

5: Warren EH, Fujii N, Akatsuka Y, Chaney CN, **Mito JK**, Loeb KR, Gooley TA, Brown ML, Koo KK, Rosinski KV, Ogawa S, Matsubara A, Appelbaum FR, Riddell SR. Therapy of relapsed leukemia after allogeneic hematopoietic cell

transplant with T cells specific for minor histocompatibility antigens. Blood. 2010 Jan 13.

6: **Mito JK**, Riedel RF, Dodd L, Lahat G, Lazar AJ, Dodd RD, Stangenberg L, Eward WC, Hornicek FJ, Yoon SS, Brigman BE, Jacks T, Lev D, Mukherjee S, Kirsch DG. Cross species genomic analysis identifies a mouse model as undifferentiated pleomorphic sarcoma/malignant fibrous histiocytoma. PLoS One. 2009 Nov 30;4(11):e8075.

7: Tykodi SS, Fujii N, Vigneron N, Lu SM, **Mito JK**, Miranda MX, Chou J, Voong LN, Thompson JA, Sandmaier BM, Cresswell P, Van den Eynde B, Riddell SR, Warren EH. C19orf48 encodes a minor histocompatibility antigen recognized by CD8+ cytotoxic T cells from renal cell carcinoma patients. Clin Cancer Res. 2008 Aug 15;14(16):5260-9.

8: Rosinski KV, Fujii N, **Mito JK**, Koo KK, Xuereb SM, Sala-Torra O, Gibbs JS, Radich JP, Akatsuka Y, Van den Eynde BJ, Riddell SR, Warren EH. DDX3Y encodes a class I MHC-restricted H-Y antigen that is expressed in leukemic stem cells. Blood. 2008 May 1;111(9):4817-26.

9: Warren EH, Vigneron NJ, Gavin MA, Coulie PG, Stroobant V, Dalet A, Tykodi SS, Xuereb SM, **Mito JK**, Riddell SR, Van den Eynde BJ. An antigen produced by splicing of noncontiguous peptides in the reverse order. Science. 2006 Sep 8;313(5792):1444-7

10: Brickner AG, Evans AM, **Mito JK**, Xuereb SM, Feng X, Nishida T, Fairfull L, Ferrell RE, Foon KA, Hunt DF, Shabanowitz J, Engelhard VH, Riddell SR, Warren EH. The PANE1 gene encodes a novel human minor histocompatibility antigen that is selectively expressed in B-lymphoid cells and B-CLL. Blood. 2006 May 1;107(9):3779-86.